Mass-balanced stratigraphy

Data-model comparison within a closed sedimentary system (Adriatic Sea, Italy)

Proefschrift

ter verkrijging van de graad van doctor aan de Technische Universiteit Delft, op gezag van de Rector Magnificus prof. dr. ir. J.T. Fokkema, voorzitter van het College voor Promoties, in het openbaar te verdedigen

op dinsdag 3 november 2009 om 10.00 uur

door

Marit Bente BROMMER

doctorandus in de aardwetenschappen geboren te Amsterdam Dit proefschrift is goedgekeurd door de promotor: Prof. dr. S.B. Kroonenberg

Copromotor: Dr. G.J. Weltje

Samenstelling promotiecommissie:

Rector Magnificus voorzitter

Prof. dr. S.B. Kroonenberg Technische Universiteit Delft, promotor Dr. G.J. Weltje Technische Universiteit Delft, copromotor

Prof. dr. ir. M.J.F. Stive Technische Universiteit Delft

Prof. dr. ir. A.E. Mynett Technische Universiteit Delft & UNESCO-IHE

Prof. dr. P.L. de Boer Universiteit Utrecht

Prof. dr. C. Amos University of Southampton, United Kingdom

Dr. A. Cattaneo IFREMER, France

Prof.dr. J.J.G. Reijmer Technische Universiteit Delft, reservelid

ISBN: 978-90-8570-418-8

Copyright © 2009 by M.B. Brommer, Section of Applied Geology, Faculty of Civil Engineering and Geotechnology, Delft University of Technology. All rights reserved, no parts of this thesis may be reproduced, stored in any retrieval system or transmitted, in any forms or by any means, electronic, mechanical, photocopying, recording or otherwise without the prior written permission of the author.

This research project has been funded by the Netherlands Organisation for Scientific Research (NWO) under contract number 813.03.005. Printed with generous financial support of Delft University of Technology.

Printed by Wöhrmann Print Service Zutphen

Mass-balanced stratigraphy

Data-model comparison within a closed sedimentary system (Adriatic Sea, Italy)

Contents

Intro	duction	1
1.1	General introduction	1
1.2	Why study the Adriatic Basin?	2
1.3	Objectives of the thesis	2
1.4	Outline of the thesis	4
rates	nstruction of sediment supply from mass accumulation in the Northern Adriatic Basin (Italy) over the past	7
	00 years	_
2.1	Introduction	7
2.2	Study Area	ç
	2.2.1 The Adriatic Basin	
	2.2.2 Northern Adriatic shelf	10
	2.2.3 Po Delta	10
0.0	2.2.4 Mid-Adriatic Deep	13
2.3	Stochastic analysis of the stratigraphic record	14
	2.3.1 Geostatistical modelling	14
	2.3.2 Time-depth conversion	16
	2.3.3 Sediment mass calculation	16
	2.3.4 Uncertainty estimation of sediment mass	19
0.4	2.3.5 Deposits in the Po Delta and MAD	20
2.4	Results	21
	2.4.1 Spatial distribution of sediment thickness	21
	2.4.2 Total sediment mass per lithosome	23
	2.4.3 Basin-wide mass accumulation rates	23
2.5	Interpretation and discussion	24
	2.5.1 Statistical Test	24
	2.5.2 Relation to sediment supply	25
	2.5.3 Analysis of the HST-2 lithosome	27
	2.5.4 Spatial-temporal scales of mass accumulation	27
	rates	
2.6	Conclusions	29
appli	nent budget modelling of multi-sourced basin fills: cation to recent deposits of the Northern Adriatic mud Italy)	37
3.1	Introduction	37
3.2	Study area	38
~ . -	3.2.1 Adriatic Basin	38
	3.2.2 Geology of the river basins	40
	3 2 3 Hydrodynamics	40

		3.2.4 Sediment transport	41
	3.3	Grain-size analysis of river and surface samples	41
		3.3.1 Sampling and grain-size analysis	41
		3.3.2 Results	42
		3.3.3 Spatial distribution of grain-size	48
	3.4	Geochemical analysis of river samples	4'
		3.4.1 Introduction	4'
		3.4.2 Geochemical analysis and data processing	4
		3.4.3 Results	48
	3.5	Modelling sediment supply	52
		3.5.1 Sediment supply model	52
		3.5.2 Input data and results	53
	3.6	Dispersal patterns on the shelf	58
		3.6.1 Geochemical end-members	5
		3.6.2 Unmixing of surface samples	5
		3.6.3 Dispersal patterns of the C and S fractions	5
	3.7	Integrated analysis of provenance and dispersal	6
		3.7.1 Combining grain-size and chemistry	6
		3.7.2 Source-specific accumulation patterns	60
		3.7.3 Sediment budget and model calibration	6
	3.8	Discussion and conclusion	6
4	19.00 appro		
4	19.00 appro 4.1	0 years: data-model comparison using a mass-balance each Introduction	7
4	19.00 appro	0 years: data-model comparison using a mass-balance bach Introduction Setting	7 ! 7! 7'
4	19.00 appro 4.1	O years: data-model comparison using a mass-balance bach Introduction Setting 4.2.1 The Adriatic Basin	7: 7: 7:
4	19.00 appro 4.1 4.2	O years: data-model comparison using a mass-balance bach Introduction Setting 4.2.1 The Adriatic Basin 4.2.2 River basins	7: 7: 7: 7:
4	19.00 appro 4.1 4.2	O years: data-model comparison using a mass-balance bach Introduction Setting 4.2.1 The Adriatic Basin 4.2.2 River basins Sediment supply model	7: 7: 7: 8:
4	19.00 appro 4.1 4.2	O years: data-model comparison using a mass-balance bach Introduction Setting 4.2.1 The Adriatic Basin 4.2.2 River basins Sediment supply model Input data	7 7 7 7 8 8
4	19.00 appro 4.1 4.2	O years: data-model comparison using a mass-balance bach Introduction Setting 4.2.1 The Adriatic Basin 4.2.2 River basins Sediment supply model Input data 4.4.1 Area (A) and elevation (R)	77 77 77 80 8
4	19.00 appro 4.1 4.2	Introduction Setting 4.2.1 The Adriatic Basin 4.2.2 River basins Sediment supply model Input data 4.4.1 Area (A) and elevation (R) 4.4.2 Sediment storage and release (B)	75 77 75 80 8 8
4	19.00 appro 4.1 4.2 4.3 4.4	Introduction Setting 4.2.1 The Adriatic Basin 4.2.2 River basins Sediment supply model Input data 4.4.1 Area (A) and elevation (R) 4.4.2 Sediment storage and release (B) 4.4.3 Discharge (Q) and temperature (T)	7 7 7 7 8 8 8 8 8 8
4	19.00 appro 4.1 4.2 4.3 4.4	Introduction Setting 4.2.1 The Adriatic Basin 4.2.2 River basins Sediment supply model Input data 4.4.1 Area (A) and elevation (R) 4.4.2 Sediment storage and release (B) 4.4.3 Discharge (Q) and temperature (T) Uncertainty analysis	7 7 7 8 8 8 8 8 8 8
4	19.00 appro 4.1 4.2 4.3 4.4	Introduction Setting 4.2.1 The Adriatic Basin 4.2.2 River basins Sediment supply model Input data 4.4.1 Area (A) and elevation (R) 4.4.2 Sediment storage and release (B) 4.4.3 Discharge (Q) and temperature (T) Uncertainty analysis Upscaling of model output	7 7 7 7 8 8 8 8 8 8 8
4	19.00 appro 4.1 4.2 4.3 4.4	Introduction Setting 4.2.1 The Adriatic Basin 4.2.2 River basins Sediment supply model Input data 4.4.1 Area (A) and elevation (R) 4.4.2 Sediment storage and release (B) 4.4.3 Discharge (Q) and temperature (T) Uncertainty analysis Upscaling of model output Statistical analysis of results	77 77 77 88 88 88 88 88 88
4	19.00 appro 4.1 4.2 4.3 4.4	Introduction Setting 4.2.1 The Adriatic Basin 4.2.2 River basins Sediment supply model Input data 4.4.1 Area (A) and elevation (R) 4.4.2 Sediment storage and release (B) 4.4.3 Discharge (Q) and temperature (T) Uncertainty analysis Upscaling of model output Statistical analysis of results 4.7.1 Model output	77 77 77 88 88 88 88 88 88 88
4	19.00 appro 4.1 4.2 4.3 4.4	Introduction Setting 4.2.1 The Adriatic Basin 4.2.2 River basins Sediment supply model Input data 4.4.1 Area (A) and elevation (R) 4.4.2 Sediment storage and release (B) 4.4.3 Discharge (Q) and temperature (T) Uncertainty analysis Upscaling of model output Statistical analysis of results 4.7.1 Model output 4.7.2 Statistical test	77 77 77 88 88 88 88 88 88 88
4	19.00 appro 4.1 4.2 4.3 4.4 4.5 4.6 4.7	Introduction Setting 4.2.1 The Adriatic Basin 4.2.2 River basins Sediment supply model Input data 4.4.1 Area (A) and elevation (R) 4.4.2 Sediment storage and release (B) 4.4.3 Discharge (Q) and temperature (T) Uncertainty analysis Upscaling of model output Statistical analysis of results 4.7.1 Model output 4.7.2 Statistical test 4.7.3 Test result	7 7 7 7 8 8 8 8 8 8 8 8 8 8 8 8 8 8
4	19.00 appro 4.1 4.2 4.3 4.4	Introduction Setting 4.2.1 The Adriatic Basin 4.2.2 River basins Sediment supply model Input data 4.4.1 Area (A) and elevation (R) 4.4.2 Sediment storage and release (B) 4.4.3 Discharge (Q) and temperature (T) Uncertainty analysis Upscaling of model output Statistical analysis of results 4.7.1 Model output 4.7.2 Statistical test	77 77 77 88 88 88 88 88 88 89
5	19.00 appro 4.1 4.2 4.3 4.4 4.5 4.6 4.7	Introduction Setting 4.2.1 The Adriatic Basin 4.2.2 River basins Sediment supply model Input data 4.4.1 Area (A) and elevation (R) 4.4.2 Sediment storage and release (B) 4.4.3 Discharge (Q) and temperature (T) Uncertainty analysis Upscaling of model output Statistical analysis of results 4.7.1 Model output 4.7.2 Statistical test 4.7.3 Test result Discussion and conclusions	7; 7; 7; 8; 8; 8; 8; 8; 8; 9; 9;
	19.00 appro 4.1 4.2 4.3 4.4 4.5 4.6 4.7	Introduction Setting 4.2.1 The Adriatic Basin 4.2.2 River basins Sediment supply model Input data 4.4.1 Area (A) and elevation (R) 4.4.2 Sediment storage and release (B) 4.4.3 Discharge (Q) and temperature (T) Uncertainty analysis Upscaling of model output Statistical analysis of results 4.7.1 Model output 4.7.2 Statistical test 4.7.3 Test result Discussion and conclusions ment budget, growth pattern and stratal architecture of	77 77 77 88 8 8 8 8 8 8 8 8 9
	19.00 appro 4.1 4.2 4.3 4.4 4.5 4.6 4.7	Introduction Setting 4.2.1 The Adriatic Basin 4.2.2 River basins Sediment supply model Input data 4.4.1 Area (A) and elevation (R) 4.4.2 Sediment storage and release (B) 4.4.3 Discharge (Q) and temperature (T) Uncertainty analysis Upscaling of model output Statistical analysis of results 4.7.1 Model output 4.7.2 Statistical test 4.7.3 Test result Discussion and conclusions	7
	19.00 appro 4.1 4.2 4.3 4.4 4.5 4.6 4.7	Introduction Setting 4.2.1 The Adriatic Basin 4.2.2 River basins Sediment supply model Input data 4.4.1 Area (A) and elevation (R) 4.4.2 Sediment storage and release (B) 4.4.3 Discharge (Q) and temperature (T) Uncertainty analysis Upscaling of model output Statistical analysis of results 4.7.1 Model output 4.7.2 Statistical test 4.7.3 Test result Discussion and conclusions ment budget, growth pattern and stratal architecture of ate-Holocene Adriatic mud belt: an integrated model	77 77 77 88 88 88 88 88 89 99

		5.3.1 Introduction	102
		5.3.2 Mass balance	102
		5.3.3 Longshore transport	104
		5.3.4 Provenance	105
		5.3.5 Preservation Potential	105
	5.4	Results	107
	5.5	Discussion	110
		5.5.1 Long-term trends	110
		5.5.2 Transience versus persistence	111
	- 0	5.5.3 Local versus basin-wide measurements	112
	5.6	Conclusions	112
6		ainable coastal zone management: a concept for	115
		asting long-term and large-scale coastal evolution	
	6.1	Introduction	115
	6.2	Scientific disciplines and their view on the coastal system	117
		6.2.1 Stratigraphic community	117
		6.2.2 Geo)morphological community	117
		6.2.3 Coastal engineering community	118
	6.3	Scientific disciplines and the primary scale relationship	119
	6.4	Sediment dynamics and long-term coastal evolution	121
		6.4.1 Sediment fluxes	121
		6.4.2 Sediment budgets	123
		6.4.3 Modelling of sediment supply	123
	6.5	Discussion	125
		6.5.1 Sediment dynamics	125
		6.5.2 Natural versus Social Systems	125
		6.5.3 Linking human impact to natural coastal dynamics	127
		6.5.4 Morphodynamic forecasts	127
		6.5.5 Uncertainties	128
	6.6	Conclusions	128
		References	129
		Samenvatting	145
		Acknowledgements	149
		Curriculum Vitae	151
		List of proceedings and publications	153
		mor or proceedings and publications	TOO

Chapter 1

Introduction

1.1 GENERAL INTRODUCTION

Understanding responses of sedimentary systems to rapid sea level rise is of fundamental interest to sedimentary geology and crucial to forecasting the effects of near-future climate change on coastal regions. About 90% of the sediment generated by erosion on land is deposited on continental shelves, where it is (temporarily) stored in major deltas, as shelf deposits, and on the continental slope.

The natural unit in the "source-to-sink" view of earth-surface dynamics is the sediment dispersal system, which comprises an erosional basin in which sediments are generated (the source) and a sedimentary basin in which they are deposited (the sink). Source-to-sink analysis of sediment dispersal systems attempts to make optimal use of geo(morpho)logical information through integration of observations and models of earth-surface dynamics and the stratigraphic record. Knowledge of rates of mass transfer from source to basin on geological timescales forms an essential link between stratigraphic and geomorphologic modelling (e.g. Leeder, 1997; Weltje et al., 1998; Paola and Swenson, 1998; Yoo et al., 2007). The archives of terrigenous sediments on continental margins are the most logical candidates for investigation of source-to-sink dynamics through time (Sommerfield, 2006).

The recent trend in the earth-science community to consider earth-surface evolution within a holistic ("source-to-sink") framework has been motivated by the prospect of providing new insights into the responses of our planet to (anthropogenic) environmental perturbations. This development is exemplified by the Community Surface Dynamics Modeling System (CSDMS; http://csdms.colorado.edu), which is aimed at developing, supporting and disseminating integrated software modules that predict the erosion, transport, and deposition of sediment and solutes in landscapes and sedimentary basins. The aim to systematically address problems of earth-surface dynamics raises pertinent questions about the extent to which geological data sets are capable of providing benchmarks for such integrated models. These questions are centered on one of the most fundamental problems in the earth sciences: geological observations on different temporal and spatial scales indicate that inferences from core data cannot be readily upscaled to obtain quantitative

reconstructions of the entire basin fill. The first logical step in a source-to-sink analysis would be to quantify sediment fluxes through the system.

However, direct comparisons of sediment fluxes in source and sink are almost non-existent, and conservation of mass, a basic principle of physics, plays a subordinate role in quantitative models of earth-surface evolution and analysis of sediment dispersal systems. Implementing mass conservation constraints on the stratigraphic record is extremely difficult, which is attributable to its incompleteness and transient nature (Sadler, 1981; Sommerfield, 2006; Jerolmack and Sadler, 2007).

The upscaling problem and the difficulty of implementing mass-balance constraints on sediment dispersal systems explain why data-model comparisons spanning geological timescales and covering the spatial scale of an entire basin are virtually non-existent.

1.2 WHY STUDY THE ADRIATIC BASIN?

Sediment dispersal systems that are the most likely candidates for successful mass-balanced source to sink analyses are the so-called "closed" basins, i.e. those in which no sediments have bypassed the site of deposition (over the time interval of interest). In basins which behave as closed systems on geological time scales, the quantity of sediment supplied by the source equals the quantity of sediment deposited in the sink, because mass is conserved. But even in "closed" basins, a direct translation of mass-accumulation rates into rates of sediment supply calculations is only valid if the quantity of sediment subjected to intrabasinal erosion and recycling is insignificant relative to the amount of sediment supplied to the basin (Einsele and Hinderer, 1998). Another pertinent requirement for mass-balanced studies is the accurate and precise age estimation of (presumably) isochronous key surfaces of basin-wide extent (Lowe et al., 2007). In addition, the fact that most fine-grained sediment dispersal systems have been fed by multiple sediment sources (river systems) implies that the stratigraphic record inevitably will be composed of a complex mixture of sediments. Mass-balanced studies of fine-grained sediment dispersal systems can only yield successful results when the stratigraphic analysis allows for decomposition of the total sediment budget into contributions from individual source areas.

In summary, the ideal study area for mass-balanced stratigraphic analysis would be a closed sedimentary system that has already been studied in great detail and is easily accessible for (additional) sampling. Over the past fifteen years several large-scale research programmes have been commissioned by North-American and European funding agencies to enhance the scientific understanding of fluvial versus glacial dominated margin strata formation and to assess regional variability. The STRATAFORM programme was initiated in 1994 by the US Office of Naval Research to develop a comprehensive strategy to analyse and model the formation of continental margin stratigraphy

(Nittrouer and Kravitz, 1996). After the success of STRATAFORM, six major research programmes were launched, funded by various US and EC institutions, in which some fifty research groups operate. The North American programmes are NA-EuroSTRATAFORM and PASTA (ONR), MARGINS and its satellite CSDMS (NSF); the EU-funded programmes are PROMESS, EC-EuroSTRATAFORM and EURODELTA.

The closed basin of the northern Adriatic Sea, Italy, was selected as one of the target areas in the above programmes, with the aim to study the formation of fine-grained shelf stratigraphy and relate present-day sedimentary processes to the stratigraphic record.

In addition to the data collected in the above programmes, the CNR Institute of Marine Sciences (ISMAR), in Bologna, Italy, has been mapping large parts of the Adriatic Sea, in order to set up a basin-wide stratigraphic framework. The transgressive and high-stand deposits at the Northern Adriatic shelf have been mapped in great detail based on high-resolution 2-D seismic data (>40.000 km of CHIRP-sonar and 3.5 kHz sub-bottom profiles), supplemented by analyses of a large number of sediment cores (Trincardi et al., 1994; Cattaneo and Trincardi, 1999; Correggiari et al., 2001; Cattaneo et al., 2003). The wealth of information generated by these programmes and the high quality of their output provides a unique opportunity for successful mass-balanced source-to-sink analysis.

1.3 OBJECTIVES OF THE THESIS

Quantitative source-to-sink analyses of sediment dispersal systems covering a geological time interval are rare, for a variety of reasons discussed above. The overarching objective of this thesis is to present a mass-balanced stratigraphic analysis of a closed basin. This challenging task was broken down into the following series of sub-tasks:

- Reconstruct basin-wide sediment supply from the stratigraphic record;
- Develop and test a sediment-budget model for present-day multisourced basin fills;
- Simulate sediment supply based on the characteristics of the source and perform a data-model comparison using the concept of mass balance;
- Infer the relations between growth patterns, stratal architecture, and spatial variability of sediment properties within a sedimentdispersal system;
- Expand the above results into a conceptual model of coastal management on various temporal and spatial scales.

At the heart of this thesis lies the development of a generic methodology for addressing the above aims, and its application to a carefully selected study area, the Adriatic Sea, Italy. The relation between the aims that correspond to the chapters of this thesis, and their methodological aspects are summarized in the next section.

1.4 OUTLINE OF THE THESIS

In Chapter 2, time-averaged mass accumulation rates in the Northern Adriatic Sea (Italy) over the past 19 kyr and the associated uncertainties are presented. Sediment masses of five lithosomes and their uncertainties have been derived by means of stochastic simulation, since the nature of stratigraphic data does not permit the use of simple analytical rules of error propagation. Quantification of the uncertainties of the estimates is required to compare mass-accumulation rates across a series of time intervals, in order to decide whether basin-wide changes in time-averaged rates of sediment supply can be inferred from the stratigraphic record.

In Chapter 3, a straightforward approach to quantitative analysis and modelling of fine-grained sediment dispersal systems with multiple sources is demonstrated in order to obtain more insight into the growth pattern of mud belts on decadal to millennial time scales. Analysis of the physical and chemical properties of surface sediments, in conjunction with measurements of modern sediment accumulation rates allows us to calculate the rates of sediment supply from two distinct source areas in the Northern Adriatic basin. These rates were used to calibrate a numerical model of sediment delivery from fluvial drainage basins.

In Chapter 4, the most recent version of HydroTrend, a numerical model of water and sediment delivery from fluvial drainage basins to river mouths (Kettner and Syvitski, 2007; Syvitski and Milliman, 2007) is applied to simulate sediment supply to the Northern Adriatic based on palaeo-climate proxies derived from Global Circulation Models and drainage-basin physiography. The fact that the Adriatic basin is a closed system allows us to perform a data-model comparison based on the principle of mass balance, which serves as the first quantitative test of the BQART/HydroTrend model on geological time scales. Fundamental requirements for the comparison are: (1) Independent estimates of mass-transfer and accumulation rates covering the two domains of the sediment dispersal system, i.e. source and sink; (2) A statistically rigorous comparison of these rates, which implies that the uncertainties associated with all estimates must be quantified.

Chapter 5 synthesizes the results of the preceding three chapters to present a spatially distributed model of sediment transfer from source to sink in the northern Adriatic mud belt (highstand systems tract). Spatial patterns of sediment accumulation on three temporal scales within the Adriatic Basin serve as the starting point of this modeling exercise. The mass-balanced

analysis is complemented by high-resolution seismic cross-sections, which illustrate the late-Holocene stratal architecture of the mud belt. A sediment budget model is then applied to quantify the long-term average rates of longshore transport, the preservation potential of sediments, and the dispersal of sediments with different provenance. The results of this work shed light on the temporal scales at which transient stratigraphy ("active layer") gives way to persistent stratigraphy (which will be preserved under present-day forcing conditions).

In Chapter 6, it is illustrated how geological information derived from mass-balanced stratigraphic analysis helps to assess the long-term trend of the coastal system. The methods developed and used in this thesis come together in this concluding Chapter, which demonstrates the crucial importance of forecasting the effects of near-future climate-change scenarios on coastal regions.

Chapter 2

Reconstruction of sediment supply from mass accumulation rates in the Northern Adriatic Basin (Italy) over the past 19.000 years

2.1 INTRODUCTION

The recent trend in the earth-science community to consider earth-surface processes within a holistic ("source-to-sink") framework has been motivated by the prospect of providing new insights into the responses of our planet to (anthropogenic) environmental perturbations. This development is exemplified by the Community Surface Dynamics Modeling System (CSDMS; http://csdms.colorado.edu), which is aimed at developing, supporting and disseminating integrated software modules that predict the erosion, transport, and deposition of sediment and solutes in landscapes and sedimentary basins. The aim to systematically address problems of earth-surface dynamics raises pertinent questions about the extent to which geological data sets are capable of providing benchmarks for such integrated models. In this contribution, we will focus on a topic that has received comparatively little attention in the earth-science community: the derivation of long-term sediment budgets from the stratigraphic record. The importance of such studies is that they potentially allow earth scientists to incorporate a fundamental law of physics in datamodel comparisons, i.e. conservation of mass.

The natural unit in the "source-to-sink" view of earth-surface dynamics is the sediment dispersal system, which comprises an erosional basin in which sediments are generated (the source) and a sedimentary basin in which they are deposited (the sink). Knowledge of rates of mass transfer from source to basin on geological timescales forms an essential link between stratigraphic and geomorphologic modeling (Leeder, 1997; Weltje et al., 1998; Paola and Swenson, 1998). The frequency bands in which variations of sediment supply are widely believed to be concentrated range from 10^3 to 10^5 years (Hovius and Leeder, 1998). In the Quaternary, this time scale coincides with glacio-eustatic cycles, which profoundly affected drainage-basin evolution and governed basin-fill architecture through high-amplitude sea level changes. Since the Last Glacial Maximum (LGM, \approx 21 ka BP), fluvial sediment fluxes have varied significantly (Blum and Törnqvist, 2000; Walling, 2006), and deglaciation

following the LGM has led to an acceleration of erosion in glaciated catchment areas (Hallet et al., 1996; Molnar and England, 1990).

Reconstructing sediment supply from the stratigraphic record is not a straightforward task, which explains the limited knowledge on rates of sediment supply to basins on geological time scales (Hovius and Leeder, 1998). One of the fundamental problems in reconstructing sediment supply is the incompleteness of the stratigraphic record (Sadler, 1981; Sommerfield, 2006; Jerolmack and Sadler, 2007), which reflects the limited preservation potential of continental-margin deposits. Therefore, sediment dispersal systems that are the most likely candidates for successful reconstructions of palaeo-sediment fluxes are the so-called "closed" basins, i.e. those in which no sediments have bypassed the site of deposition (over the time interval of interest). However, even in "closed" basins, direct calculation of long-term mass accumulation rates from the stratigraphic record is only valid if the quantity of sediment subjected to intrabasinal erosion and recycling is insignificant relative to the amount of sediment supplied to the basin (Einsele and Hinderer, 1998). Another requirement for such studies is the accurate and precise age estimation of (presumably) isochronous key surfaces of basin-wide extent (Lowe et al., 2007). If all of these conditions are fulfilled, calculation of basin-wide sediment accumulation rates on geological time scales would constitute the first step towards the development of generic methods to reconstruct sediment supply from the stratigraphic record.

In this Chapter, we present time-averaged mass accumulation rates and their associated uncertainties within a well-documented closed basin, the Northern Adriatic Sea (Italy) spanning the time interval from 19 ka BP to the present. Quantification of the uncertainties of our estimates is required to compare mass-accumulation rates across a series of time intervals, in order to decide whether basin-wide changes in time-averaged rates of sediment supply can be inferred from the stratigraphic record. We derive the sediment masses of five lithosomes and their associated uncertainties by means of stochastic simulation, since the nature of stratigraphic data does not permit the use of simple analytical rules of error propagation. Our approach is based on standard procedures employed in the oil and gas industry to analyze the hydrocarbon content of reservoirs (commonly referred to as "Stock Tank Oil Initially In Place" (STOIIP) or "Gas Initially In Place" (GIIP)). Basic requirements to accurately derive the value of the STOIIP/GIIP are, amongst others, estimation of the bulk volume of the rock containing oil or gas, as well as the porosity of the rock, which determines the total pore volume available for storage of hydrocarbons (White and Gehman, 1979; Agarwal et al., 1999 and references therein). Our aim is to estimate the complement of pore volume: the sediment volume, which can be converted to mass for the purpose of obtaining basin-wide accumulation rates.

The stochastic simulation used to derive the time-averaged mass accumulation rates and their uncertainties are described in the first part of this Chapter. The

second part of the Chapter consists of the interpretation and discussion of the results.

2.2 STUDY AREA

2.2.1 The Adriatic Basin

The Northern Adriatic shelf (Fig. 2.1 is shallow and has a low gradient of approximately 0.05° (Trincardi et al., 1994). Sediment input is restricted to the Northern and Western side of the basin (Cattaneo et al., 2003). The Mid-Adriatic Deep (MAD), a depression in the centre of the Adriatic, acted as a sediment trap since the Last Glacial Maximum (LGM), which allows us to regard the Adriatic Basin as a closed sedimentary system (Cattaneo et al., 2003; Ridente and Trincardi, 2005). After the LGM, sea level rose and the areal extent of the basin increased, which caused a counter-clockwise longshore current to become active at around 14 ka BP (Cattaneo and Trincardi, 1999). From that time on, fine-grained sediment dispersed to the Adriatic Sea by Alpine and Apennine Rivers was conveyed to the Southwest to form an elongate shore-parallel prodelta, which extends to the area south of the Gargano peninsula.

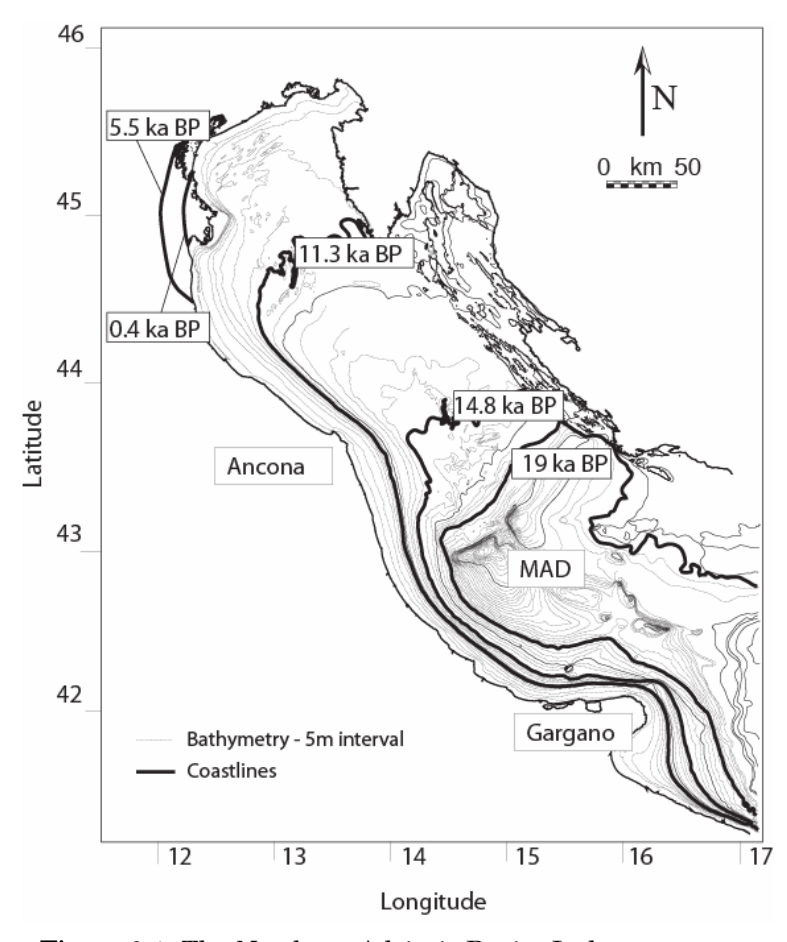


Figure 2.1: The Northern Adriatic Basin, Italy

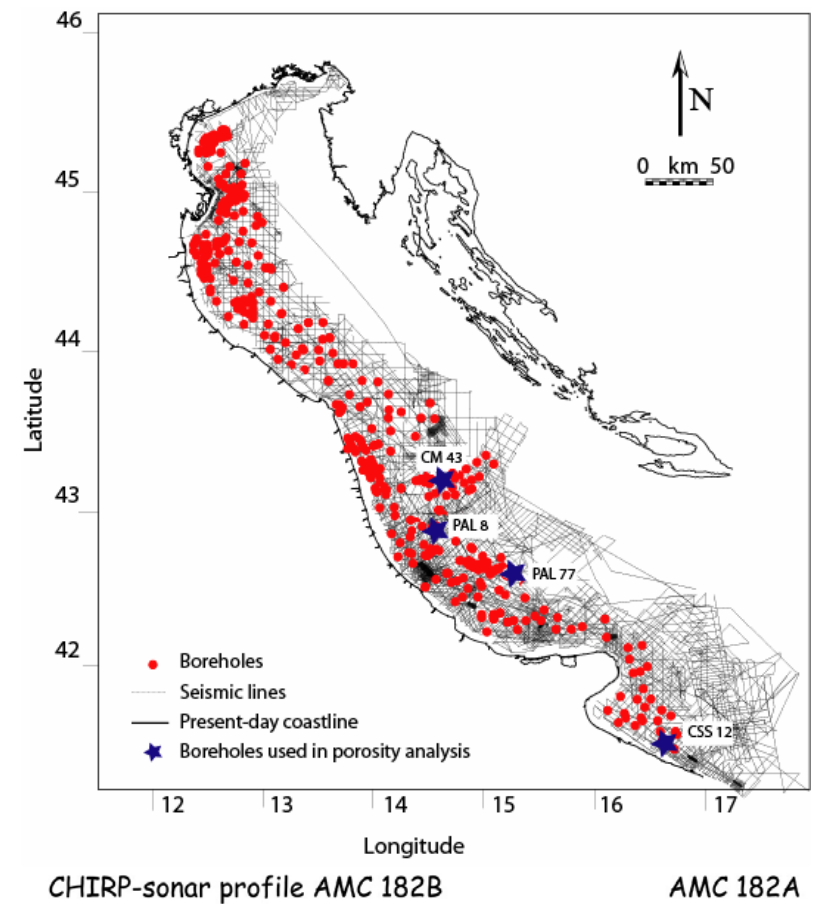
2.2.2 Northern Adriatic shelf

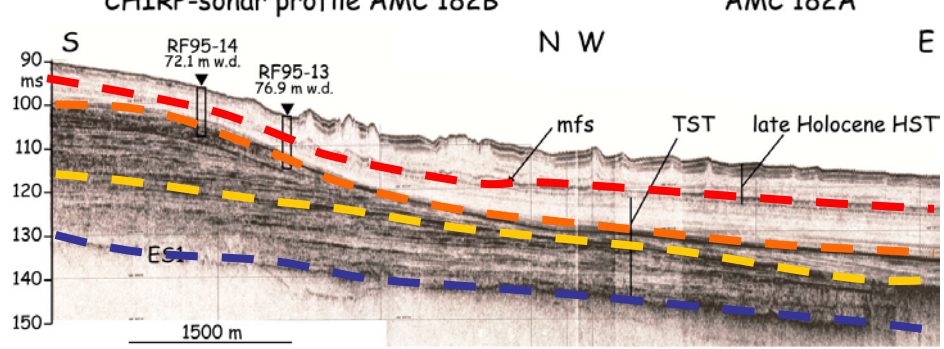
The transgressive and highstand deposits at the Northern Adriatic shelf have been mapped in great detail, based on high-resolution 2-D seismic data (>40.000 km of CHIRP-sonar and 3.5 kHz sub-bottom profiles), supplemented by analyses of a large number of sediment cores (Trincardi et al., 1994; Cattaneo and Trincardi, 1999; Correggiari et al., 2001; Cattaneo et al., 2003). Figure 2.2 provides an overview of the seismic lines and borehole data and presents a selected example of the seismic-stratigraphic record of the Adriatic Basin. Additional data can be retrieved from a public data base stored online at www.pangea.de containing geoscientific and environmental metadata acquired during several EU-funded projects (EuroStrataform and Eurodelta).

Four basin-wide stratigraphic surfaces have been recognized, whose ages were established by 14C dating (Trincardi et al., 1994; Correggiari et al., 2001; Cattaneo et al., 2003; Asioli et al., 2001). Correggiari et al. (2001) subdivided the Highstand Systems Tract (HST) into an upper unit (HST-2; 0.4-0 ka BP) and a lower unit (HST-1: 5.5 - 0.4 ka BP). These two units are bounded by conformable surfaces, the lowermost of which represents the maximum flooding surface (MFS). The three lithosomes comprising the Transgressive Systems Tract (TST), which contain the record of abrupt deglacial sea level rise, are the upper unit (TST-3; 11.3-5.5 ka BP), the middle unit (TST-2; 14.8-11.3 ka BP), and the lower unit (TST-1; 19.0-14.8 ka BP) (Cattaneo and Trincardi, 1999). These units are separated by unconformable ravinement surfaces (S1 and S2 (Fig. 2.2)), with the exception of the TST-1 unit, which is bounded locally by the maximum regressive surface (MRS) in places where this surface has not been cut by the lowermost ravinement surface (TS) (Fig. 2.2) (Trincardi et al., 1994). Two-way travel time maps have been constructed for each of these five seismic-stratigraphic lithosomes (Fig. 2.3A and 2.3B).

2.2.3 Po Delta

The transgressive record of the Po Plain was compiled from published stratigraphic data (Fig. 2.4; Amorosi et al., 1999; 2003; 2005; Amorosi and Milli, 2001; Farabegoli et al., 2004; Stefani and Vincenzi, 2005). The transgressive wedge in the Po plain has a maximum thickness of 15 meters, and is attributed to the uppermost TST unit (TST-3). The coastline at the time of maximum flooding (5.5 ka BP) was located 50 km inland of the present coastline (Fig. 2.1; Correggiari et al., 2001). The MFS is located at a depth of 29 m below the surface of the modern Po Delta (Correggiari et al., 2005; Stefani and Vincenzi, 2005), which is consistent with long-term subsidence rates of the Po plain (Carminati and Martinelli, 2002). The highstand deposits are on average 12-15 meters thick. The onshore part of the HST was subdivided into a lower and upper unit, in accordance with the offshore deposits.





MFSS2S1TS

Figure 2.2: Example of the Adriatic seismic stratigraphic record (Chirp Sonar profile AMC 182; modified from Cattaneo and Trincardi, 1999). The maximum flooding surface (MFS) separates the highstand systems tract (HST) from the underlying transgressive systems tract (TST). The TST has been subdivided into three units (TST-1, TST-2, and TST-3) by two unconformable surfaces (S1 and S2). The lower boundary of the TST is formed by the maximum regressive surface (MRS), which at most localities has been cross-cut by a transgressive surface (TS).

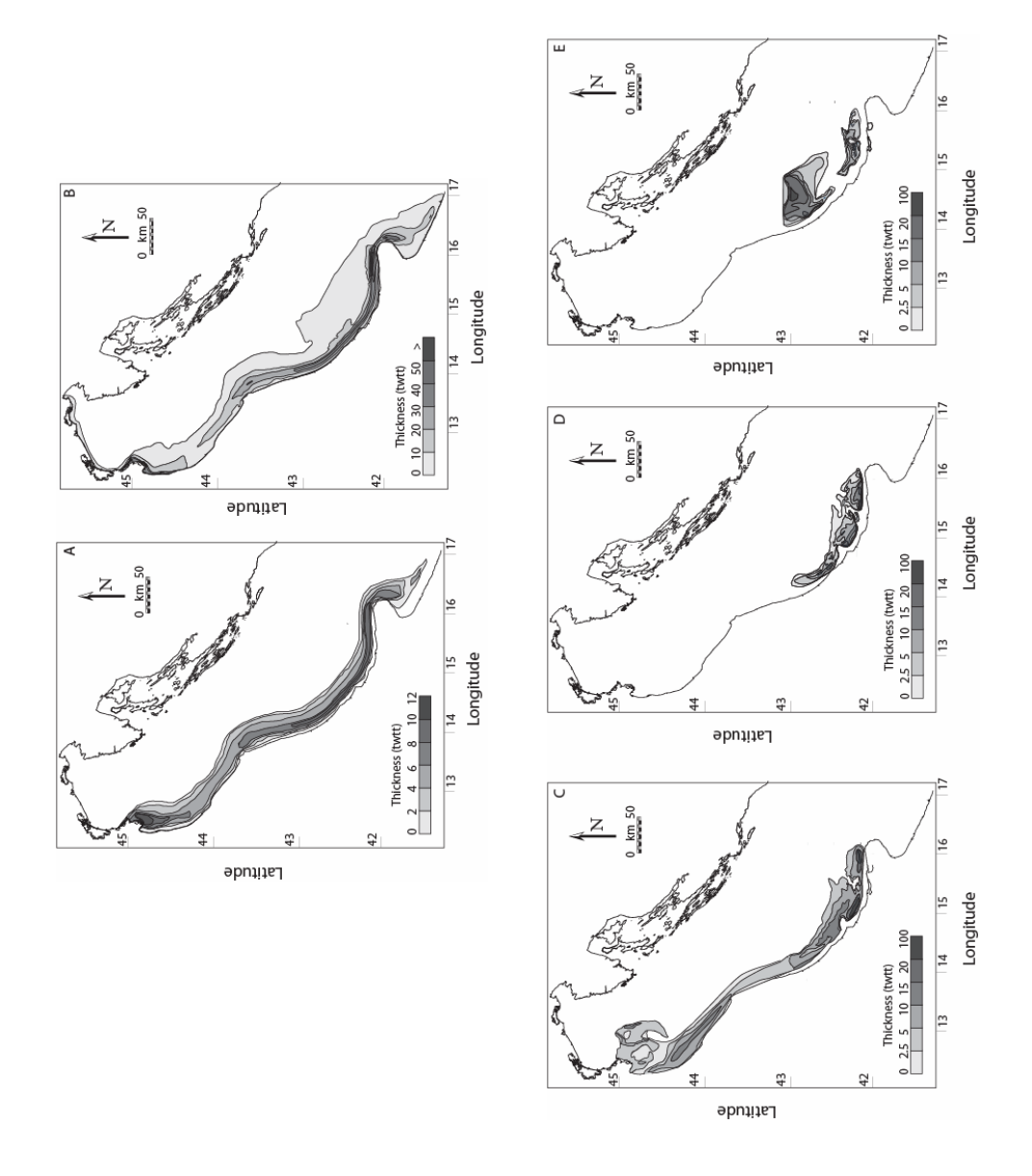


Figure 2.3: Two way travel time maps of two HST and three TST lithosomes at the Adriatic shelf: (A) Upper unit (HST-2); (B) Lower unit (HST-1); (C) Upper unit (TST-3); (D) Middle unit (TST-2) and Lower unit (TST-1).

2.2.4 Mid-Adriatic Deep

The thicknesses of the TST and HST units within the MAD were derived from published data on sediment accumulation rates from several sediment cores (Fig. 2.4; Trincardi et al., 1996; Asioli, 1996; Langone et al., 1996; Alvisi and Frignani, 1996). These data were interpolated in order to construct surfaces for the TST-2 and TST-3 units. The TST-3 and HST-1 units in the MAD have been mapped from seismic profiles.

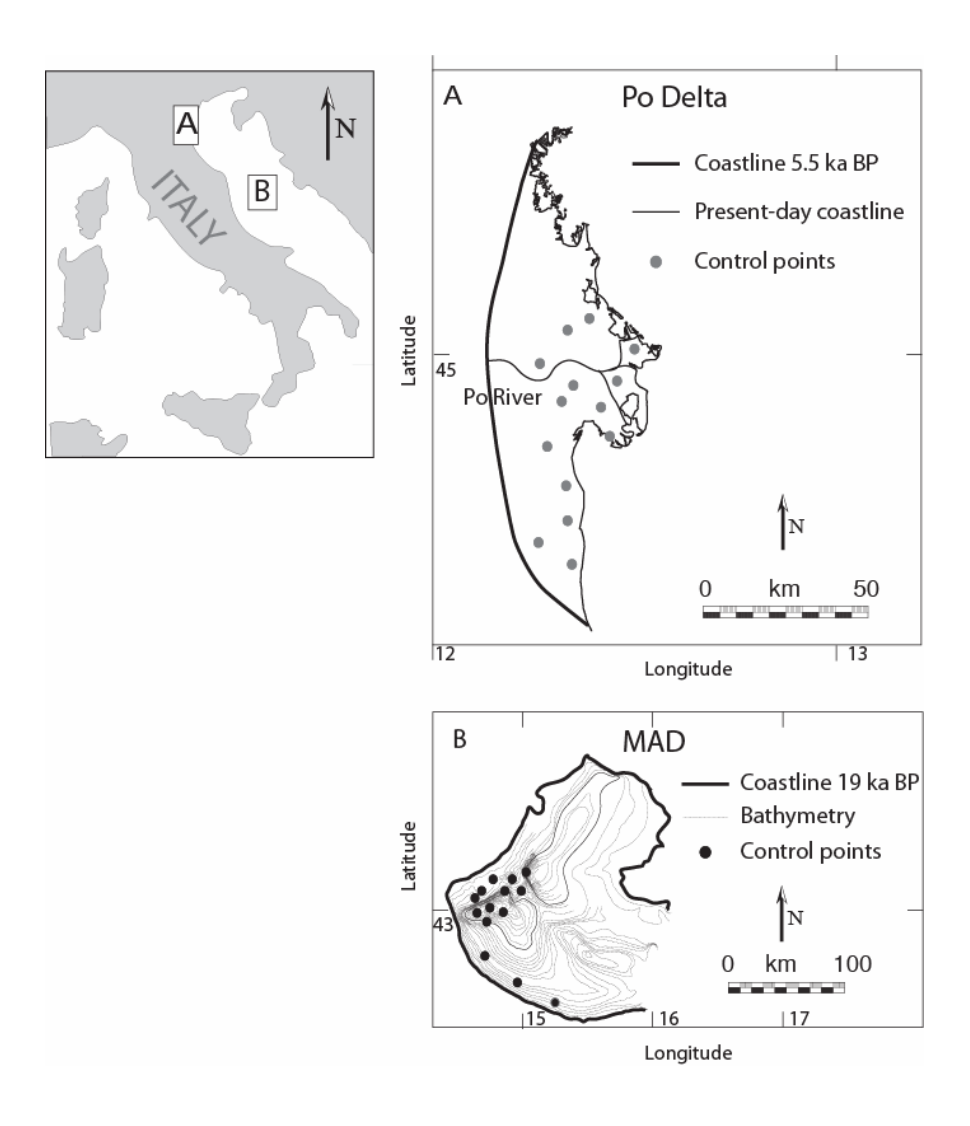


Figure 2.4: Detailed overview of the Po Delta (A) and the Mid-Adriatic Deep (MAD) (B) with control points used to derive isopach maps.

2.3 Stochastic analysis of the stratigraphic record

2.3.1 Geostatistical modelling

The analysis started with digitization of the contour lines of the five hand-drawn two-way travel time maps of the Adriatic shelf lithosomes (Fig. 2.3A and 2.3B). The result of this operation was a series of (x,y,t) vectors wherein x and y are the spatial coordinates (latitude, longitude) and t represents two-way travel time [ms] of the seismic signal. Equally spaced grids with 3 by 3 km grid cells were produced by geostatistical interpolation (ordinary kriging) of irregularly spaced control points. Geostatistical interpolation was preceded by the following transformation of t:

$$\widetilde{t} = \log(t + \varepsilon) \tag{2.1}$$

where ε is a small positive constant ($\varepsilon = 10^{-6}$ [ms]). The interpolated \tilde{t} values were subjected to an inverse transform that prevents the occurrence of negative travel times:

$$t = \begin{cases} \exp(\widetilde{t}) - \varepsilon & \text{if } \exp(\widetilde{t}) > \varepsilon \\ 0 & \text{if } \exp(\widetilde{t}) \le \varepsilon \end{cases}$$
 (2.2)

The semi-variogram required for geostatistical interpolation cannot be estimated from the discrete \widetilde{t} values corresponding to the contour lines of the digitized data. To avoid the bias related to input points being aligned along contour lines (Favalli and Pareschi, 2004), we constructed hypothetical measurements by connecting each data point with its nearest neighbour on an adjacent contour line. The \widetilde{t} value corresponding to a randomly chosen point (x,y) on each constructed line was estimated by means of linear interpolation of the two bounding \widetilde{t} values. We fitted spherical semi-variogram models to these hypothetical data points for each lithosome separately. Figure 2.5 illustrates the semi-variogram model of the HST-1 unit. It captures the difference in lateral continuity parallel (NW-SE: 1450) and perpendicular (NE-SW: 0450) to the shoreline by means of an anisotropy ratio of 2.0 for the range.

The two-way travel time maps of the five lithosomes are based on a large number of seismic lines and sediment cores. However, the fact that we do not know how many measurements were used to construct these maps, nor the exact locations of the control points, introduces a sampling error. We assessed the magnitude of this uncertainty associated with the finite number of control points by random sampling of control points from each lithosome. We constructed 100 subsets of 100, 300, 600 and 1000 control points each, and used these to examine the relation between the number of control points and the variance of the estimated sediment mass (full mass calculation given below). Figure 2.6 illustrates the result of this exercise for the HST-1 lithosome. The uncertainty of the estimated sediment mass is clearly influenced by sampling

error if the number of randomly selected control points is less than 600. Beyond 600 control points, however, the standard deviations of sediment-mass estimates become constant. Based on these and similar experiments with the other lithosomes, the number of control points was set to 1000.

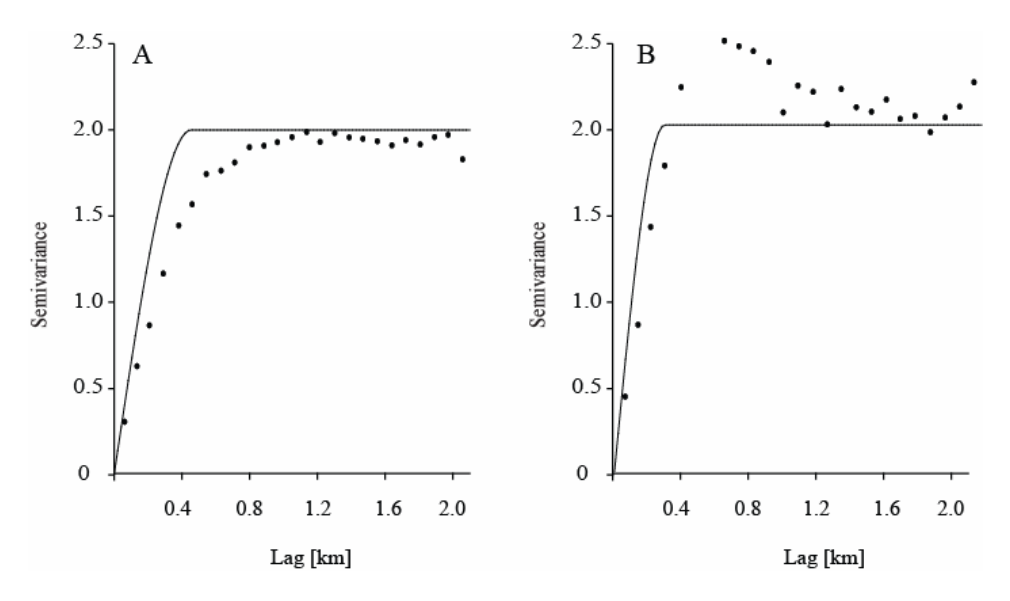


Figure 2.5: Anisotropic semi-variogram model illustrated for HST-1 lithosome. (A) shore parallel and (B) shore-normal.

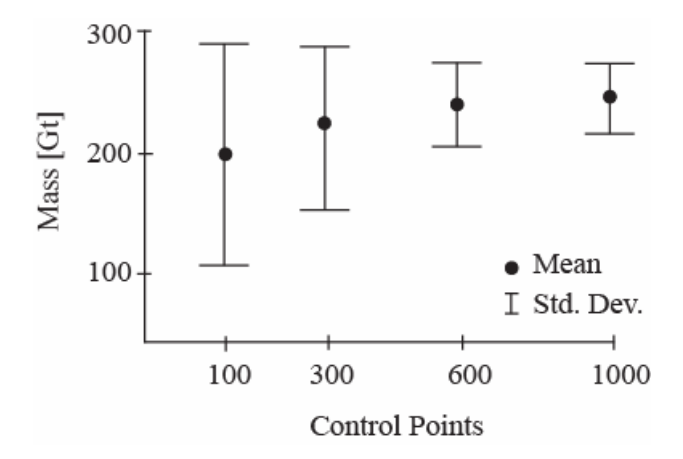


Figure 2.6: Mean and standard deviations of sediment mass (each estimate based on 10000 realizations) for different-sized subsets, illustrated for HST-1 lithosome.

2.3.2 Time-depth conversion

A velocity-depth model is required for time-depth conversion of reflectors. We assumed that velocity does not differ significantly with depth, in view of the shallow nature of the deposits and their limited thickness. The velocity of a (seismic) wave through seawater (1500 m s $^{-1}$) is often taken to be applicable to shallow-marine deposits as well (Trincardi et al., 1994; Bertrand and MacBeth, 2003). However, some authors propose a velocity of 1550 to 1600 m s $^{-1}$ (Park et al., 2000; Missiaen, pers. comm., 2006). In our stochastic simulation, we used a normally distributed velocity of 1550 \pm 15 m s $^{-1}$ (mean \pm standard deviation), to ensure that the velocity falls between 1500 and 1600 m s $^{-1}$ (Table 2.1). Time-thickness conversion of seismo-stratigraphic units was performed as follows:

$$d_{i} = z_{T} - z_{R} = V_{s}(t_{R} - t_{T})$$
(2.3)

where d_i is the estimated lithosome thickness of the \dot{r} th gridcell [m], z is depth below the surface [m], V_s is seismic velocity [m ms⁻¹] and t is two-way travel time [ms]. Subscripts T and B refer to the top and bottom of the lithosome.

2.3.3 Sediment mass calculation

Conversion of sediment volume to mass requires a careful estimate of the porosity profile of each lithosome. Core data and surface samples (Asioli et al., 1996; Langone et al., 1996; Trincardi et al., 1996; Asioli et al., 2001; Frignani et al., 2005) indicate an average near-surface porosity of 0.65 to 0.80 and a consistent downcore decrease to about 0.35. Investigation of marine sediments with burial depths up to 1 km, mostly in drill cores from the Deep Sea Drilling Project (DSDP) and Ocean Drilling Program (ODP), show that different porosity-depth relationships (exponential, linear) may apply for different types of sediments in specific geological settings (e.g. Bayer and Wetzel, 1989; Bruckmann, 1989; Huang and Gradstein, 1990). Bartetzko and Kopf (2007) investigated the upper 50 m of 168 ODP sites in order to derive porosity-depth relationships, and found that for a small number of sites an exponential equation gives a higher correlation coefficient than a linear porosity-depth equation. For the majority of the sites, the difference in correlation for linear and exponential porosity-depth relationships is relatively small.

An exponential relationship implies that the largest change in porosity takes place in the uppermost meters of the sediment column (i.e. shallow burial depth), which is often the case in shallow marine environments as opposed to deeper waters (Bartetzko and Kopf, 2007). The reason for this abrupt change in the uppermost meters of the sediment column is the presence of an active sediment-water interface. Beyond 5m burial depth, a more or less linear porosity-depth relationship is found which gradually becomes constant at depths > 30-50m. At even greater burial depths of several kms, this linear behaviour gives way to an exponential function, reflecting the asymptotic approach of porosity values to a lithology-specific minimum.

The exponential porosity-depth equation proposed by Athy (1930) forms the conceptual basis of most algorithms used today. Examples of the use of Athy's porosity-depth equation in various geological settings are discussed in detail by Giles (1996), whereas Bahr et al. (2001) provided a physical interpretation of its parameters. Athy's exponential porosity-depth equation is based on measurements at >500m burial depth, which is beyond the depth range of (sub)recent sedimentary environments (0-500m). However, the similarity between very shallow (several meters) and very deep (several kilometers) porosity profiles suggests that Athy's porosity-depth equation may also be used to capture the decreasing rate of porosity reduction with depth in the shallow muddy sediments of the Northern Adriatic.

In this study we used a modified form of Athy's equation to ensure that porosity ϕ [-] at "infinite" depth reaches the fixed minimum value ϕ_b of 0.35 (cf. Boudreau and Bennett, 1999).

Our parameterized exponential porosity equation is:

$$\phi = \phi_0 e^{-cz} + \phi_b \tag{2.4}$$

where z is depth below the surface [m], $\phi_0 + \phi_b$ is the porosity [-] at the surface (z=0), c is a constant [m⁻¹], and ϕ_b is the porosity [-] at infinite depth. The parameter values and their standard deviations used in our calculations are based on four sediment cores, CM 43, CSS 12, PAL 8, and PAL 77, whose locations are given in Fig. 2.2. The resulting mean values (μ) and standard deviations (σ) of the parameters are listed in Table 2.1. Figure 2.7 shows porosity profiles of the four cores, together with the envelope of simulated porosity profiles based on the parameter settings of Table 2.1.

Table 2.1: Parameters of shelf, MAD, and Po Delta deposits used in stochastic time-depth conversion.

	Shelf & MAD		De	lta
Parameter	μ	σ	μ	σ
ϕ_0 [-]	0.35	0.03	0.25	0.02
c [-]	0.22	0.03	0.22	0.03
ϕ_b [-]	0.35	-	0.25	-
$V_s [\mathrm{m} \; \mathrm{s}^{ ext{-}1}]$	1550	15	-	-

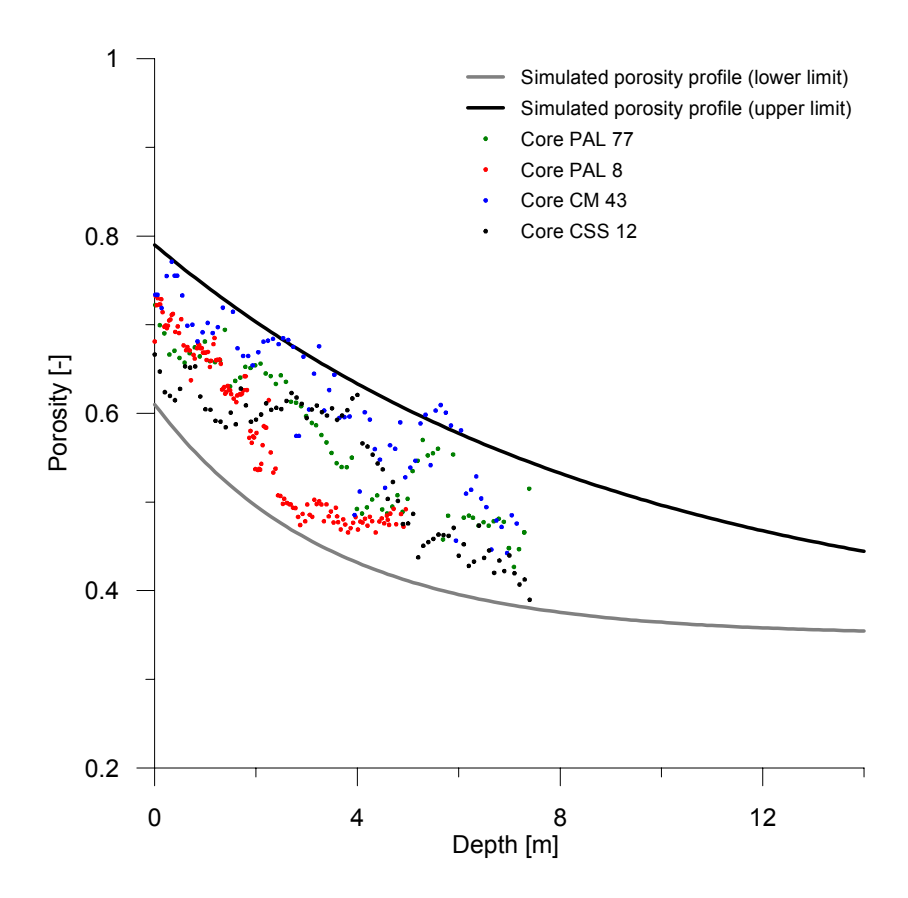


Figure 2.7: Parameterization of the porosity-depth relation in Adriatic shelf sediments. The envelope of porosity-depth profiles covers mean parameter values \pm three standard deviations.

The conversion from bulk volume (thickness \times area) to net sediment mass was carried out as follows. The mean porosity $\overline{\phi}_i$ [-] of a sediment column with thickness d_i [m] is given by:

$$\overline{\phi}_{i} = \frac{1}{d_{i}} \int_{z_{T}}^{z_{B}} (\phi_{0} e^{-cz} + \phi_{b}) dz$$
(2.5)

The geostatistical estimate of sediment mass \tilde{M} [Gt] of a lithosome is the sum of the sediment masses of the grid cells with $d_i > 0$, which for N cells is given by:

$$\tilde{M} = \rho A \sum_{i=1}^{N} (1 - \overline{\phi_i}) d_i \tag{2.6}$$

where sediment density (ρ) is assumed to be 2.65 Gt km⁻³, and the area of one grid cell, $A = 9 \text{ km}^2$.

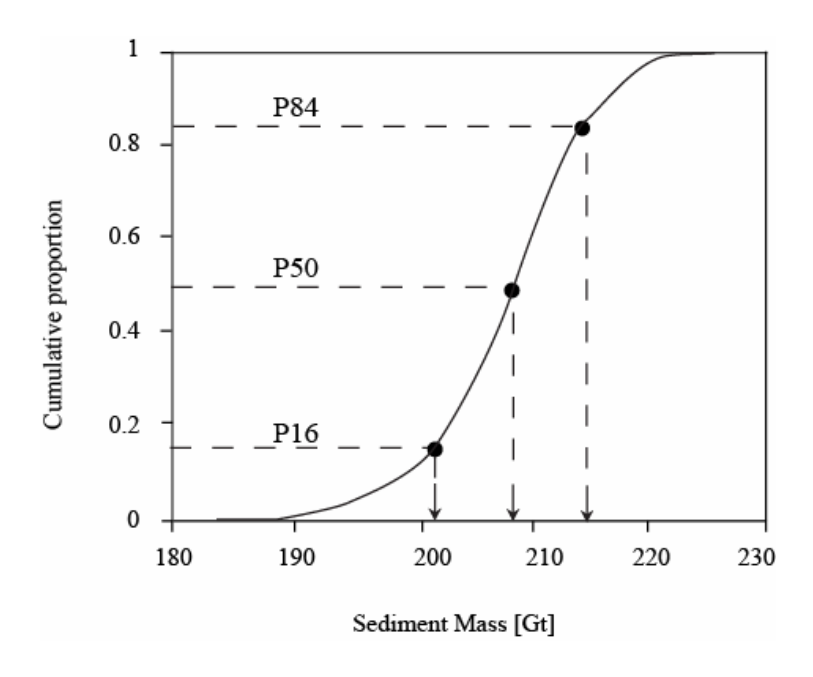


Figure 2.8: Derivation of μ and σ from cumulative distribution function of sediment mass illustrated for HST-1 lithosome.

2.3.4 Uncertainty estimation of sediment mass

The sediment-mass estimation procedure outlined above was carried out 10.000 times for each shelf lithosome. Each geostatistical estimate of shelf mass (\tilde{M}) was based on a set of 1000 randomly selected control points, in conjunction with a stochastic realization of the three parameter set (V_s, c, ϕ_0) . For each lithosome, the results of the stochastic simulations were summarized as follows. The representative value of the shelf sediment mass is the median (50th percentile) of 10.000 realizations (Fig. 2.8):

$$\mu_{shelf} = \tilde{M}_{50} \tag{2.7}$$

The absolute uncertainty (or standard deviation, i.e. the 68 % confidence interval) is derived from the difference between the 16th and the 84th percentile of the shelf mass distribution:

$$\sigma_{shelf} = \frac{(\tilde{M}_{84} - \tilde{M}_{16})}{2} \tag{2.8}$$

The fractional uncertainties derived from stochastic simulation of sediment masses on the shelf are in the range of $\approx 10\%$.

2.3.5 Deposits in the Po Delta and MAD

Mass calculations of the onshore deposits and the deposits in the MAD followed largely the same method with a few adaptations. The volumes of sediment deposited in the onshore part of the Po delta (TST-3, HST-1, and HST-2) were estimated from stratigraphic profiles. The volumes of offshore deposits in the MAD (TST-2, TST-3, and HST-1) were estimated from accumulation rates measured in sediment cores. These thicknesses were interpolated to construct isopach maps in (x,y,z), where x,y are the spatial coordinates and z is the depth of the bounding surface. For the onshore deltaic deposits, we adopted a porosity of about 0.50 near the surface, declining with depth to about 0.25 due to compaction. The porosity profile of deposits in the MAD was assumed to be identical to that of the shelf deposits (Table 2.1).

The MAD deposits contribute ≈ 15 % to the total sediment mass of the TST-2 and TST-3 units, and only 2% to the total sediment mass of the HST-1 unit (Table 2.2). Data coverage in the MAD is poor; we therefore adopted a fractional uncertainty of 40% for the sediment-mass estimates of these units. It should be noted that this somewhat arbitrary choice is not critical to our results. If we alter the fractional uncertainties of the sediment masses in the MAD to for instance 30% or 50%, absolute uncertainties of the total sediment mass in the TST-2 and TST-3 lithosomes change by no more than a few percent, and the change in absolute uncertainty of the HST-1 mass is negligible.

Table 2.2: Sediment masses Ma (all estimates (μ) and standard deviations (o) in Gt). Symbol "-" indicates mass is negligible.

	De	lta	Sh	elf	MA	AD	Tot	tal
Lithosome	μ	σ	M	σ	μ	σ	μ	σ
HST-2	2	1	17	2	-	-	18	2
HST-1	14	7	222	26	4	1	236	28
TST-3	5	2	177	27	30	12	212	40
TST-2	-	-	98	8	19	8	116	16
TST-1	-	-	37	4	121	18	158	22

2.4 RESULTS

2.4.1 Spatial distribution of sediment thickness

The results of the stochastic analysis are presented in Figure 2.9A and 2.9B which show the integrated thickness maps of the five lithosomes in the Northern Adriatic Basin. Figure 2.9A presents the thickness maps [m] of the two HST lithosomes (HST-1 and HST-2). Figure 2.9B presents the thickness maps of the three TST lithosomes (TST-1, TST-2 and TST-3).

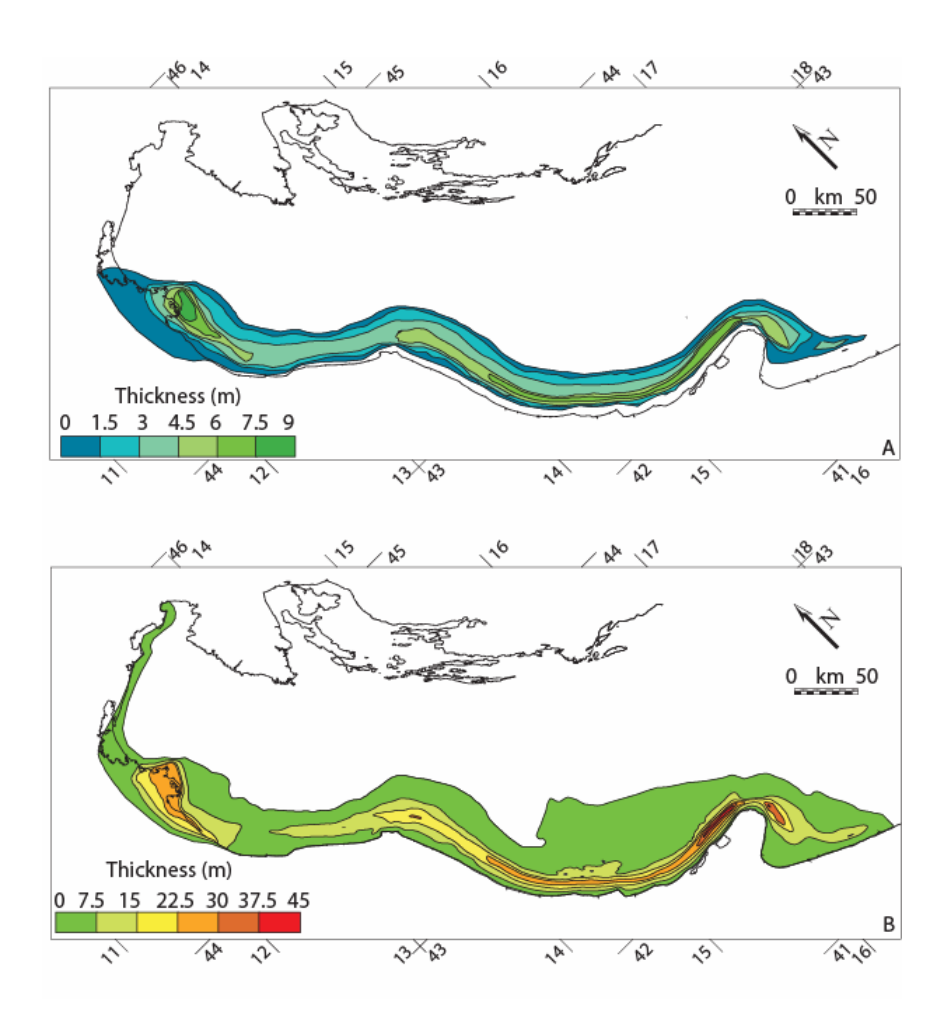


Figure 2.9A: Isopach maps [m] of the HST resulting from the stochastic analysis: (A) HST-2 and (B) HST-1.

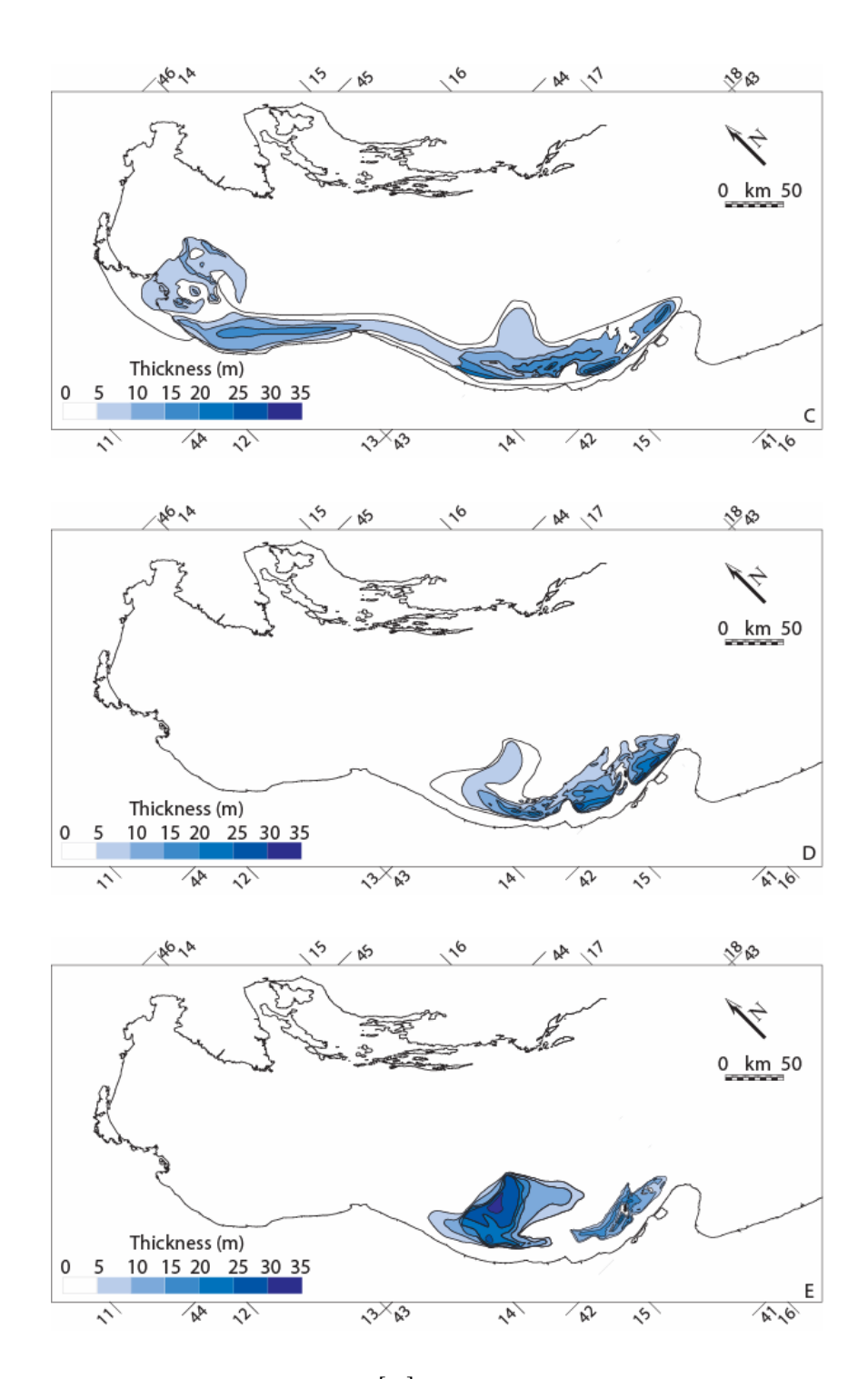


Figure 2.9B: Isopach maps [m] of the TST resulting from the stochastic analysis: (C) TST-3; (D) TST-2; and (E) TST-1.

2.4.2 Total sediment mass per lithosome

The sediment mass of an entire lithosome (M_a) and its uncertainty (δM_a) are obtained as follows (Taylor, 1982):

$$M_a = \mu_{delta} + \mu_{shelf} + \mu_{MAD} \tag{2.9}$$

$$\delta M_a = \sqrt{(\sigma_{delta})^2 + (\sigma_{shelf} + \sigma_{MAD})^2}$$
(2.10)

Note that the uncertainties associated with the sediment masses of the shelf and MAD deposits are not independent, because they are based on the same parameterization of seismic velocity and porosity. The uncertainties associated with the sediment masses of the onshore Po Delta deposits are assumed to be uncorrelated to $\sigma_{\textit{shelf}}$ and $\sigma_{\textit{MAD}}$. This leads to the specific form of Equation (2.10). Fractional uncertainties of the total sediment mass are in the range of 10% to 20% (Table 2.2).

2.4.3 Basin-wide mass accumulation rates

The ages of the bounding surfaces of the seismic-stratigraphic units were estimated from 14 C measurements. Based on the inferences of Lowe et al. (2007), we assigned a fractional uncertainty of 3% to the age estimates of the bounding surfaces of the Adriatic units, with the exception of the boundary between the HST-1 and HST-2 units, to which we assigned a fractional error of 10% (Table 2.3). These age assignments (a) and their absolute uncertainties (δa) were converted into estimates of the duration of the time slices corresponding to the five lithosomes (τ) with associated absolute uncertainties (τ) by means of root-sum-squares (RSS) approximation (Taylor, 1982) under the assumption of uncorrelated errors (Table 2.3).

Table 2.3: Estimated ages of bounding surfaces, α [kyr], duration of time slices τ [kyr], and net accumulation rates S_{α} [Gt kyr⁻¹].

Bounding surface	а	δα	Lithosome	τ	δτ	S_{α}	δS_a
HST-2/HST-1	0.4	0.04	HST-2	0.4	0.04	45	7
HST-1/TST-3 (MFS)	5.5	0.17	HST-1	5.1	0.17	46	6
TST-3/TST-2	11.3	0.34	TST-3	5.8	0.38	37	7
TST-2/TST-1	14.8	0.44	TST-2	3.5	0.56	33	7
TST-1/LST (MRS)	19.0	0.57	TST-1	4.2	0.72	38	8

We calculated the basin-wide mean mass accumulation rate (S_a) for each lithosome as follows:

$$S_a = M_a / \tau \tag{2.11}$$

Its fractional uncertainty may be obtained by RSS approximation, because uncertainties in mass and duration are uncorrelated:

$$\frac{\delta S_a}{S_a} = \sqrt{\left(\frac{\delta M_a}{M_a}\right)^2 + \left(\frac{\delta \tau}{\tau}\right)^2} \tag{2.12}$$

In the above equations, S_a is the estimated mass accumulation rate [Gt kyr⁻¹] of each lithosome and δS_a [Gt kyr⁻¹] is the associated absolute uncertainty. Relative uncertainties of basin-wide mass-accumulation rates are in the order of $\approx 20\%$ (Table 2.3).

2.5 INTERPRETATION AND DISCUSSION

2.5.1 Statistical test

An adaptation of the well-known Z-test (e.g. Taylor, 1982; Davis, 2002) was used to examine if net basin-wide mass-accumulation rates are likely to have varied between time slices. The test was modified to enable a pair-wise comparison of rates (see Appendix 1 for derivation of test statistic). Strictly speaking, the five mass accumulation rates constitute a time series, which means that they may be serially correlated. However, since we are only assessing the probability that the five estimates are equal, their time order, and consequently, the presence or absence of serial correlation, is irrelevant.

The null hypothesis (equality of two mass-accumulation rates) is considered acceptable if its probability exceeds a significance level α , which was set at 0.1 (this represents the risk of erroneously rejecting the null hypothesis). The results of applying the Z-test to the five mass-accumulation rates ($H_{\mathcal{O}}$: $S_a(i) = S_a(j)$, for $i \neq j$) are given in Table 2.4. The conclusion from this test is that the stratigraphic record does not show evidence of significant variations in basin-wide mass-accumulation rates between the five time slices, because the variation is indistinguishable from random error.

Calculation of long-term averages of S_a , representative of the entire HST and TST, involves the total sediment masses in the two systems tracts as well as their total durations, which reduces their fractional uncertainties (Table 2.5). The resulting estimates accentuate the difference between net accumulation rates of the TST and HST lithosomes. Application of the Z-test to these two long-term average rates gives a probability of 0.11 that the two are equal, which is slightly above the significance level. This result shows that equality of

the two mean rates is possible but not very likely. Similar Z-tests, in which accumulation rates of individual lithosomes from one systems tract were compared to the average accumulation rate of the other systems tract, failed to reveal significant differences. The grand mean rate of net basin-wide mass accumulation in the Northern Adriatic over the past 19 kyr is equal to 39 ± 3 Gt kyr⁻¹ (Table 2.5).

Table 2.4: Pairwise comparison of net accumulation rates S_a [Gt kyr⁻¹] in terms of probabilities under the null hypothesis (equality of estimates).

	HST-2	HST-1	TST-3	TST-2
HST-1	0.89			
TST-3	0.40	0.31		
TST-2	0.24	0.17	0.74	
TST-1	0.50	0.41	0.92	0.68

Table 2.5: Masses M_a [Gt] and accumulation rates S_a [Gt kyr⁻¹] of the HST, TST, and HST+TST lithosomes with their absolute uncertainties.

Lithosome	M_{α}	δM_{lpha}	$S_{\!lpha}$	δS_{α}
HST	254	28	46	5
TST	486	48	36	4
HST+TST	740	56	39	3

2.5.2 Relation to sediment supply

The result of our data analysis refers to the preserved part of the geological record of the Northern Adriatic basin, i.e. to the net basin-wide accumulation rates within a series of lithosomes. Basin-wide correlation of the surfaces that separate these lithosomes was made possible by the fact that most of them are (at least locally) marked by unconformities. This applies to the lower bounding surface of all three TST units (Trincardi et al., 1994). In the case of unconformity-bounded units, the relation between net basin-wide mass accumulation rates (MARs) extracted from the stratigraphic record and rates of sediment supply is obscured by intrabasinal erosion and redistribution of sediments, which are particularly common on geological time scales, because the boundary conditions of sediment dispersal systems change due to eustatic and climatic variations (Sadler, 1981; Sommerfield, 2006; Jerolmack and Sadler, 2007). Other surfaces, such as the MFS, which separates the upper TST from the lower HST unit, and the boundary between the lower and upper HST

units, are conformable. Recycling of sediment across conformable bounding surfaces is likely to be insignificant relative to the uncertainty of our estimates.

If a lithosome in a "closed" sedimentary basin is bounded by conformable (nonerosional) surfaces, the quantity of sediments preserved within that unit is expected to be equal (within the limits of uncertainty) to the quantity of sediment supplied during the time interval corresponding to that unit. This applies to unit u1 (Fig. 2.10A). In Figure 2.10B, unit u2 is bounded on top by an erosional surface, which indicates that some of the material originally deposited in unit u2 has been recycled into unit u3. Hence, if we would base our MAR calculations solely on unit u₃, we would overestimate the amount of sediment supplied during the time interval corresponding to that unit. Likewise, the MAR over the time interval corresponding to unit u2 would be underestimated. However, the two units u2 and u3 together will contain the correct quantity of sediments supplied in the combined time intervals corresponding to both units, which indicates that it should be possible to equate the average MAR over the combined duration of the two units to the average rate of sediment supply. Figure 2.10C illustrates the effects of two superimposed erosional surfaces. In this case, we have one unit that will be underestimated (u2), one that will be overestimated (u4), and one unit that may contain either more or less sediment than the quantity actually supplied in the corresponding time interval (u3), depending on the difference between the quantities recycled across the bounding surfaces. Again, a MAR that is representative of sediment supply may be calculated over the combined interval of the three units.

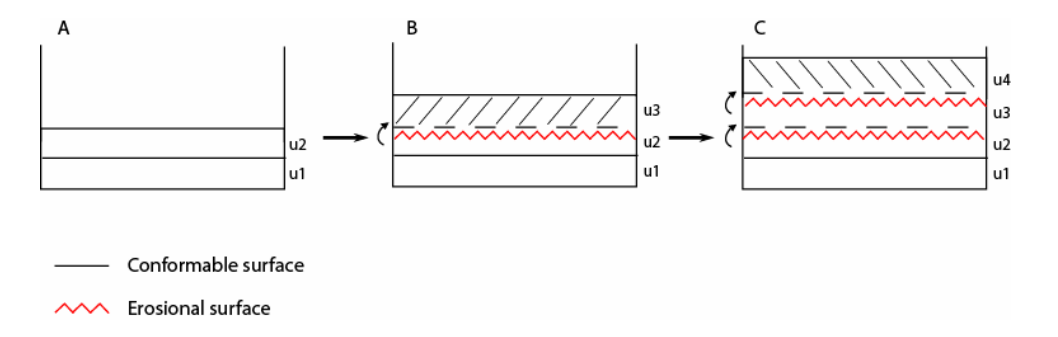


Figure 2.10: Effects of sediment recycling on mass preservation in the stratigraphic record.

Hence, from a (long-term) sequence-stratigraphic perspective, a mismatch between rates of sediment supply and mass accumulation is expected in the case of unconformity-bounded units. This implies that only our calculations pertaining to the two HST units (and the HST as a whole) can be directly interpreted in terms of basin-wide average rates of sediment supply, because

these units are bounded by conformities. The same applies to the long-term average MARs of the TST and the HST+TST reported in Table 2.5, because addition of sediment to the TST by reworking, indicated by the fact that the MRS locally coincides with a ravinement surface, is likely to be negligible relative to the uncertainty associated with our estimates.

2.5.3 Analysis of the HST-2 lithosome

The feasibility of inferring rates of sediment supply from conformity-bounded lithosomes in a "closed" basin is illustrated by a comparison of our reconstruction of the uppermost lithosome (HST-2 unit) with data on present-day MARs presented by Frignani et al. (2005). They calculated MARs over the entire Northwest Adriatic shelf based on activity-depth profiles of excess 210 Pb supported by 137 Cs depth distributions. The spatial distribution pattern and absolute values of these MARs are in broad agreement with inferences from a number of recent studies on short-term deposition rates (Wheatcroft et al., 2006; Palinkas and Nittrouer, 2007). The isotopes 210 Pb and 137 Cs have half-lives of 23 and 30 years, respectively. Therefore, calculations based on these isotopes reflect decadal averages. Based on the data of Frignani et al. (2005), the total quantity of sediments accumulating on the Northern Adriatic shelf is estimated to be ≈ 43 Mt yr $^{-1}$. This quantity is virtually identical to the independently derived estimate of Syvitski and Kettner (2007), which equals ≈ 42 Mt yr $^{-1}$ and covers essentially the same time scale.

We derived a centennial average of basin-wide MAR from the analysis of the HST-2 lithosome (0.4 - 0.0 ka BP) that occupies the Adriatic shelf and part of the on-shore Po Delta. The modern Po Delta has advanced rapidly since 1604 AD due to canalizations of the Delta tributaries (Nelson, 1970). We derived the total sediment mass of the HST-2 lithosome seaward of the \approx 1600 AD coastline (Fig. 2.1) by means of the stochastic analysis as described above. The basin-wide MAR derived from this portion of the HST-2 lithosome, which reflects a centennial average, equals 43 ± 7 Mt yr⁻¹. The two basin-wide MARs and the simulated rate of basin-wide sediment supply, which were derived by independent methods, are statistically indistinguishable. Hence, the comparison of three independent estimates of mass accumulation in the conformity-bounded HST-2 lithosome confirms the above principle and demonstrates that the Northern Adriatic Basin is a closed system.

2.5.4 Spatial-temporal scales of mass accumulation rates

From a (long-term) sequence-stratigraphic perspective, a possible mismatch between rates of sediment supply and mass accumulation should be minimal in the case of conformity-bounded units. However, formation of shelf stratigraphy is not an instantaneous process. This implies a mismatch between the two rates if time series on which local accumulation rates are based are shorter than the average time involved in displacing river-mouth sediments to a more permanent position, the so-called base level. Since the notion of base level is intimately coupled with preservation potential, it is implicitly tied to a specific

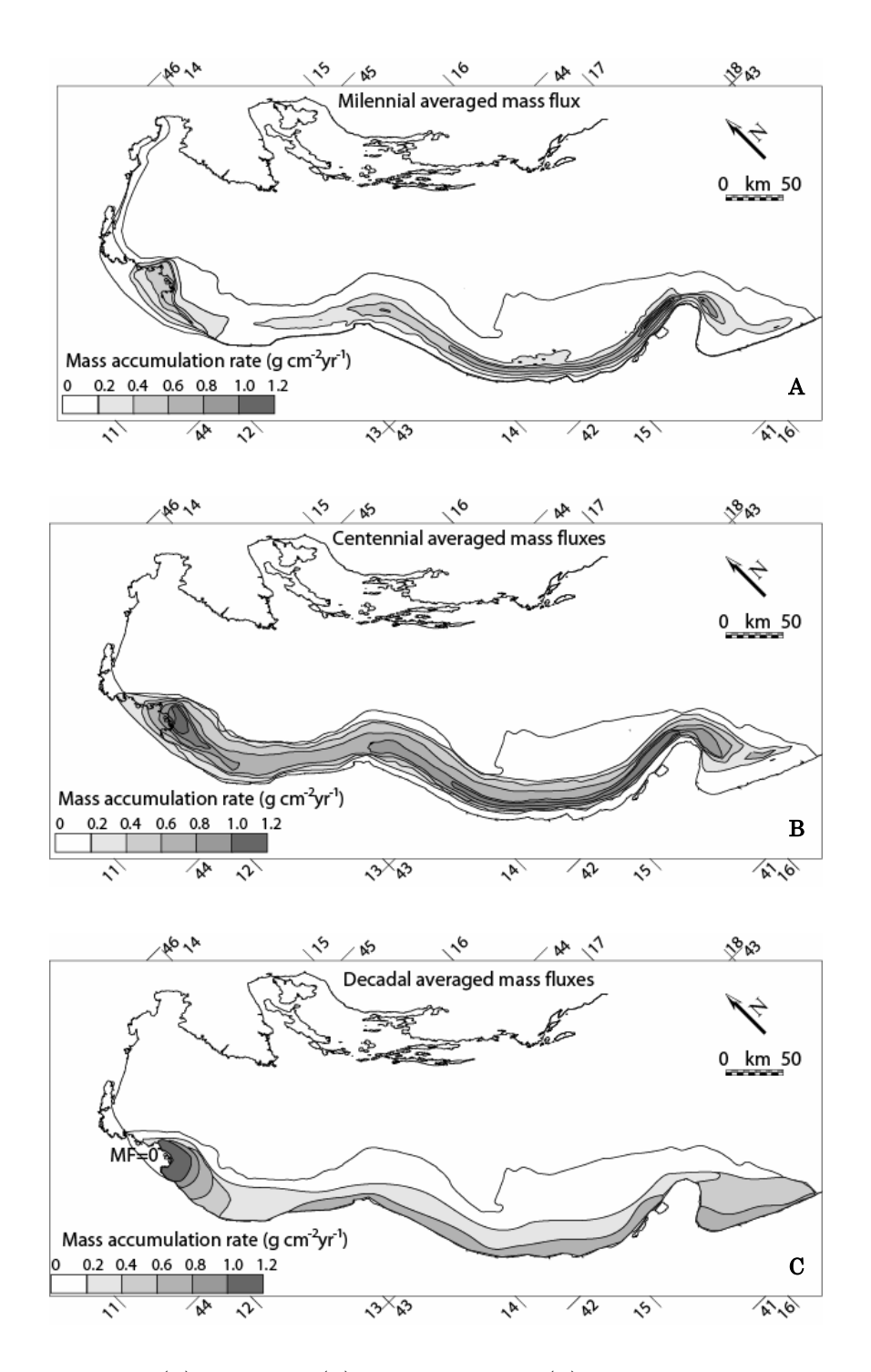


Figure 2.11: (A)Millenial, (B) centennial, and (C) decadal averaged mass fluxes [g cm $^{-2}$ yr $^{-1}$].

temporal scale (cf. Sommerfield, 2006). Jerolmack and Sadler (2007) discuss sediment accumulation rates in relation to the morphological evolution of continental shelves and coastal plains in an attempt to estimate the time scale at which transience gives way to persistence. Based on their findings the authors concluded that persistent landscapes begin to form at 10^2 to 10^3 years and are complete by 10^4 to 10^5 years.

We can clearly illustrate this concept by a comparison of the reconstruction of the lower HST lithosome (HST-1) with the uppermost lithosome (HST-2), and by a comparison of the uppermost lithosome (HST-2) with data on present-day MARs presented by Frignani et al. (2005) based on the isotopes ²¹⁰Pb and ¹³⁷Cs, which reflect decadal average MARs.

Figure 2.11A depicts the millennial averaged mass fluxes derived from the thickness distribution of the HST-1 lithosome. Figure 2.11B presents the centennial averaged mass fluxes derived from the thickness distribution of the HST-2 lithosome. Figure 2.11C presents the corresponding decadal averages calculated from the data of Frignani et al. (2005).

The spatial variation of mass fluxes brings out systematic differences between decadal, centennial and millennial averages. The decadal average mass flux (Fig. 2.11A) shows that sediments tend to accumulate near the coast and especially off the river mouths of the Po-delta distributaries. On centennial time scales (Fig. 2.11B), sediments are reworked and displaced basinward (cross-shore) along most of the Adriatic coast. In addition, the pattern also shows a net trend of longshore progradation in the most distal part of the lithosome, which reflects the growth of the recent Gargano subaqueous delta (Fig. 2.1; Cattaneo et al., 2003). Other features of interest include the area around the modern Po Delta, showing a rapid progradation which started around AD1600 (Correggiari, 2001) and the low preservation potential of sediments presently accumulating near the coast. The pattern of millennial average mass fluxes (Fig. 2.11C) is in many ways similar to the centennial average fluxes, albeit without the localized accumulation in front of the modern Po delta. Hence, much of the sediment which has accumulated over the past decades in the Northern Adriatic is likely to represent a transient stratigraphic record, because the near-surface sediments have not yet reached their longterm repositories.

2.6 CONCLUSIONS

Our quantitative analysis demonstrates that a probabilistic assessment of MARs in a well-documented "closed" basin potentially allows reconstruction of time-averaged rates of sediment supply, provided the basin fill can be subdivided into conformity-bounded units.

The data currently at our disposal permit us to adopt this approach for the two youngest lithosomes corresponding to the HST, and possibly for the TST as a whole. Indeed, our estimate of basin-wide MAR from the uppermost lithosome

(HST-2) closely matches the independent estimates of Frignani et al. (2005) and Syvitski and Kettner (2007) based on modern (decadal-averaged) rates. By comparing mass accumulation rates on three different time scales we demonstrated a low preservation potential of sediments presently accumulating near the coast. The Late Holocene evolution of the Northern Adriatic mud belt is characterized by a continuous alongshore and cross-shore sediment transport regime. The spatial variation of sediment accumulation rates over different time intervals in the mud belt indicates that the stratigraphic record which has formed during the last century must be considered transient (sensu Jerolmack and Sadler, 2007). The change from transient to persistent accumulation patterns seems to occur at the centennial to millennial time scale.

We are unable to reject the null hypothesis that the millennial-scale averages of net basin-wide MARs are equal, although the discrepancy between average MARs of the HST and TST lithosomes suggests that the long-term average rate of sediment supply has increased over the past 19 kyr. Given the fact that order-of-magnitude variations in rates of fluvial sediment supply to marine basins have been postulated by many authors working in the (Late) Quaternary (Leeder et al., 1998; Blum and Törnqvist, 2000; Meybeck and Vörösmarty, 2005), our results are perhaps perceived as disappointing. But the limitations imposed by our data base (and its uncertainties) do not allow us to draw more specific conclusions.

In view of the fractional uncertainties associated with basin-wide net MARs, which are in the range of 20%, our findings could be interpreted in terms of signal attenuation, attributable to the limited time resolution of the stratigraphic record. This problem may be overcome with a significantly improved age model that would enable us to reduce the uncertainty of the duration of the five time slices. Further improvements in estimation of sediment mass from seismics are also possible with better control on porosity profiles, which should allow us to further constrain the stochastic simulations. Further methodological improvements may ultimately lead to the distinction of more time slices within a basin fill. Undoubtedly, high-resolution analyses of basin fills conducted with a vastly improved methodology would demonstrate that variations in rates of mass accumulation also exist in the stratigraphic record. Unfortunately, none of these improvements are by themselves sufficient to aid interpretation of net basin-wide MARs in terms of rates of sediment supply. The main reason for this is recycling of sediments, which causes sediments deposited in a given time interval to be reworked and incorporated into younger units (Einsele, 2000). In view of the recycling problem, the preferred approach to sediment-supply reconstructions is to subdivide the stratigraphic record into conformity-bounded genetic sequences (Galloway, 1989).

It is clear from the above discussion that there are limits to the information that can be extracted from the stratigraphic record, which indicates that the recycling problem must be tackled in a different way. It is highly likely that the liquid and solid discharges of the rivers bordering the Northern Adriatic Basin have varied both in space and time. Numerical models of water and sediment delivery, such as HydroTrend (Syvitski and Kettner, 2007), could be employed to simulate sediment supply in order to constrain the sediment budget of a "closed" basin such as the Northern Adriatic based on palaeo-data derived from proxies and Global Circulation Models. If successful, this approach will lead to a mass-balanced model of supply and accumulation, which may shed more light on the dynamics of sediment dispersal, deposition, and recycling on geologically relevant time scales.

List of Abbreviations and symbols

Abbreviations

HST: HST-1:	Highstand Systems Tract [5.5 – 0.0 ka BP] Lower HST unit [5.5 - 0.4 ka BP]
HST-2:	Upper HST unit [0.4 - 0.0 ka BP]
LGM:	Last Glacial Maximum
LST:	Lowstand Systems Tract
MAD:	Mid-Adriatic Deep
MAR:	Mass Accumulation Rate
MFS:	Maximum Flooding Surface, separating the TST from the HST [5.5 ka BP]
MRS:	Maximum Regressive Surface, separating the LST from the TST [19.0 ka BP]
TST:	Transgressive Systems Tract [19.0 – 5.5 ka BP]
TST-1:	Lower TST unit [19.0 - 14.8 ka BP]
TST-2:	Middle TST unit [14.8 - 11.3 ka BP]
TST-3:	Upper TST unit [11.3 - 5.5 ka BP]

Symbols

Symbol	Definition	Unit
A	Area of grid cell	$[km^2]$
a	Age of bounding surface	[kyr]
δa	Absolute uncertainty of a	[kyr]
c	Constant (porosity-depth Equation)	$[\mathbf{m}^{\cdot 1}]$
d	Thickness	[m]
\mathcal{E}	Constant (geostatistical	[ms]
	interpolation)	
ϕ	Porosity at depth z	[-]
ϕ_0	Surface porosity	[-]
ϕ_{b}	Porosity at infinite depth	[-]
$rac{\pmb{\phi}_b}{\pmb{\phi}}$	Vertically-averaged porosity	[-]
$ ilde{M}$	Stochastic realization of sediment	[Gt]
$\mu_{ extit{shelf}}$	mass Median sediment mass of shelf deposits	[Gt]
$\mu_{ extit{delta}}$	Median sediment mass of delta deposits	[Gt]
$\mu_{{\scriptscriptstyle MAD}}$	Median sediment mass of MAD deposits	[Gt]
M_a	Sediment mass of entire lithosome	[Gt]
δM_a	Absolute uncertainty of M_a	[Gt]

$egin{array}{c} ho \ S_a \end{array}$	Sediment (grain) density Basin-wide mass accumulation	[Gt km ⁻³] [Gt kyr ⁻¹]
$\delta S_a \ \sigma_{shelf}$	rate Absolute uncertainty of S_a Absolute uncertainty of μ_{shelf}	[Gt kyr ⁻¹] [Gt]
$\sigma_{ extit{delta}}$	Absolute uncertainty of $\mu_{\scriptscriptstyle delta}$	[Gt]
$\sigma_{{\scriptscriptstyle MAD}}$	Absolute uncertainty of μ_{MAD}	[Gt]
t	Two-way travel time of seismic signal	[ms]
$ ilde{t}$	Transformed t value	[ms]
$ ilde{t}$	t from surface to bottom of lithosome	[s]
	t from surface to bottom of lithosome t from surface to top of lithosome	[s]
t_B t_T $ au$ $\mathcal{S} au$	t from surface to bottom of lithosome	[s]
t_B t_T $ au$	t from surface to bottom of lithosome t from surface to top of lithosome Duration of time slice Absolute uncertainty of τ	[s] [s] [kyr]

Appendix 2.1: Z-test for equality of two quantities with associated errors

Let $x_1 \pm \delta x_1$ and $x_2 \pm \delta x_2$ be two estimated quantities (with associated standard deviations) we wish to test for equality. The fractional errors of the two quantities are defined as $\frac{\delta x_1}{|x_1|}$ and $\frac{\delta x_2}{|x_2|}$, respectively.

Commonly used tests of equality of means, such as the two-sample t-test, cannot be applied in this case, because these require specification of sample sizes (Davis, 2002). An alternative is provided by the familiar Z-test, which relates normally distributed variables to the standard normal distribution M(0,1) by applying the transformation:

$$Z = \frac{X - \mu}{\sigma},$$

where Z is a standard normal deviate, i.e. a number drawn from M(0,1), X is the quantity of interest, assumed to be distributed as $M(\mu, \sigma)$, μ is the population mean, and σ is the population standard deviation (Taylor, 1982; Davis, 2002).

Our adaptation of the Ztest is based on evaluation of the ratio of the two estimated quantities. Because the ratio of two identical numbers with associated normally distributed errors follows a Log-normal distribution, we take the logarithm of the ratio, which leads to the following log-ratio test.

The quantity of interest is defined as $y = \ln q$, where $q = \frac{x_1}{x_2}$. If the errors δx_1 and δx_2 are uncorrelated, the fractional error associated with q equals:

$$\frac{\delta q}{|q|} = \sqrt{\left(\frac{\delta x_1}{|x_1|}\right)^2 + \left(\frac{\delta x_2}{|x_2|}\right)^2}.$$

The absolute error associated with y is given by: $\delta y = \left(\frac{dy}{dq}\right)\delta q$.

Because $\frac{dy}{dq} = \frac{d \ln q}{dq} = \frac{1}{q}$, we obtain an absolute error $\delta y = \frac{\delta q}{|q|}$, and it follows

that:
$$\delta y = \sqrt{\left(\frac{\delta x_1}{|x_1|}\right)^2 + \left(\frac{\delta x_2}{|x_2|}\right)^2}$$
.

The test statistic Z is then defined as:

$$Z = \frac{-|y|}{\delta y}.$$

We can test the hypothesis H_0 : $x_1 = x_2$ (which is equivalent to Z = 0) by evaluation of the integral of $\mathcal{N}(0,1)$:

 $P(H_0) = 2 \int_{-\infty}^{Z} \frac{1}{\sqrt{2\pi}} e^{-x^2/2} dx$, which gives the two-sided probability P under the

null hypothesis. The value of $P(H_0)$ represents the probability of observing a difference greater than or equal to $\left|x_1-x_2\right|$ if the two are in fact identical.

Chapter 3

Sediment budget modelling of multi-sourced basin fills: application to recent deposits of the Northern Adriatic mud belt (Italy)

3.1 INTRODUCTION

Dispersal of fine-grained sediments on continental shelves has been the subject of intensive research (Chen et al., 2000; Diaz et al., 1996; Labaune et al., 2005; Lesueur et al., 2002; Li et al., 1998; Liquete et al., 2007, 2008; Lobo et al., 2004; Owen, 2004; Sternberg et al., 1996; Tesson et al., 2005). Numerous studies have shown that dispersal pathways of fine-grained sediments are complex, because transfer of material from river plumes to the shelf and beyond is accomplished through a variety of transport mechanisms operating on different temporal and spatial scales (Kineke et al., 1996; Mulder and Syvitski, 1995; Goodbred and Kuehl, 1999; Kuehl et al., 2003; Traykovski et al., 2007). In some areas, detached subaqueous delta deposits form far away from parent river mouths (Kuehl et al., 1997; Goodbred and Kuehl, 1999; Cattaneo et al., 2003) which underscores the importance of understanding the fate of fine-grained sediments.

The hydrodynamic behaviour of fine-grained marine sediments is governed by their degree of cohesion, which is not a simple function of grain size. In general, marine clays and very fine silts are subject to flocculation, a process in which clays and very fine silts form large aggregates or flocs. Flocculation alters settling velocities relative to those of the individual particles and induces selective transport and deposition (McCave, 1984; Kranck et al., 1996a; Kranck et al., 1996b; McCave and Hall, 2006). However, flocs are fragile and break up easily (Hunt, 1986; Burban et al., 1989; Manning et al., 2006). The resuspension of (un)flocculated particles in high-energetic environments (e.g. tidal areas, turbiditic environments, estuaries) has been studied extensively under field and laboratory conditions (McCave, 1984; Kranck et al., 1996a; Kranck et al., 1996b; Eisma, 1990, 1997; Bass et al., 2002, 2003; Curran et al., 2004; Mikkelsen et al., 2004; Manning et al. 2006). These studies, which yielded insight into the break-up of flocs and resuspension of (un)flocculated particles, cover small temporal scales (hours to days). The hydrodynamic behaviour of fine-grained sediment on longer time scales, which is of particular relevance to the formation of muddy stratigraphic sequences, remains poorly understood.

This Chapter is based on: Weltje, G.J. and Brommer, M.B (2009). Sediment budget modelling of multi-sourced basin fills: application to recent deposits of the Northern Adriatic mud belt (Italy). Submitted to Journal of Basin Analysis.

In this study, we present a straightforward approach to quantitative analysis and modelling of fine-grained sediment dispersal in systems with multiple sources, in order to obtain more insight into the growth pattern of mud belts on decadal to centennial time scales. We consider the modern fine-grained sediments on the Northern Adriatic Shelf, Italy (Fig. 3.1) an ideal test case for our integrated source-to-sink approach to quantitative provenance analysis (Weltje and Von Eynatten, 2004) and sediment-budget modelling. The Northern Adriatic system has been studied extensively and is fully accessible for sampling (Trincardi et al., 1994; Correggiari et al., 2001; Asioli et al., 2001; Cattaneo et al., 2003; Palinkas and Nittrouer, 2007; Milligan et al., 2007).

We start by presenting grain-size analyses of samples from the Alpine and Apennine rivers and surface sediments from the Adriatic mud belt. The multimodal grain-size distributions allow us to identify two size fractions, representing clay and very fine silt (O, dominantly transported as aggregates, and fine to medium silt (S), dominantly transported as single grains, respectively. After physical separation, the two fractions were subjected to geochemical analysis. Each of the two size fractions of the river samples was subdivided into statistically significant provenance groups, using a cluster analysis in conjunction with stochastic simulation (permutation test). The last step in the provenance analysis of the river samples is the calculation of compositional fingerprints (end members) of each provenance group for each size fraction. These end members are estimated as mixtures of supply-weighted compositions of river-mouth sediments. Relative supply rates of the rivers belonging to a provenance group were derived from an uncalibrated numerical model of fluvial sediment delivery (Syvitski and Milliman, 2007). A linear mixing model employing these fluvial end-member sediments was used to unmix the surface sediments of the northern Adriatic mud belt. Integration of the unmixed chemical data with bulk accumulation rates (Frignani et al., 2005) allowed us to map the accumulation rates of sediments derived from each of the two major source areas (Po/Adige vs. Apennines) across the mud belt. The estimates of bulk accumulation rates from each of the provenance groups were used to calibrate the source-specific sediment supply rates derived from the numerical model. We close with an evaluation of this integrated quantitative approach to sediment-budget analysis of muddy shelf sediments.

3.2 STUDY AREA

3.2.1 Adriatic Basin

The Northern Adriatic shelf is shallow and has a low gradient (0.05°) (Fig. 3.1) (Trincardi et al., 1994). Sediment input is restricted to the Northern and Western side of the basin (Cattaneo et al., 2003). Sea level started to rise after the Last Glacial Maximum (LGM) and a counter-clockwise longshore current became active at around 14 ka BP (Cattaneo and Trincardi, 1999). From that time on, fine-grained sediment dispersed to the Adriatic Sea by Alpine and Apennine Rivers has been conveyed to the south to form an elongate shore-

parallel prodelta of the Alpine and Apennine rivers that extends to the area south of the Gargano promontory. Brommer et al. (2009) presented quantitative estimates of bulk sediment accumulation rates on the Northern Adriatic mud belt over the past 5500 years, based on conversion of high-resolution seismic and porosity profiles from cores, coupled with $^{14}\mathrm{C}$ datings. Their results, which are consistent with modern accumulation rates based on activity-depth profiles of excess $^{210}\mathrm{Pb}$ supported by $^{137}\mathrm{Cs}$ depth distributions (Frignani et al., 2005) and simulations of sediment supply from the fluvial drainage basins surrounding the Northern Adriatic (Syvitski and Kettner, 2007), indicate that the mud belt receives $\approx\!42~\mathrm{Mt}$ of sediment annually.

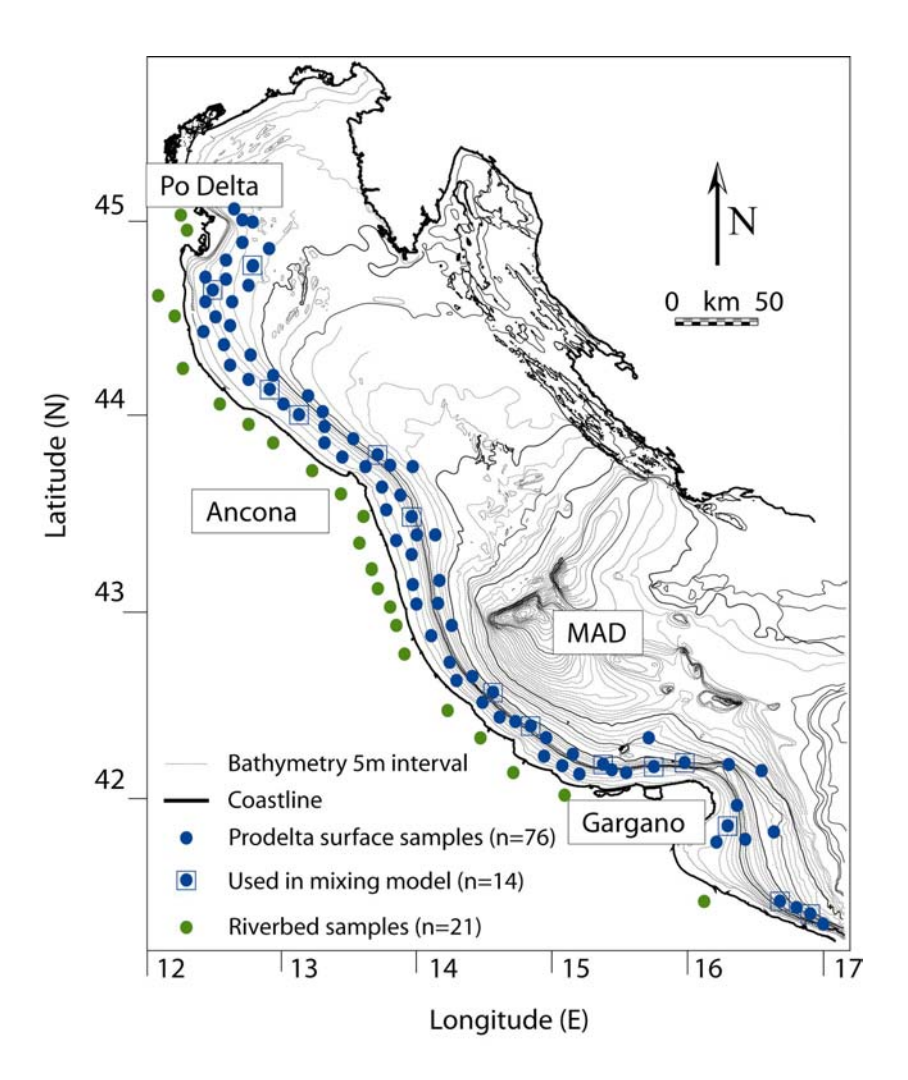


Figure 3.1: Adriatic Basin (Italy) with sampling stations.

3.2.2 Geology of the river basins

The river basins surrounding the Northern Adriatic Sea have been subdivided into four groups: the Eastern Alpine rivers, the Adige River, the Po River, and the Apennine rivers (Fig. 3.1). The Eastern Alpine rivers predominantly drain carbonate lithologies (limestones and dolostones) of the Calcareous Southern Alps (Castellarin and Vai, 1982), and their drainage basins are of similar dimensions. The Adige River cuts into metamorphic rocks of the Austroalpine platform in its upper reaches and into porphyries of the Atesine platform in its lower reaches (Dinelli and Lucchini, 1999). The Po River drains both the Alps and Apennines. The western Alps consist of metamorphic rocks of the crystalline basement (micaschist, gneiss, phyllites and marbles) and various kinds of intrusive rocks (granites, syenites, peridotites). Po tributaries from the central Alps mainly drain sedimentary rocks such as limestones and dolostones, whereas Apennine tributaries of the Po River drain shales, calcareous mudstones and sandstones (Dinelli and Lucchini, 1999). The Apennine mountain chain is also lithologically heterogeneous. Northern Apennine rivers drain sandstones and (calcareous) mudstones of the Marnoso-Arenacea Formation (Dinelli and Lucchini, 1999). The Central Apennine rivers drain turbidites (sandstones and calcareous mudstones) of the Laga Formation, as well as Pliocene (calcareous) mudstones (Dinelli and Lucchini, 1999). The Southern Apennine Rivers drain limestones and dolostones of the Apennine Mesozoic platform, and Plio-Pleistocene sands and calcareous mudstones (Dinelli and Lucchini, 1999).

3.2.3 Hydrodynamics

The Adriatic Sea is characterized by a microtidal regime and is dominated by a cyclonic anti-clockwise circulation driven by thermohaline currents (Malanotte-Rizzoli and Bergamasco, 1983; Bondesan et al., 1995; Cattaneo et al., 2003). The surface circulation of the Adriatic is strongly affected by seasonal wind forcing: the catabatic Bora wind blows from the Northeast during winter and the Scirocco wind blows from the Southeast during summer. The dominant cyclonic circulation traps fresh fluvial water and sediments along the western side of the basin (Poulain, 2001). The southward current is continuous, approaching 1 m s⁻¹, and is fastest in the Apennine region (Palinkas and Nittrouer, 2007). The strong southward transport creates a conveyor belt of sediment starting at the Po Delta and ending at the Gargano Promontory, where the highest accumulation rates are observed (> 1 cm yr⁻¹). The wave climate is characterized by mean wave heights of ≈1 m with maximum heights of ≈ 4 m, and wave periods of 4 to 8 s, causing velocities in the near-bottom wave boundary layer of ≈40 cm s⁻¹ (Harris et al., 2004). Water and sediment discharge to the Adriatic Basin peak during late autumn and late spring (Cattaneo et al., 2003; Syvitski and Kettner, 2007).

3.2.4 Sediment transport

Sediment transport from the Po Delta and the Apennine rivers towards the Gargano promontory is governed by erodibility, settling velocity and physical forcing (Palinkas and Nittrouer, 2007). The erodibility shows significant seasonal and spatial (Po versus Apennine) variability. Po River sediments are initially deposited near the river mouth, whereas sediment from Apennine Rivers can traverse long distances during floods. Milligan et al. (2007) demonstrated that 90% of the fine-grained sediment discharged by the Po River is deposited in the immediate vicinity of the Po river mouth in the form of large flocs, whereas the rest moves further alongshore as small flocs and single particles. However, Po River sediment is remobilized by energetic waves soon after delivery and some of the material may reach depocentres offshore the Gargano Promontory within a single storm season (Harris et al., 2004). Resuspension of fine-grained sediments occurs mostly during Bora events, and rates of along shelf sediment transport are at least one order of magnitude higher than cross-shelf transport (Fain et al., 2007; Traykovski et al., 2007). According to Milligan et al. (2007), particles with diameters smaller than the floc limit d_t act as cohesive material and are transported and deposited predominantly within flocs. Particles larger than de act as non-cohesive material, which implies that they are transported and deposited primarily as single grains. The observed floc limit in the Adriatic prodelta samples is in the range of 5 to 18 µm (Milligan et al., 2007). The median diameter of the flocs varies from 5 to 38 µm (Milligan et al., 2007). Settling velocities of cohesive sediments range from 0.48 to 1.35 mm s⁻¹ in the Adriatic Sea (Mikkelsen et al., 2007). Their average settling velocity (1 mm s⁻¹) is typical for a wide range of environments (Hill et al., 2000). Single quartz grains ranging in size between 20 and 63 μm have settling velocities on the order of 1-3 mm s⁻¹ (Gibbs et al., 1971; LeRoux, 2002).

3.3 GRAIN-SIZE ANALYSIS OF RIVER AND SURFACE SAMPLES3.3.1 Sampling and grain-size analysis

The tops (0-5 cm) of 76 prodelta sediment cores were sampled for grain-size analysis. The cores were retrieved from variable water depths (Fig. 3.1). In addition, 21 river beds were sampled with a Van Veen grab sampler (Fig 3.1). Samples were treated with 10 ml of 30% $\rm H^2O^2$ in order to remove organic matter and boiled until the peroxide was destroyed. The beakers were filled with de-ionized water to remove dissolved cations. After decantation of the clear water until 100 ml, 0.2 g of $\rm Na^4P^2O^7.10H^2O$ (a peptizing agent) was added, after which the samples were boiled for ≈ 1 minute. This treatment causes any aggregates or flocs conceivably present in the sediment to be dispersed. Grain-size analysis of the samples was carried out on a FRITSCH Analysette 22 Laser Particle Sizer according to the conventions of Konert and Vandenberghe (1997).

3.3.2 Results

Grain-size distributions (GSDs) of the river and offshore surface samples are mainly composed of clay and silt-sized particles (≈95%). Variable, but mostly small proportions of sandy sediments are present in samples from shallow water nearby river mouths (Fig. 3.2). Figure 3.3 presents a river sample (Bevano River), which was scaled-up by a factor 1.15 to illustrate the sandy admixture relative to the average offshore sample.

Apart from a highly variable sandy admixture (> 60 μ m), the GSDs of nearly all samples display a bimodal distribution, comprising a population of clays up to medium silt (referred to as C fraction: < 18 μ m), and a population of coarse to very coarse silt (referred to as S fraction: 18 – 60 μ m). In the Adriatic, the finest particles up to \approx 18 μ m in size are subject to flocculation (Milligan et al., 2007). Particles coarser than \approx 18 μ m are predominantly transported and deposited as single grains. The boundary between the C and S fractions thus coincides with the floc limit measured by Milligan et al. (2007).

The results of the grain-size analysis of the prodelta samples are presented in Appendix 3.1 (Table 3.1). The mass fractions of the three size ranges are

defined as $\mathbf{g} = [g_C, g_S, h]'$, subject to the unit-sum constraint $\mathbf{1}'\mathbf{g} = 1$. A useful grain-size measure for hydrodynamic interpretation is the proportion of cohesive (C) relative to the sum of cohesive (C) and cohesionless (S) sediments:

$$M = \frac{g_C}{g_C + g_S} \tag{3.1}$$

Figure 3.4 illustrates the mean grain sizes of the three fractions (C, S, and sand) plotted against M. The means of the C and S fractions display a consistent pattern of low variability and strong correlation with M. The grain size of the sandy admixture does not show any correlation with M, confirming the idea of apparently random addition suggested by Figure 3.2. We also calculated for each sample the logarithm of mean grain size without the sandy admixture, i.e. the C and S fractions combined:

$$\overline{\log D} = M \overline{\log D_C} + (1 - M) \overline{\log D_S}$$
(3.2)

where $\overline{\log D}_C$ is the logarithm of mean grain size [μ m] of the C fraction, and $\overline{\log D}_S$ is the logarithm of mean grain size [μ m] of the S fraction.

The relation between summary statistics M and $\overline{\log D}$ is expected to be linear only if size sorting effects are negligible. Figure 3.4 clearly shows that this is the case for the offshore surface samples, which implies that the samples may be regarded as simple linear mixtures of two subpopulations (i.e. fractions C and S) with approximately constant properties across the area:

$$\overline{\log D} = -1.214M + 1.705 \tag{3.3}$$

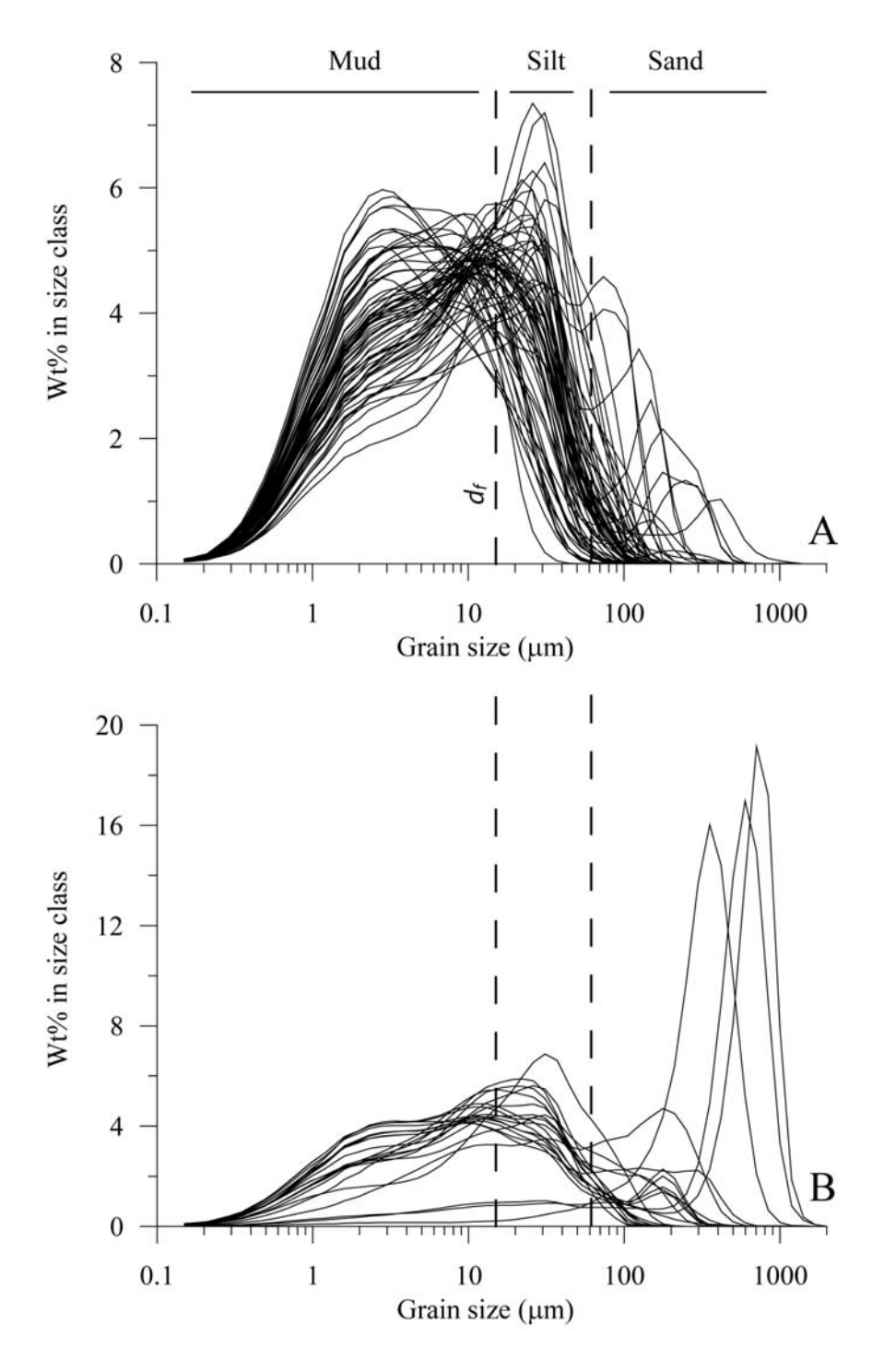


Figure 3.2: Grain-size distributions of prodelta (A) and river samples (B), subdivided into three size ranges. The floc limit $d_{\rm f}$ was used to define the boundary between the C fraction (<18 μ m) and the S fraction (18-60 μ m).

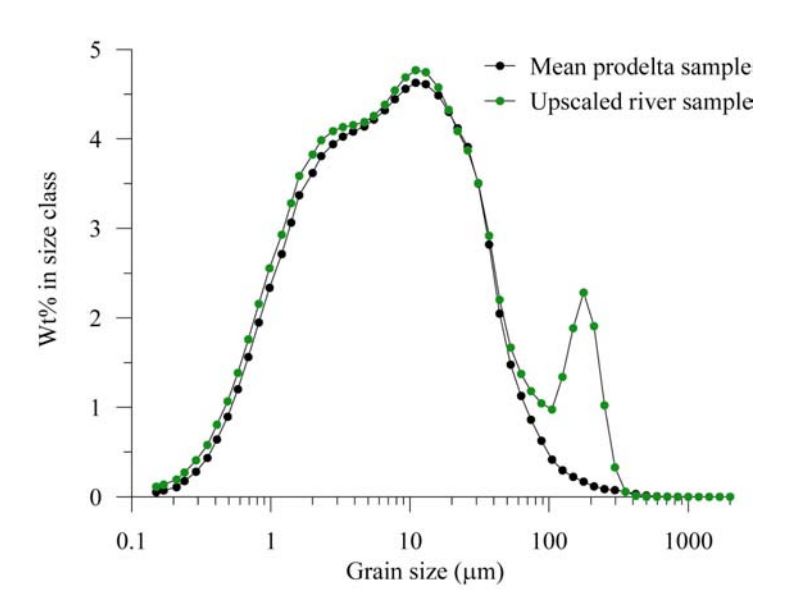


Figure 3.3: Mean grain-size distribution of the mud-belt samples (n = 76) and one upscaled river sample (Bevano River) to illustrate sandy admixture.

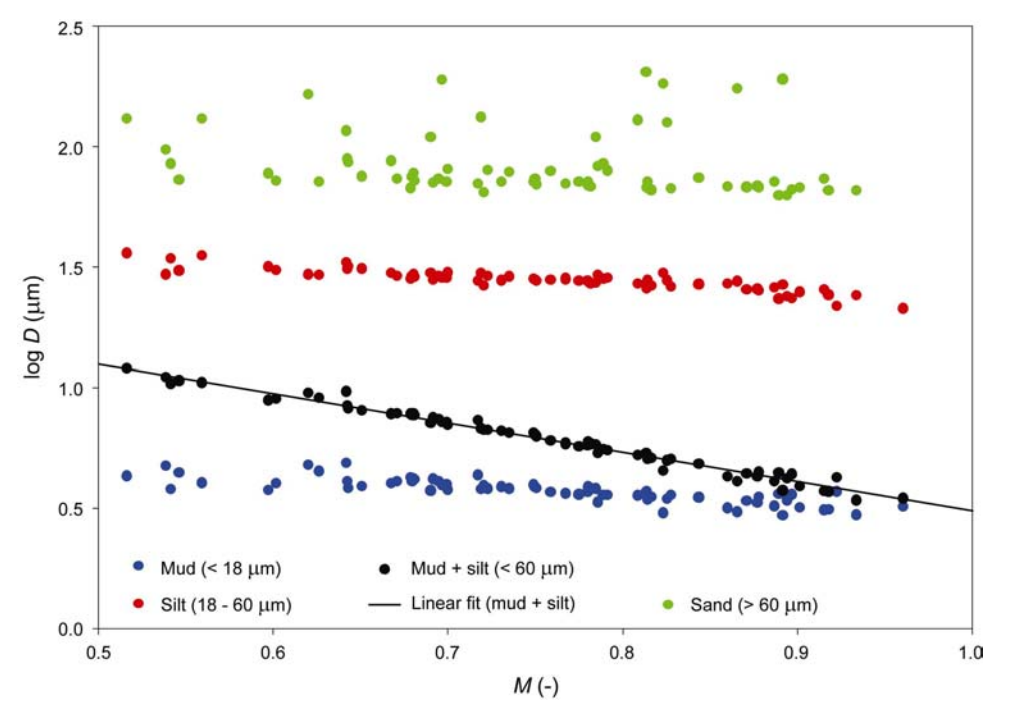


Figure 3.4: Relation between M and the mean grain-size of the C, S, and sand fractions. The regression line shows the strong linear correlation between M and the mean size of the C and S fractions combined.

Indeed, Figure 3.2 illustrates that the GSD of the cohesive fraction is constant across the data set, with a median grain size of $\approx 3~\mu m$. This apparently fixed distribution likely reflects sediment provenance (i.e. the mechanism of sediment generation). It does not exclude the occurrence of selective transport and deposition within the C fraction, but merely suggests that the size of the flocs, which controls the settling velocity of the C fraction, is independent of the size of the clay and silt particles that make up the flocs. Figure 3.4 indicates that size-sorting effects in the S fraction (sortable silt; McCave, 1984) appear to be minor as well, and may be ignored in our first-order approach. The excellent fit of Equation 3.3 to the data ($R^2 = 0.985$) indicates that M allows a close determination of the mean grain size of the sediment below 60 μ m, which is sufficient for the purpose of our study.

3.3 Spatial distribution of grain-size

Geostatistical modelling was used to visualize the spatial distribution of various grain-size and compositional parameters on the Northern Adriatic shelf. Smooth equally spaced grids with cells of 0.5×0.5 km were produced by ordinary kriging of irregularly spaced data points. Spherical semi-variogram models fitted to the data points were designed to capture the difference in lateral continuity parallel (NW-SE: 145°) and perpendicular (NE-SW: 45°) to the shoreline by means of an anisotropy ratio of 2.0. Parameters of the semi-variogram models are listed in the corresponding figure captions. Further details are given in Appendix 1. Figure 3.5A shows a map of \overline{D} with fining trends perpendicular and parallel to the Adriatic coast. In the vicinity of the Po Delta and close to the shoreline, the seabed consists of relatively coarse sediment. The finest sediment is found offshore the Central and Southern Apennines. Figure 3.5B illustrates the spatial distribution of h, the proportion of sand (fraction > $60~\mu m$). Sandy sediment is present in the near-shore area close to river mouths and directly North of the Gargano promontory.

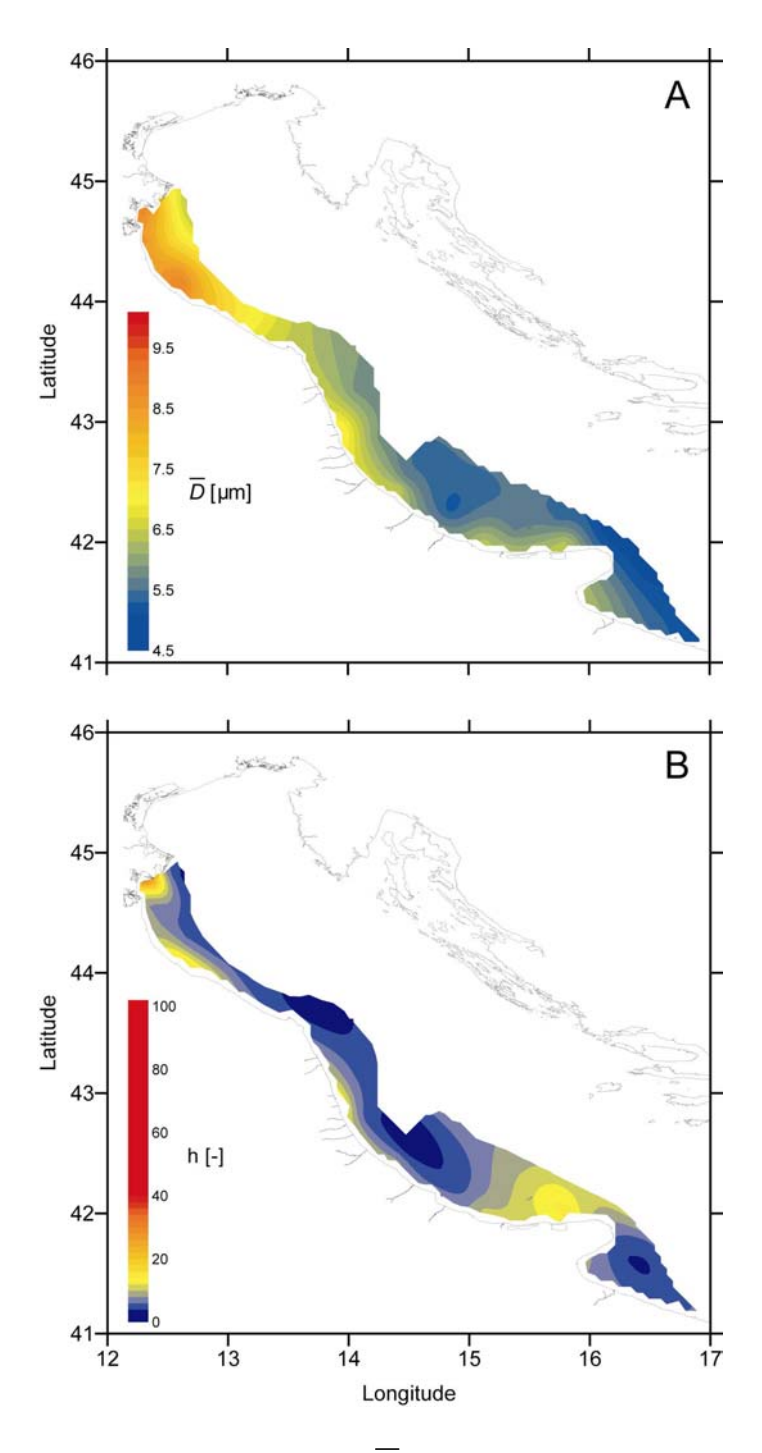


Figure 3.5: (A) Mean grain size \overline{D} [µm] of the fraction below 60 µm. Note the fining trend both cross-shore and long-shore. Semivariance = 1.0, Range = 5.0 km, Nugget = 0.05; (B) Proportional contribution of sand [-]. Semivariance = 1, Range = 15 km, Nugget = 0.5.

3.4 GEOCHEMICAL ANALYSIS OF RIVER SAMPLES

3.4.1 Introduction

Fine-grained sediments originating from different source areas (groups of river basins) thoroughly mix along the pathway from source to sink, owing to repeated resuspension, transport and deposition under the influence of waves. Spatial variations in composition and texture of locally deposited sediments therefore reflect provenance as well as fractionation during selective transport. Compositional variation induced by selective transport should be removed if the objective of sediment analysis is to extract a provenance signal from a series of samples (Weltje, 2004). The inferred average settling velocities of the $C (< 18 \mu m)$ and $S (18-60 \mu m)$ fractions and their coherent spatial distribution pattern (Fig. 3.5) indicate that these two size ranges correspond to different dynamic populations (Weltje & Prins, 2003). In the analysis presented below, we assume that these dynamic populations are transport invariant. Transport invariance of a grain assemblage implies that grains are transported under similar conditions (irrespective of the transporting medium or the mode of transport, i.e. as individual particles or as aggregates). Hence, the composition of such grain assemblages is insensitive to fractionation and independent of the grain-size distribution and the bulk chemical composition of the sediment (Weltje, 2004).

Under conditions of transport invariance, all compositional variation should reflect mixing of different source materials in the size range under investigation. The purpose of the geochemical analysis presented below is to determine whether the chemical composition of the river sediments supplied to the northern Adriatic mud belt is sufficiently heterogeneous on the scale of the entire dispersal system to permit extraction of significant provenance signals from the geochemical data. We therefore analysed the C and S fractions of the river sediments separately, and subjected the data to a cluster analysis in order to investigate whether the river sediments may be subdivided into discrete provenance groups.

3.4.2 Geochemical analysis and data processing

The bulk samples were split into three size fractions by using meshes of 20 μm and 63 μm . The coarse fraction (> 63 μm) was not analyzed. The other two fractions were dried at 60 ^{0}C and ground in an agate mortar. The C fraction (< 20 μm) was analyzed by XRF in the form of pearls. The S fraction (20 - 63 μm) was analyzed by ICP-AES. The results of the geochemical analyses are presented in Appendix 3.1 (Tables 3.2 and 3.3). We used a cluster analysis in conjunction with a permutation test to examine if significantly different provenance groups (groups of contiguous river basins comprising distinct source areas) can be distinguished within the C and S fractions on the basis of chemical composition.

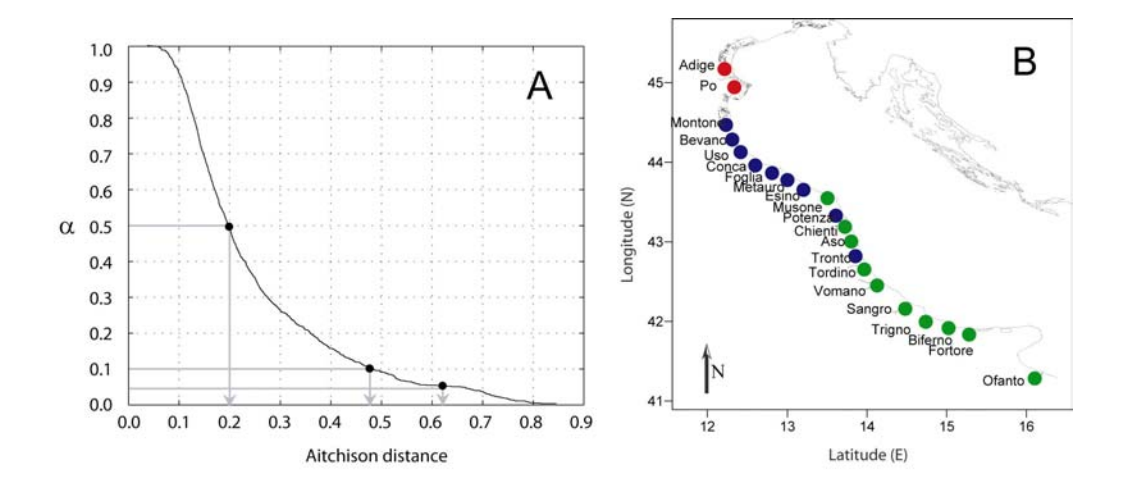
Empirical classification of compositional data was carried out by means of cluster analysis according to Ward's method, with the Aitchison distance as criterion for assignment of individual observations to clusters (Davis, 2002; Pawlowsky-Glahn and Olea, 2004). The data transformation and cluster analysis are discussed in Appendices 3.2 and 3.3. We carried out a permutation test in order to test the significance of the cluster assignment. A permutation test is a stochastic simulation technique, based on repeated analysis of randomized data. A particularly attractive property of the permutation test is that it does not require assumptions about possible causes of random or systematic error in the data, or of the probability distributions of the variables subjected to clustering. The randomization procedure destroys any correlation among the variables while preserving their marginal distributions. Any significant cluster arrangement is therefore destroyed, and the randomized data may be used to build an empirical probability distribution of the desired test statistic under the null hypothesis. In our case, the test statistic is the Aitchison distance between clusters. By running the cluster analysis of our randomized data many times, and saving the Aitchison distances obtained in each run, we construct the cumulative distribution function (CDF) of Aitchison distances. We select the upper $(1-\alpha)$ point of this CDF as the critical distance, which has a probability of α of occurring under the null hypothesis. Hence, all clusters separated by Aitchison distances, which are equal to or larger than the critical distance are significant at the 100 α % level. We adopted $\alpha = 0.1$ as the significance level in all tests. Details of the permutation test are listed in Appendix 3.4.

3.4.3 Results

We generated 1000 permutation distributions of Aitchison distances by repeated randomization of the data for each of the two dynamic populations (C and S fractions). Figure 3.6A shows the CDF of the recorded distances corresponding to the C fraction. The critical Aitchison distance corresponding to $\alpha = 0.1$ is 0.47. Figure 3.6C combines the results of the cluster analysis and the permutation test. The x-axis denotes the individual observations (river samples). The y-axis at the left hand side of the diagram depicts the Aitchison distance, and the right-hand side shows the corresponding significance levels under the null hypothesis (α). Figure 3.6B shows that the river samples are assigned to three clusters: a red cluster (Po and Adige rivers), a blue cluster (Northern Apennine rivers), and a green cluster (Southern Apennine rivers). The three clusters are plotted in Fig. 3.6C, from which it can be seen that the cluster assignment corresponds to three contiguous source areas, i.e. the rivers, which have been assigned to a cluster are geographically close to each other and drain similar lithologies (Dinelli and Lucchini, 1999). Figure 3.7A shows the CDF of the recorded Aitchison distances corresponding to the S fraction. Figure 3.7B is analogous to Figure 3.6B and shows the results of the cluster analysis combined with the permutation test. The critical Aitchison distance for $\alpha = 0.1$ is 0.90. Figure 3.7B shows that at this significance level the river

samples are assigned to two geographically distinct clusters: a red cluster (Po and Adige rivers) and a black cluster (Apennine rivers), which are presented in Fig. 3.7C.

Our results indicate that each cluster corresponds to a section of the hinterland which carries a distinct geochemical provenance signal — a compositional fingerprint. In order to derive the representative compositional fingerprint of each provenance group, we should take into account that the Alpine and Apennine rivers are quite different from each other in terms of their liquid and solid discharges. The next step is therefore to estimate the rates of sediment supply from all rivers, and calculate the desired compositional fingerprints as supply-weighted averages of the compositions belonging to each cluster.



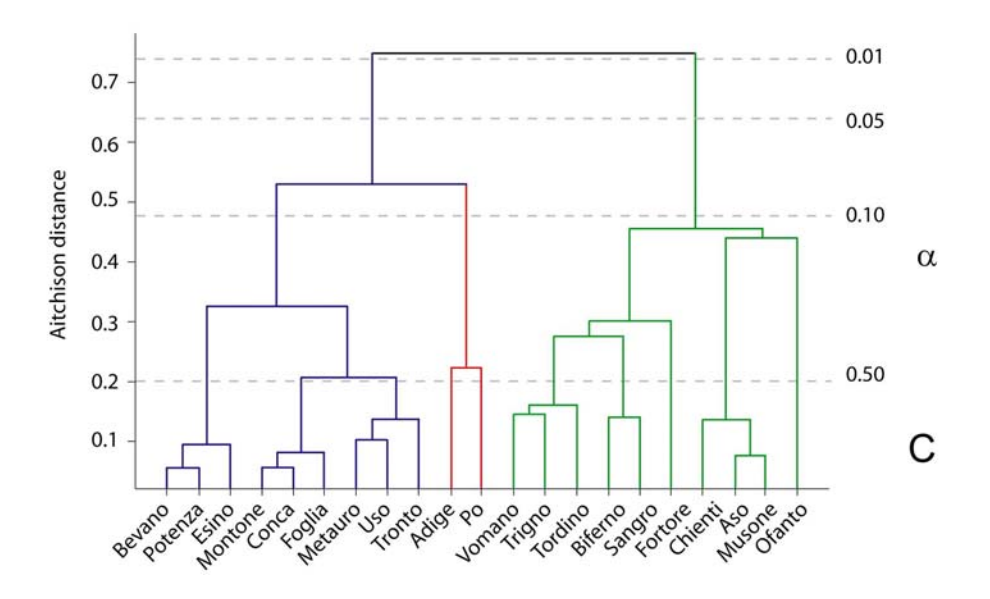
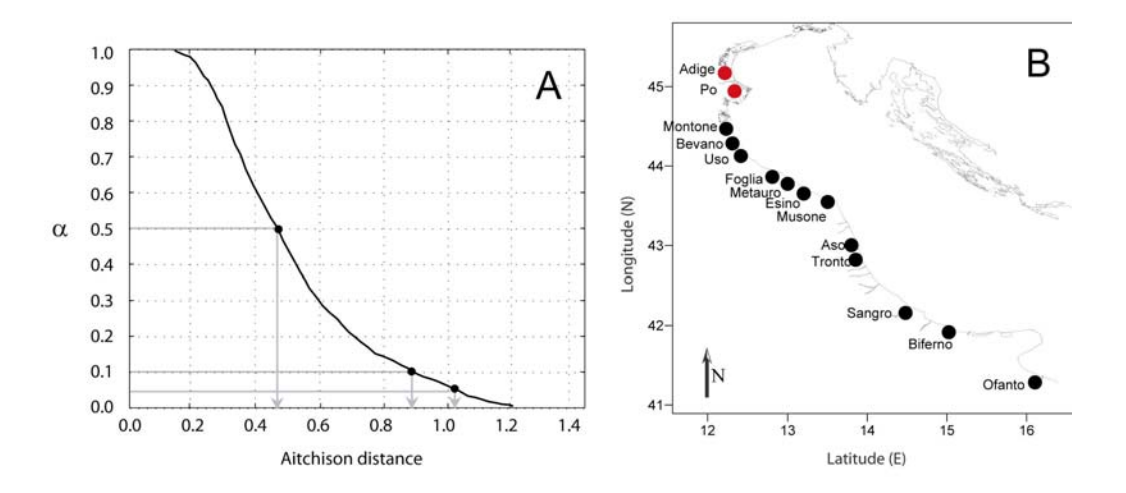


Figure 3.6: (A) Result of permutation test for the C fraction; (B) Sampling stations with colors corresponding to the three clusters. (C) Dendrogram of river-mouth samples;



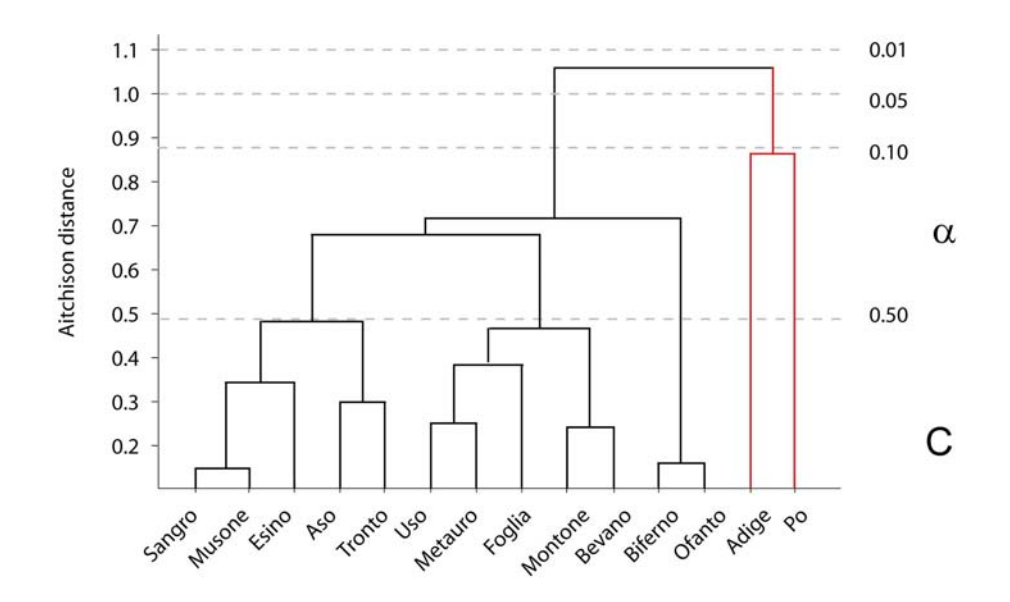


Figure 3.7: (A) Result of permutation test for the S fraction; (B) Sampling stations with colours corresponding to the two clusters. (C) Dendrogram of river-mouth samples;

3.5 MODELLING SEDIMENT SUPPLY

3.5.1 Sediment supply model

The long-term average suspended-sediment discharges (*Qs*) of the rivers debouching into the northern Adriatic Sea were estimated with the HydroTrend model (Kettner and Syvitski, 2007). At the heart of this model lies the BQART Equation (Syvitski and Milliman, 2007):

$$Qs = \omega B \left(\frac{Q}{Q_0}\right)^{0.31} \left(\frac{A}{A_0}\right)^{0.5} RT \tag{3.4}$$

where Qs is the long-term average sediment load [Mt yr¹], A is the drainage area [km²], R is the maximum elevation in the drainage basin [km], and T is the basin-averaged temperature [°C] for the case T > 2 °C (otherwise $T \equiv 2$ °C). Q is the long-term average discharge [km³ yr¹]. $A_0 \equiv 1$ [km²] and $Q_0 \equiv 1$ [km³ yr¹] are reference values introduced to non-dimensionalize area and long-term average discharge. The constant $\omega = 0.0006$ [Mt yr¹ °C ¹ km²]. Parameter B [-] represents the long-term balance of sediment generation, storage and release, which incorporates various geological and human impact factors to account for deviations of Qs with respect to the reference case B = 1 (Syvitski and Milliman, 2007).

For the purpose of modeling sediment supply, we subdivided the hinterland into different source areas, based on lithology, area, and maximum elevation in the drainage basins. We assumed that the eastern Alpine rivers do not contribute sediment to the area South of the Po Delta (Brommer et al., 2009). In order to obtain a sediment budget for the mud belt, we modelled the sediment supply of the Adige and Po rivers, and selected four representative rivers draining different parts of the Apennines: Metauro, Tronto, Sangro and Biferno (from North to South). The sediment supply from the reference basins was used to obtain estimates for the entire source area using the following procedure.

Let Q = qA, where q is defined as the liquid discharge produced per unit area of the drainage basin [km yr⁻¹]. Equation 3.4 may be rewritten as:

$$Qs = \omega B \left(\frac{q}{q_0}\right)^{0.31} RT \left(\frac{A}{A_0}\right)^{0.81}$$
(3.5)

The constant $q_0 \equiv 1$ [km yr⁻¹] is a quantity needed to non-dimensionalize the term within brackets. We assume that the values of q and B within each source area are constant, and define constant k:

$$k = \omega B \left(\frac{q}{q_0}\right)^{0.31} \tag{3.6}$$

The constant k [Mt yr⁻¹] is the characteristic rate parameter of the source area. Substitution of Equation 3.6 into Equation 3.5 gives the following expression:

$$Qs_r = kR_r T_r \left(\frac{A_r}{A_0}\right)^{0.81} \tag{3.7}$$

The subscript r indicates that Equation 3.7 applies to the reference basin for the source area. The sediment supply of other basins belonging to the same source area (indicated by the subscript i) may be derived from Equation 3.8:

$$Qs_i = kR_i T_i \left(\left(\frac{A_i}{A_r} \right) \left(\frac{A_r}{A_0} \right) \right)^{0.81}$$
(3.8)

3.5.2 Input data and results

River basin area (A) and maximum elevation (R) of the drainage basins (Table 3.4) were derived from the Shuttle Radar Topography Mission (SRTM) digital elevation models (http://srtm.usgs.gov/). Present-day temperature and precipitation data were derived from the National Oceanic and Atmospheric Administration (NOAA) database (http://www.noaa.gov/). These two variables were converted to discharges and basin-averaged temperatures by HydroTrend (Kettner and Syvitski, 2007), based on a water-balance model (Syvitski et al., 1998) and drainage-basin hypsometry, respectively.

Estimation of the source-specific parameter B, which represents the long-term balance of sediment generation, storage and release, was not attempted at this stage of the modelling exercise. Instead, sediment supply of the Adige, Po, and Apennine rivers was calculated by assuming that B=1. This default value is sufficient to determine the supply-weighted compositional fingerprint of each source area (cluster), because weighing is based on relative magnitudes of sediment supply only. As will be shown below, calibration of default sediment-supply rates was carried out on the basis of quantitative estimates of source-specific accumulation rates derived from the compositional analysis. All input parameters of the model and default sediment-supply rates are shown in Table 3.4.

Table 3.4: Parameters used for sediment supply modelling and calculation of fluvial end-members (EM = end-member); RR = representative river; * = reference basin. NB: Qs is uncalibrated (B= 1).

River Basin	EM (<i>C</i>)	EM (S)	RR (<i>C</i>)	RR (S)	$\begin{array}{c} Q \\ [km^3 \ yr^{\text{-}1}] \end{array}$	A [km²]	R [km]	T [°C]	Qs [Mt yr ⁻¹]
Adige *	PC	PS	-	-	9.60	14441	3.85	15.2	8.51
Po *	PC	PS	-	-	48.00	74259	4.75	14.1	36.36
Reno			Mon- tone	Mon- tone	2.96	4700	1.0	16.0	1.95
Lamone			Mon- tone	Mon- tone	0.32	515	1.0	16.0	0.21
Montone	A1C	AS			0.76	1204	1.0	16.0	0.50
Bevano	A1C	AS			0.16	250	1.0	16.0	0.10
Savio			Bevano	Bevano	0.38	600	1.0	16.0	0.25
Rubicone			Uso	Uso	0.13	210	1.0	16.0	0.09
Uso	A1C	AS			0.17	275	1.0	16.0	0.11
Marecchia			Conca	Foglia	0.33	530	1.0	16.0	0.22
Conca	A1C			Foglia	0.10	160	1.0	16.0	0.07
Foglia	A1C	AS			0.44	700	1.0	16.0	0.29
Metauro *	A1C	AS			0.87	1381	1.7	15.8	0.57
Cesano			Esino	Esino	0.26	410	1.1	16.0	0.17
Esino	A1C	AS			0.76	1200	1.1	16.0	0.50
Musone	A2C	AS			0.40	640	1.4	15.9	0.27
Potenza	A2C			Mu- sone	0.49	775	1.5	15.9	0.32
Chienti	A2C			Aso	0.82	1300	1.5	15.9	0.92
Aso	A2C	AS			0.21	275	2.0	17.0	0.19
Tronto *	A2C	AS			0.90	1190	2.5	16.8	0.84
Tordino	A2C			Tronto	0.35	460	2.0	17.0	0.33
Vomano	A2C			Tronto	0.58	765	2.2	16.8	0.54
Saline			Vo- mano	Tronto	0.41	540	1.5	17.0	0.34
Pescara			Sangro	Sangro	2.41	3190	2.2	16.8	1.98
Sangro *	A2C	AS			0.65	1712	2.8	17.5	1.06
Sinello			Trigno	Sangro	0.17	450	1.4	17.8	0.28
Trigno	A2C			Sangro	0.46	1200	2.2	17.7	0.75
Biferno *	A2C	AS			0.87	1285	2.05	17.7	0.75
Fortore	A2C			Biferno	0.98	1450	2.0	17.5	0.84
Ofanto	A2C	AS			1.02	1500	2.0	17.5	0.87

3.6 DISPERSAL PATTERNS ON THE SHELF

3.6.1 Geochemical end-members

The supply-weighted compositional fingerprint (**F**) of each provenance group may be derived by taking the suspended sediment load of individual rivers into account:

$$\mathbf{F} = \frac{\sum_{i=1}^{n} Q s_i \mathbf{x}_i}{\sum_{i=1}^{n} Q s_i}$$
(3.9)

where Qs_i is the suspended sediment supply of the individual rivers (i = 1, n) belonging to a provenance group, and \mathbf{x} represents the geochemical composition

vector $\mathbf{x} = \begin{bmatrix} x_1, x_2, x_j, ..., x_k \end{bmatrix}'$ of each observation (river sample). Rivers for which no geochemical data are available were taken into consideration by adding their suspended loads to neighbouring "representative" rivers (Table 3.4). The resulting supply-weighted compositional fingerprints of the five provenance groups are presented in Table 3.5. We have also combined the two Apennine fingerprints (\mathbf{F}_{AIC} and \mathbf{F}_{A2C}) into a single Apennine fingerprint (\mathbf{F}_{AC}) for the purpose of robust analysis. With this set of end members, the bulk chemistry of the Adriatic surface samples can be unmixed and described in terms of provenance and grain size.

3.6.2 Unmixing of surface samples

Fine-grained sediments originating from different source areas are thoroughly mixed along the pathway from source to sink. In shallow marine areas, mixing of surface sediment occurs by means of wave-induced resuspension of previously deposited material. The composition of surface sediments at the site of final deposition is determined by the net result of multiple resuspension events. Consequently, spatial variations in composition and texture of these locally deposited sediments reflect provenance as well as fractionation during selective transport.

The surface samples of the mud belt were geochemically analyzed according to the same procedures outlined for the river samples. The geochemical composition of the C and S fractions of Adriatic surface samples can be expressed as mixtures of the end members \mathbf{F} , to yield insight into the proportional contributions of the sediment sources contributing to each size fraction:

$$\mathbf{Fm} = \mathbf{x} \tag{3.10}$$

subject to:

$$m \ge 0.1' m = 1$$
 (3.11a,b)

where the matrix \mathbf{F} represents the end members of the C or S fraction (Table 3.5), and \mathbf{x} the geochemical composition vector of the corresponding size fraction of each Adriatic surface sample (Tables 3.2 and 3.3). The vector \mathbf{m} represents the proportional contributions of the end members to each observation, subject to non-negativity and constant-sum constraints (Weltje, 1997). For each surface sample, this exercise provides two mixture vectors (one for each size fraction):

$$\mathbf{m}_{C} = \left[m_{PC}, m_{AC}\right]', \quad \mathbf{m}_{S} = \left[m_{PS}, m_{AS}\right]' \tag{3.12a,b}$$

For the C fraction, we have also calculated the three-part mixture vector:

$$\mathbf{m}_{C}^{*} = \left[m_{PC}, m_{A1C}, m_{A2C} \right]' \tag{3.13a,b}$$

Table 3.5: Chemical compositions [g kg^{-1}] of fluvial end-members (EM=end-member)

EM	Na	Mg	Al	Si	Р	K	Са	Ti	Cr	Mn	Fe	Zn	Rest
PC	10	25	57	199	7	25	111	4	-	1	49	-	512
A1C	13	17	61	179	9	16	133	4	-	1	42	-	524
A2C	26	13	64	177	18	15	119	4	-	1	44	-	519
AC	21	14	63	178	15	15	125	4	-	1	43	-	521
PS	4	14	32	-	-	8	164	2	0.1	1	19	.1	756
AS	8	12	39	-	-	11	120	2	0.1	1	18	.1	789

3.6.3 Dispersal patterns of the C and S fractions

In order to depict the dispersal pattern of the C fraction, we have plotted the mixing vectors of the three provenance groups (Eqns. 3.12b and 3.13). For surface samples located to the north of Ancona (Fig. 3.1) we impose $m_{\scriptscriptstyle A2C}=0$ as an additional constraint, based on the *a priori* information that fine-grained sediments are transported southward by the longshore surface current.

Figure 3.8A displays the dispersal pattern of the C fraction originating from the Po/Adige provenance group. Offshore sediment adjacent to the Po Delta consists of approximately 80 to 90% of Po/Adige derived material. Essentially the same applies to the S fraction of Po/Adige provenance (Fig. 3.8B). The Cfraction in the area surrounding the Gargano Promontory is composed of ≈ 45 % material of the Po/Adige provenance group (Fig. 3.8A). In the area to the south of the Gargano Promontory, the S fraction is composed of $\approx 15\%$ Po/Adige material (Fig. 3.8B). The contribution of the Apennine provenance group to the S fraction is the exact complement of Figure 3.8B, and ranges from 25-40% in the area directly south of the Po Delta to almost 85% in the southern part of the Adriatic mud belt. The contribution of the Northern Apennine provenance group to the C fraction ranges from $\approx 75\%$ in the area to the south of the Po Delta to $\approx 15\%$ in the area surrounding the Gargano promontory (Fig. 3.9A). Figure 3.9B shows that the Southern Apennines provenance group becomes dominant (up to $\approx 40\%$) in the C fraction North of the Gargano Promontory. In the area to the South of the Gargano Promontory the contribution of the Southern Apennines provenance groups equals the contribution of the Po/Adige provenance group ($\approx 45\%$).

The mixing model calculations thus indicate that material originating from the northernmost provenance group (Po and Adige rivers) is transported over a distance of 500 km to be deposited at the southernmost extension of the subaqueous delta, in the area South of the Gargano Promontory. This is a consistent spatial pattern in both C and S fractions. The only difference between the two fractions is that the quantity of Po and Adige material present in the surface samples within the C fraction is approximately 45%, whereas the S fraction of surface samples consists of approximately 15% of Po and Adige derived material. These findings suggest that the C fraction, consisting of cohesive particles, is more susceptible to resuspension along the pathway from source to sink. Given the different transport mechanisms and terminal fall velocities of both fractions, it seems logical that sediments of the C fraction have a lower preservation potential than sediments of the S fraction.

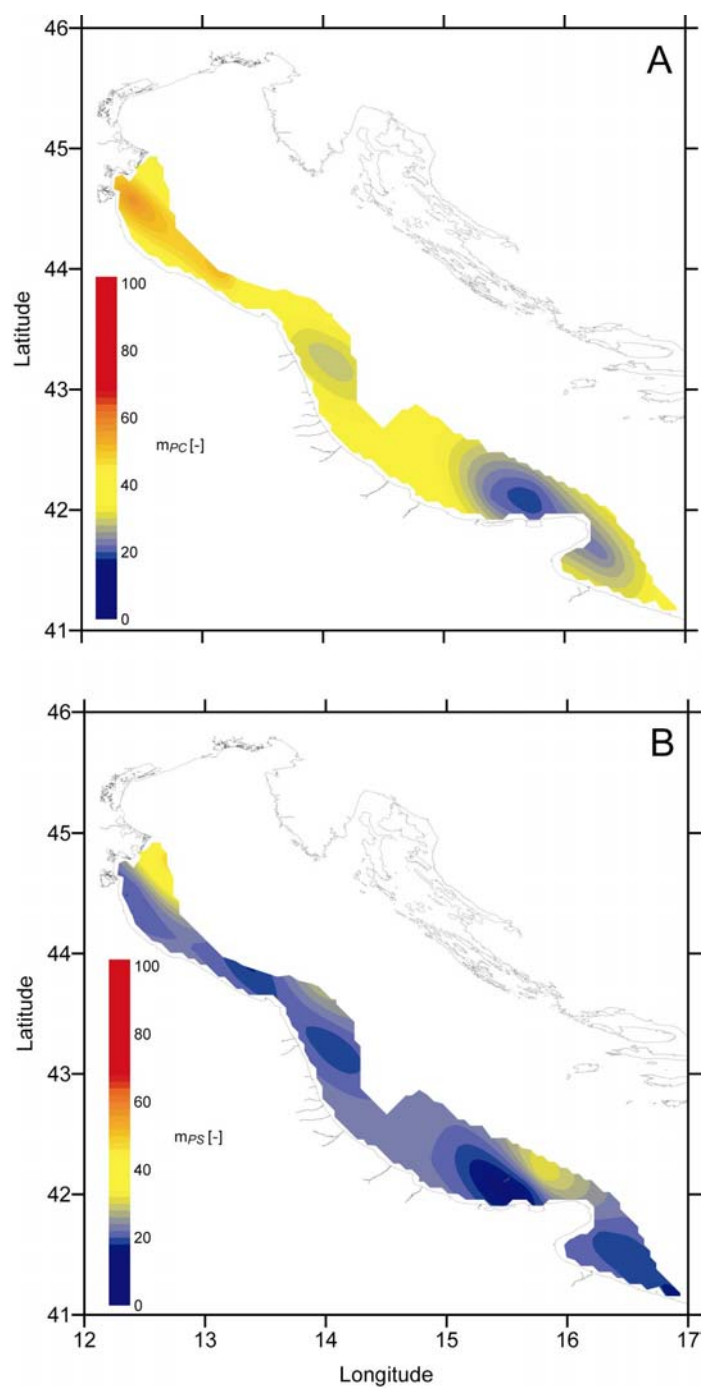


Figure 3.8: (A) Proportional contribution of rivers Po and Adige to the C fraction. Semivariance = 1.0, Range = 3.0 km, Nugget = 0.05; (B) Proportional contribution of rivers Po and Adige to the S fraction. Semivariance = 0.8, Range = 2.5 km, Nugget = 0.05.

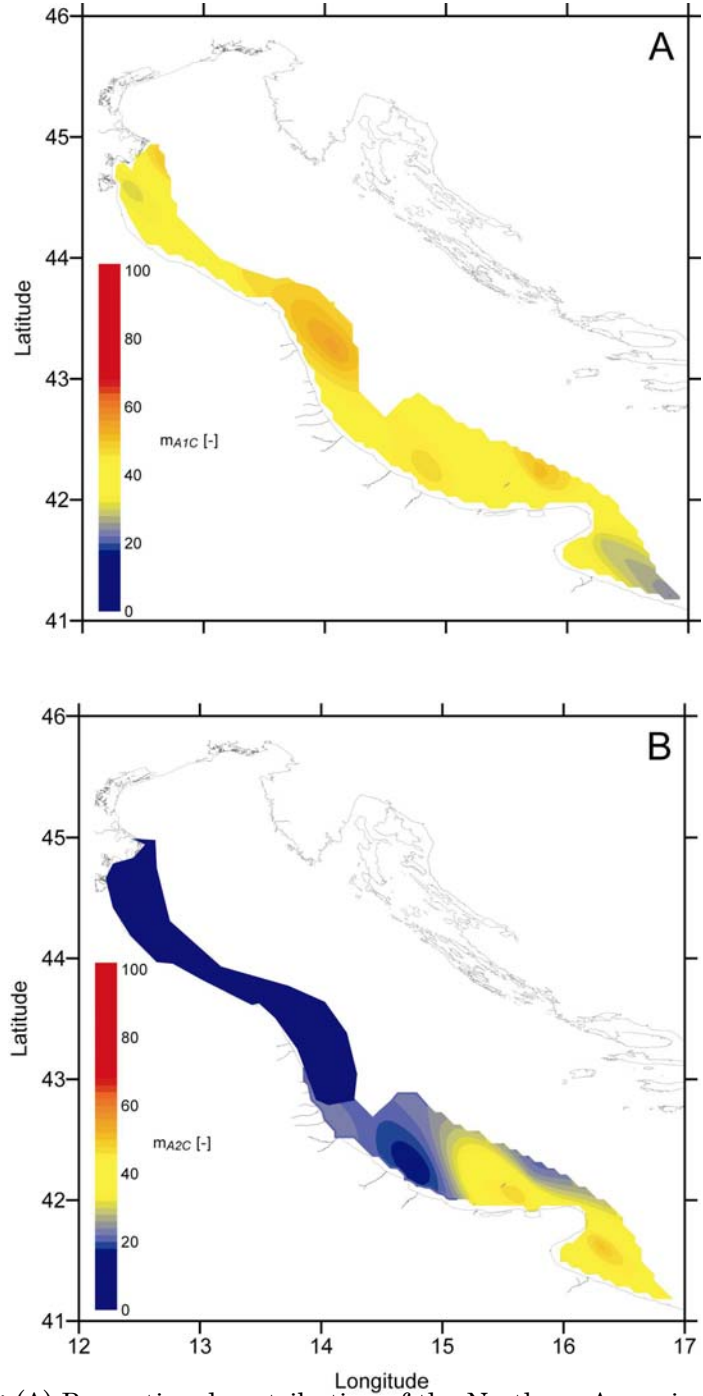


Figure 3.9: (A) Proportional contribution of the Northern Apennine rivers to the C fraction. Semivariance = 1.0, Range = 3.0 km, Nugget = 0.05; (B) Proportional contribution of the Southern Apennine rivers to the C fraction. Semivariance = 1.0, Range = 3.0 km, Nugget = 0.05.

3.7 INTEGRATED ANALYSIS OF PROVENANCE AND DISPERSAL

3.7.1 Combining grain-size and chemistry

The results of the cluster analysis show that the Adriatic mud belt is predominantly sourced by two distinct provenance groups, the Po/Adige and Apennine provenance group. The results of the linear mixing model allow us to infer the dispersal patterns of the two provenance groups within the C and S fractions separately. In addition, we have captured the ratio of the two size fractions with the variable M. The next logical step is to combine these inferences into one overall model of provenance and size-selective dispersal by establishing the relation between the mixing coefficients within each fraction and the spatial grain-size variation across the mud belt. This may be achieved by defining the two-component mixing vector \mathbf{p} , which sums to unity $(\mathbf{1'p} = 1)$:

$$p_{A} = M m_{AC} + (1 - M) m_{AS}$$

$$p_{P} = M m_{PC} + (1 - M) m_{PS}$$
(3.14a,b)

The vector \mathbf{p} gives the proportions of the two provenance groups in the combined size range covered by the C and S fractions, which allows source-specific accumulation patterns to be mapped.

3.7.2 Source-specific accumulation patterns

The spatial distribution of "modern" bulk sediment accumulation rates across the Adriatic mud belt, based on activity-depth profiles of excess ^{210}Pb supported by ^{137}Cs depth distributions (Frignani et al., 2005), is shown in Figure 3.10A. Accumulation rates of the sand fraction (> 60 µm), as well as source-specific accumulation rates of the size fraction < 60 µm may be obtained from these bulk rates as follows:

$$\begin{split} V_A &= p_A (1-h) V \\ V_P &= p_P (1-h) V \\ V_S &= h V \end{split} \tag{3.15a-c}$$

where V is defined as the bulk sediment accumulation rate ($V = V_A + V_P + V_S$), h is the proportion of sand (> 60 μ m), V_S is the accumulation rate of the sand fraction, and V_A and V_P represent the accumulation rates of sediments (< 60 μ m) derived from the Apennines and Po/Adige, respectively.

Figure 3.10B illustrates that sand accumulates mainly in front of the Po Delta and the Apennine rivers. An additional depocentre of sand is present directly North of the Gargano promontory.

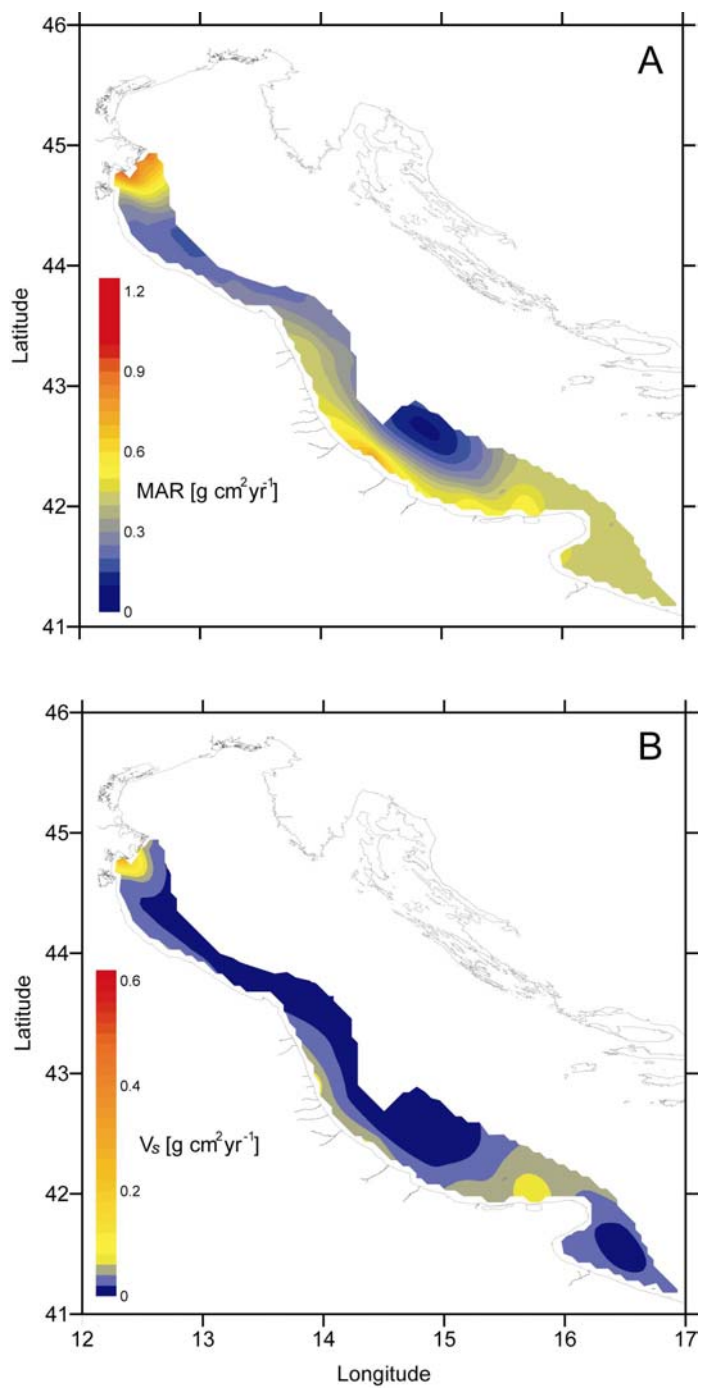


Figure 3.10: (A) Present-day bulk mass accumulation rates (after Frignani et al., 2005). Semivariance = 1.0, Range = 6 km, Nugget = 0.2; (B) Sand accumulation rates. Semivariance = 1, Range = 15 km, Nugget = 0.5.

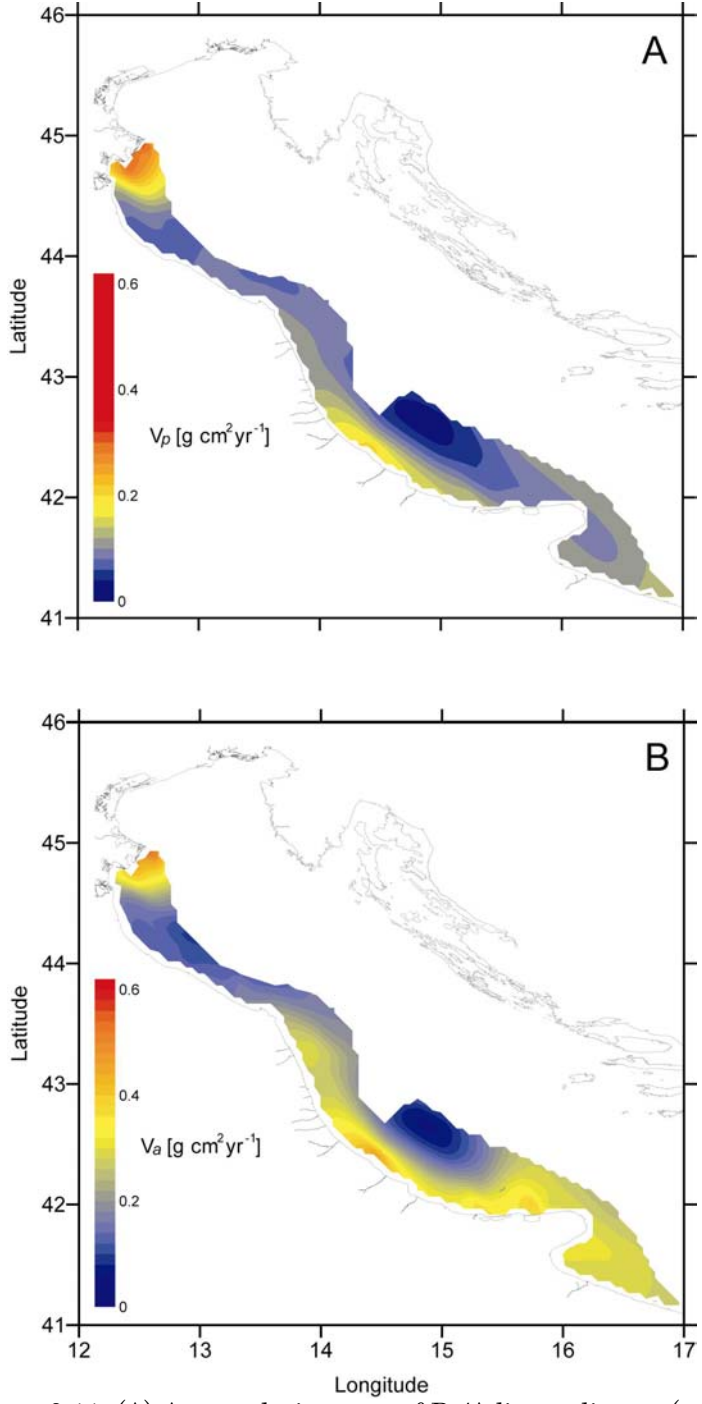


Figure 3.11: (A) Accumulation rate of Po/Adige sediment (< 60 μ m) on the northern Adriatic shelf. Semivariance = 1.0, Range = 6 km, Nugget = 0.2; (B) Accumulation rate of Apennine sediment (< 60 μ m) on the northern Adriatic shelf. Semivariance = 1.0, Range = 6 km, Nugget = 0.2

Figure 3.11A and B illustrate the source-specific sediment accumulation patterns on the Adriatic mud belt. Sediments derived from the Po and Adige rivers (Fig. 3.11A) accumulate in the vicinity of the Po Delta, along the Apennine coast, and at the southernmost tip of the mud belt (South of Gargano). Sediments from the Apennine rivers (Fig. 3.11B) dominate the southern part of the mud belt, especially the area around Gargano.

3.7.3 Sediment budget and model calibration

The results of our grain-size calculations indicate that the mean annual supply of sediment to the mud belt comprises ≈ 29 Mt of mud ($< 20 \, \mu m$), ≈ 10 Mt of silt ($20-60 \, \mu m$), and ≈ 3 Mt of sand ($> 60 \, \mu m$). Table 3.6 summarizes the sediment budgets of the two source areas. On average, the Po and Adige rivers supply ≈ 17 Mt annually, whereas the mean annual supply of the Apennines equals ≈ 25 Mt. We may use these totals to calibrate the sediment storage and release parameter B of the BQART model (Eqns. 3.4-3.7). A good fit of our data to BQART model predictions is obtained by setting B = 0.4 for the Po and Adige rivers, and B=1.5 for the Apennine rivers (Table 3.6). It should be noted that this approach to model calibration, which is based on analysis of accumulation rates, grain size and sediment composition, is independent of the procedure used to derive geochemical end members. In the latter, use was made of relative supply rates only, based on the assumption that the value of B is constant among the rivers belonging to a particular provenance group.

Table 3.6: Source-specific rates [Mt yr-1] of sediment accumulation and supply (* = sand equally divided between source areas; ** = calibrated: BP = 0.4; BA = 1.5)

Size range	Po/Adige (P)	Apennines (A)	Total
Mud/silt (< 60 µm)	15.6	23.4	39
Sand (> 60 μ m) *	1.5	1.5	3
Bulk	17	25	42
Qs (calibrated) **	18	23	41

3.8 DISCUSSION AND CONCLUSION

Our study of the northern Adriatic mud belt illustrates the steps needed to produce a quantitative model of sediment supply and dispersal on muddy continental shelves sourced by many different fluvial systems. We present a straightforward approach to quantifying sediment supply, provenance, and selective dispersal of surface sediments, based on the integration of grain-size analysis, geochemical analysis of specific size fractions, bulk accumulation rates, a numerical model of sediment supply, and statistical algorithms designed for compositional data. The integrated sediment-budget modelling

approach presented in this study is based on well-established techniques, and is potentially applicable to any basin.

Our first-order approach is designed to be internally consistent and produces reasonable results. Breakdown of the bulk sediment budget (Frignani et al., 2005) was achieved by combining grain-size and geochemical analyses. Multimodal GSDs of river-bed and offshore sediments were subdivided into two hydrodynamically distinct sub-populations (C and S fractions) by using the floc limit (Milligan et al., 2007). Statistically significant provenance groups in the C and S fractions correspond to contiguous and lithologically distinctive river basins. Based on the provenance analysis of the river samples and simulated sediment loads of corresponding river basins, we were able to calculate compositional fingerprints (end members) for both size fractions as linear combinations of supply-weighted compositions of river sediments. By means of a linear mixing model that employed these end members, the bulk chemistry of the Adriatic surface samples could be described in terms of provenance and grain size, and the sediment-dispersal patterns of the different provenance groups on the Northern Adriatic shelf could be visualized.

Mixing coefficients are sensitive to noise in cases where end members are compositionally similar. In general, such errors are expected to be random and will cancel each other if a sufficiently large number of samples are available for mapping. The limited number of mud-belt surface samples on which the sourcespecific mixing patterns are based thus imply that local deviations from expected patterns may occur. The apparent accumulation of Po/Adige sediment in front of the Apennine river mouths (Fig. 3.11A), as well as the apparent accumulation of Apennine sediment in the vicinity of the Po Delta (Fig. 3.11B) most likely represent artefacts of the unmixing procedure. However, we can observe that apparent underestimation of the proportion of Po/Adige sediment at one location (close to the Po Delta) is counterbalanced by apparent overestimation elsewhere (in front of the Apennine river mouths). Because proportions are constrained to unit sum, two opposite and similarly cancelling apparent systematic deviations are present in the accumulation pattern of Apennine sediment. Our estimates of source-specific accumulation rates (Table 3.6) closely match estimates of sediment-supply rates obtained by independent methods (Cattaneo et al., 2003; Syvitski and Kettner, 2007). We therefore conclude that the source-specific rates of sediment accumulation derived from our results are accurate, and allow us to calibrate the BQART model of sediment supply (Syvitski and Milliman, 2007) for present-day conditions. Similarly, our estimate of the rate of sand supply to the northern Adriatic mud belt (≈3 Mt yr¹) seems reasonable in the light of available bedload data of the Po and selected Apennine rivers collected between 1970 and 1990 (Preti, 1999). Our findings thus indicate that the integrated quantitative analysis of sediment supply, provenance and dispersal yields interpretable results.

On the decadal time scale associated with bulk accumulation rates based on ²¹⁰Pb and ¹³⁷Cs, the dispersal patterns of silt and mud already show signs of southward long-shore transport. On this time scale, Po/Adige sediments accumulate close to the Po delta (Fig. 3.11A), but Apennine sediments mainly accumulate in the area around the Gargano promontory where direct input of river sediments is limited (Fig. 3.11B). Accumulation of sand takes place around the Po delta and along parts of the Apennine coast, as well as directly North of the Gargano promontory (Fig. 3.10B). Brommer et al. (2009) show that the pattern of centennial averaged mass fluxes (1600 AD to present) indicates a significant cross-shore and along-shore displacement of sediments relative to the present-day situation (decadal average), which points to the low preservation potential of surface sediments. The dispersal patterns obtained from our analysis of modern surface sediments thus represent snapshots of transient features (cf. Jerolmack and Sadler, 2007). Consequently, one does not expect the underlying stratigraphic record to be a one-to-one image of the surface sediments. In order to examine if this is indeed the case, the integrated approach advocated in this study could be extended to the subsurface by geochemical analysis of sediment cores, provided seismic data and time control permit subdivision of the stratigraphic record into basin-wide time slices.

APPENDIX 3.1: CORE LOCATIONS, GRAIN-SIZE PARAMETERS AND GEOCHEMICAL DATA

Table 3.1:Core locations and grain-size parameters (μm)

Core ID	Lon. E	Lat. N	< 18 µm	18-60 μm	> 60 µm	log D	log D	log D
			mud %	silt %	sand %	mud	silt	sand
POP01-1	12.531	44.836	70.52	27.87	1.61	0.64	1.44	1.85
AD78-177	12.665	44.800	76.89	21.76	1.35	0.57	1.44	1.85
CM94-88	12.310	44.797	4.51	4.88	90.61	0.65	1.56	2.16
GORO3	12.278	44.793	7.88	6.22	85.90	0.61	1.55	2.12
CM94-82	12.407	44.784	46.06	28.25	25.69	0.68	1.47	2.22
CM94-84	12.359	44.779	8.30	7.78	83.92	0.64	1.56	2.12
CM95-12	12.652	44.778	73.89	23.54	2.57	0.57	1.45	1.90
CM95-13	12.715	44.750	79.02	18.74	2.24	0.56	1.43	2.11
RER96-6	12.365	44.698	66.12	31.01	2.87	0.62	1.46	1.86
RER96-8	12.354	44.661	51.40	28.60	20.01	0.59	1.51	1.94
RER96-9	12.332	44.630	60.18	35.94	3.88	0.66	1.47	1.86
CM92-18	12.433	44.574	73.21	24.60	2.19	0.60	1.45	1.86
RER96-13	12.356	44.556	67.06	31.80	1.14	0.63	1.45	1.83
RER96-16	12.351	44.503	31.29	35.02	33.68	0.66	1.51	2.06
CM95-31	12.574	44.493	74.14	17.05	8.80	0.57	1.43	2.31
RER96-19	12.371	44.432	64.24	30.25	5.51	0.63	1.47	1.89
RER97-5	12.665	44.294	67.68	30.22	2.10	0.63	1.45	1.85
RER97-4	12.621	44.256	48.42	41.54	10.04	0.68	1.47	1.99
RER97-6	12.633	44.199	50.76	42.22	7.02	0.65	1.49	1.86
AD87-1	12.895	44.106	66.92	29.49	3.59	0.61	1.46	1.87
AN97-37	12.940	44.094	60.45	30.13	9.42	0.61	1.48	1.94
RER97-11	12.635	44.090	36.22	38.53	25.24	0.65	1.51	2.02
CM95-21	13.157	44.061	70.09	25.29	4.62	0.58	1.46	1.90
AD87-2	12.851	44.047	51.94	28.96	19.11	0.61	1.49	1.95
RER97-12	12.632	44.046	23.71	13.26	63.04	0.69	1.52	2.07
CM95-34	13.157	44.023	73.21	24.47	2.32	0.59	1.45	1.87
CM95-33	13.158	43.971	64.49	31.66	3.85	0.62	1.47	1.87
AN97-3	13.387	43.913	68.02	26.14	5.84	0.58	1.47	1.91
AN97-2	13.336	43.877	65.13	30.76	4.11	0.62	1.46	1.88
AN97-15	13.642	43.755	68.03	29.33	2.64	0.60	1.46	1.86
AN97-7	13.819	43.754	75.52	22.92	1.56	0.56	1.45	1.85
AN97-13	13.631	43.754	74.01	24.64	1.36	0.59	1.44	1.85
AN97-8	13.920	43.753	76.23	22.20	1.57	0.56	1.45	1.85
KS02-246	14.047	43.340	74.92	20.63	4.45	0.58	1.44	2.04
AN97-28	14.074	43.253	87.57	12.23	0.20	0.55	1.41	1.83
AN97-29	14.211	43.167	89.34	10.64	0.02	0.54	1.38	1.80

AN97-27 14.216 43.164 62.48 27.25 10.27 0.60 1.46 2.28 AD86-11 14.161 43.148 71.58 26.46 1.96 0.59 1.45 1.86 AD86-30 13.949 42.926 13.80 14.95 71.25 0.67 1.57 2.00 AD86-33 14.263 42.863 87.42 12.30 0.28 0.53 1.41 1.84	
AD86-30 13.949 42.926 13.80 14.95 71.25 0.67 1.57 2.00	
AD86-33 14.263 42.863 87.42 12.20 0.28 0.53 1.41 1.84	
11.00 00 11.200 12.000 07.42 12.00 0.20 0.00 1.41 1.04	
CSS00-24 14.165 42.785 77.59 21.73 0.68 0.59 1.43 1.84	
CSS00-23 14.165 42.785 77.20 21.81 0.99 0.59 1.44 1.84	
PAL94-9 14.493 42.585 88.19 11.29 0.52 0.51 1.42 1.85	
COS01-32 14.446 42.506 81.38 18.37 0.25 0.55 1.42 1.82	
CSS00-5 14.469 42.488 81.15 18.61 0.24 0.57 1.41 1.83	
CSS00-4 14.469 42.488 92.19 7.81 0.00 0.57 1.34 -	
CSS00-20 14.472 42.486 76.44 20.19 3.37 0.56 1.46 1.90	
CSS00-6 14.475 42.484 88.88 11.11 0.01 0.56 1.37 1.80	
CSS00-21 14.476 42.476 75.32 22.90 1.78 0.57 1.46 1.85	
RF95-15 14.452 42.453 53.94 21.15 24.91 0.58 1.48 2.12	
RF95-17 14.448 42.449 64.58 27.71 7.71 0.58 1.48 1.91	
RF95-18 14.437 42.442 52.63 35.53 11.84 0.58 1.50 1.89	
RF95-19 14.438 42.442 56.41 37.42 6.17 0.61 1.49 1.86	
COS01-23 14.431 42.441 59.56 31.99 8.45 0.60 1.50 1.88	
RF95-20 14.436 42.439 54.88 24.70 20.42 0.58 1.48 2.04	
CSS00-2 14.866 42.270 89.62 10.35 0.03 0.56 1.37 1.83	
CSS00-1 14.862 42.267 95.98 4.02 0.00 0.51 1.33 -	
RF95-13 14.906 42.238 80.19 18.31 1.50 0.54 1.45 1.86	
RF95·14 14.896 42.233 75.80 20.33 3.87 0.56 1.45 1.93	
AD85-33 15.773 42.185 93.28 6.68 0.04 0.48 1.38 1.82	
CSS00-18 16.155 42.101 91.69 8.27 0.04 0.50 1.39 1.82	
RF95-1 15.401 42.097 89.98 9.88 0.14 0.51 1.40 1.83	
COS01-9 16.339 42.092 80.42 9.82 9.76 0.47 1.43 2.28	
COS01-10 16.370 42.072 51.07 10.99 37.94 0.48 1.48 2.26	
RF93-30 15.668 42.067 82.45 17.23 0.32 0.56 1.42 1.83	
RF93-31 15.710 42.026 71.92 27.95 0.13 0.60 1.42 1.81	
COS01-25 15.140 42.015 38.03 32.23 29.75 0.58 1.54 1.93	
RF93-32 15.831 41.995 28.23 31.25 40.52 0.61 1.56 1.93	
AMC99-7 16.393 41.839 71.82 15.25 12.92 0.54 1.45 2.10	
COS01-11 16.622 41.824 74.08 11.53 14.39 0.49 1.44 2.24	
COS01-16 16.463 41.724 86.87 12.93 0.20 0.53 1.41 1.83	
COS01-18 16.463 41.724 83.41 15.52 1.07 0.55 1.43 1.87	
AMC99-12 16.319 41.632 76.83 21.68 1.49 0.57 1.45 1.85	
CSS00-7 16.846 41.221 91.18 8.50 0.32 0.50 1.41 1.87	
CSS00-12 16.899 41.164 74.28 20.27 5.45 0.53 1.47 1.92	
CSS00-11 17.242 41.045 85.56 13.98 0.46 0.50 1.43 1.83	

Table 3.2: Chemical compositions (XRF) of C fraction [g kg⁻¹].

Sample	Na	Mg	Al	Si	P	K	Ca	Ti	Mn	Fe	Rest
Adige	13.79	31.08	50.58	193.23	9.73	24.97	110.87	4.25	0.79	48.58	512.13
Po	8.56	23.13	58.52	199.95	5.92	25.36	111.15	3.31	1.05	50.16	512.89
Montone	11.66	19.65	62.81	175.89	8.48	17.70	133.39	3.85	0.76	43.84	521.97
Bevano	13.72	13.58	59.89	186.84	9.57	15.57	137.16	3.81	0.65	42.03	517.18
Uso	17.89	15.16	66.59	202.85	11.97	17.06	96.72	4.07	0.79	46.83	520.08
Conca	7.98	16.32	68.98	198.99	5.65	13.67	108.93	4.03	1.04	52.77	521.65
Foglia	14.46	22.36	63.67	183.28	9.92	18.46	117.03	3.83	0.71	42.92	523.36
Metauro	9.41	14.77	60.73	170.15	6.77	15.90	148.48	3.44	0.69	41.30	528.35
Esino	6.50	12.23	55.63	187.24	4.25	14.74	145.82	3.89	0.57	35.68	533.47
Musone	38.88	11.32	48.68	157.87	23.54	12.83	149.09	3.15	0.81	32.46	521.36
Potenza	14.99	11.60	60.24	181.72	10.17	14.41	132.06	3.71	0.57	40.40	530.13
Chienti	42.14	10.91	54.26	153.75	29.87	13.60	132.78	3.13	0.95	38.35	520.28
Aso	33.58	11.72	50.62	149.43	24.00	13.24	157.60	3.11	0.75	36.58	519.37
Tronto	21.78	16.97	54.64	162.99	15.20	15.27	144.50	3.43	0.50	36.50	528.21
Tordino	12.25	16.76	63.89	179.37	8.67	16.89	127.03	3.72	0.63	42.43	528.35
Vomano	26.76	19.19	58.17	177.34	18.91	16.74	119.15	3.65	0.65	41.46	517.99
Sangro	19.97	11.29	68.92	179.25	13.70	13.27	116.33	4.22	0.83	49.64	522.56
Trigno	14.93	15.23	65.75	179.57	10.55	15.68	127.67	3.97	0.90	43.74	522.00
Biferno	40.82	9.12	61.07	177.74	29.03	12.56	111.70	3.85	1.05	40.39	512.67
Fortore	20.10	10.54	74.75	212.88	14.46	18.90	82.45	4.46	0.74	45.79	514.93
Ofanto	38.99	9.53	65.81	174.82	27.09	14.40	116.97	3.81	1.80	43.58	503.21
CM95- 13	19.96	30.17	65.75	169.22	14.11	19.06	108.30	3.95	0.64	45.53	523.33
CM92- 18	11.53	23.44	71.47	200.52	7.98	21.13	94.37	4.30	0.79	49.03	515.44
CM95- 33	11.57	22.26	65.93	199.51	8.20	18.68	101.19	4.14	0.78	46.26	521.49

AN97- 03	15.70	21.89	65.36	192.63	11.05	18.42	111.16	4.13	0.79	44.97	513.90
AN97- 02	38.83	19.96	64.56	175.36	26.04	16.75	94.53	3.59	0.78	44.81	514.79
AN97- 08	12.27	21.65	66.73	182.88	8.63	19.66	116.30	3.89	0.84	45.84	521.30
AN97- 28	19.72	18.15	64.06	178.56	14.43	18.05	116.87	3.72	0.77	43.15	522.53
CSS00- 02	13.76	18.49	65.21	185.37	8.97	18.79	119.04	3.91	0.84	45.93	519.69
AD85- 33	30.65	16.79	66.38	167.06	21.79	15.82	107.71	3.45	0.89	46.26	523.20
RF95-01	17.69	17.34	66.57	174.60	12.37	15.32	118.37	3.72	0.76	44.68	528.57
AMC99- 14	57.64	13.96	64.83	162.22	40.68	17.53	89.78	3.31	0.59	42.36	507.10
AMC99- 12	34.67	15.37	62.30	172.88	24.28	15.22	110.86	3.75	0.71	41.98	517.99
CSS00- 07	30.04	15.69	71.56	181.91	20.21	18.10	94.47	3.94	0.72	47.42	515.94
CSS00- 12	30.04	14.24	73.91	187.07	21.35	17.20	89.14	4.14	0.66	48.94	513.31

 $\textbf{Table 3.3}: \mbox{ Chemical compositions (ICP) of S fraction [g \mbox{ kg}^{\mbox{-}1}]$.}$

Sample	Na	Mg	Al	K	Ca	Ti	\mathbf{Cr}	Mn	Fe	Zn	Rest
Adige	8.41	39.41	44.63	14.43	110.20	4.67	0.08	0.50	23.51	0.15	754.00
Po	3.29	8.44	28.80	5.94	176.07	1.36	0.05	0.74	17.87	0.05	757.40
Uso	7.57	14.77	43.90	12.37	113.12	1.92	0.10	1.02	24.99	0.07	780.17
Montone	11.18	19.46	55.05	17.78	79.87	2.22	0.08	1.36	25.08	0.06	787.86
Bevano	11.76	13.18	48.10	14.36	83.48	2.38	0.07	0.86	22.74	0.06	803.02
Foglia	9.20	23.93	43.61	14.59	92.07	2.35	0.10	0.69	17.93	0.06	795.49
Metauro	6.66	11.83	37.06	10.35	130.02	1.76	0.08	0.57	17.17	0.06	784.45
Musone	9.31	8.18	34.05	10.82	132.96	1.60	0.05	0.63	13.43	0.05	788.91
Chienti	10.22	9.45	39.43	11.25	115.93	1.90	0.06	0.61	15.90	0.04	795.21
Aso	11.53	9.65	35.64	11.63	100.12	2.00	0.04	0.37	11.04	0.04	817.92
Tronto	9.02	16.01	43.82	12.26	109.85	2.14	0.06	0.46	18.73	0.06	787.61
Sangro	7.39	10.05	31.15	8.93	149.19	1.42	0.04	0.74	13.28	0.03	777.78
Biferno	7.33	6.73	40.16	12.78	115.53	1.59	0.04	1.05	18.65	0.04	796.09
Ofanto	7.42	6.23	37.66	12.28	94.62	2.08	0.05	1.14	17.40	0.04	821.08
CM95-13	16.75	32.77	60.39	19.86	107.10	2.60	0.11	0.60	27.66	0.12	732.05
CM92-18	14.05	26.87	77.25	25.19	86.87	3.11	0.15	0.89	40.28	0.14	725.19
AN97-03	19.48	21.70	58.52	18.19	103.04	3.06	0.10	0.64	27.45	0.08	747.73
AN97-08	13.98	20.57	52.20	16.06	131.82	2.31	0.08	0.59	19.86	0.05	742.49

AN97-28	13.97	18.57	71.05	23.77	87.64	2.61	0.12	0.87	39.54	0.27	741.58
CSS00- 02	15.58	16.12	52.62	17.66	125.80	2.24	0.09	0.79	25.03	0.07	744.00
AD85-33	15.36	16.61	60.49	19.40	136.20	2.82	0.09	1.28	34.53	0.17	713.05
RF95-01	19.33	17.65	66.66	23.54	108.34	2.57	0.10	0.74	36.62	0.12	724.33
AMC99- 14	16.19	14.41	58.58	18.27	113.59	2.49	0.08	0.72	27.88	0.08	747.71
AMC99- 12	12.25	13.12	50.48	16.30	123.68	2.19	0.06	0.74	23.41	0.06	757.71
CSS00- 07	12.49	12.73	55.18	17.93	119.27	2.20	0.06	0.78	43.96	0.07	735.33

APPENDIX 3.2: COMPOSITIONAL DATA ANALYSIS

Compositional or closed data are constrained to be positive and sum to unity:

$$\mathbf{x} = [x_1, ..., x_D]', x_i > 0, \sum_{i=1}^{D} x_i = 1$$
(3.2A1)

The set of all composition vectors, denoted by S^D , forms a simplex sample space, a subspace of R^D . Application of standard statistical methods designed for use with unconstrained data can lead to meaningless results if applied to compositional data. For this reason, the family of one-to-one logratio transformations from S^D to the real space was introduced (Aitchison, 1986). In this study two types of logratio transformation are used: the additive logratio (alr) transformation and the centred logratio (ch) transformation.

Additive logratio (alr) transformation: This is a transformation from S^D to R^{D-1} , and the result for an observation $\mathbf{x} \in S^D$ are the transformed data $\mathbf{x}^{(j)} \in R^{D-1}$ with

$$\mathbf{x}^{(j)} = \left[x_1^{(j)}, ..., x_{D-1}^{(j)}\right]' = \left[\log \frac{x_1}{x_j}, ..., \log \frac{x_{j-1}}{x_j}, \log \frac{x_{j+1}}{x_j}, ..., \log \frac{x_{D-1}}{x_j}\right]'$$
(3.2A2)

The index $j \in \{1,...,D\}$ refers to the variable selected as common denominator in the transformation. The main advantage of the alr transformation is that it represents compositional data in an unconstrained form in the real space. The inverse alr transformation from R^{D-1} to S^D (also called the additive logistic transformation) is defined as:

$$x_{i} = \frac{\exp(x_{i}^{(j)})}{\exp(x_{i}^{(j)}) + \dots + \exp(x_{D-1}^{(j)}) + 1} \text{ for } i = 1, \dots, D, i \neq j$$
(3.2A3)

$$x_{j} = \frac{1}{\exp(x_{i}^{(j)}) + \dots + \exp(x_{D-1}^{(j)}) + 1} \text{ for } j \in \{1, \dots, D\}$$
(3.2A4)

Centred logratio (clr) transformation: This transformation, which is symmetrical with respect to the vector elements of \mathbf{x} , was designed for the purpose of multivariate analyses such as the cluster analysis applied in this study. Compositions $\mathbf{x} \in S^D$ are transformed to $\mathbf{y} \in R^D$, with

$$\mathbf{y} = \left[y_1, ..., y_D\right]' = \left\lceil \log \frac{x_1}{g(\mathbf{x})}, ..., \log \frac{x_D}{g(\mathbf{x})} \right\rceil'$$
(3.2A5)

where the function $g(\mathbf{x})$ represents the geometric mean of \mathbf{x} :

$$g\left(\mathbf{x}\right) = D \prod_{i=1}^{D} x_{i} \tag{3.2A6}$$

The inverse clr transformation is expressed as:

$$x_{i} = \frac{\exp(y_{i})}{\sum_{i=1}^{D} \exp(y_{i})} \text{ for } i = 1,...,D$$
(3.2A7)

Geostatistical interpolation of compositional variables is conveniently carried out by first applying a log-ratio transformation (Equation 3.2A2). The unconstrained variable is then interpolated on a regular grid, after which the interpolated values are subjected to the inverse log-ratio transformation (Equation 3.2A3).

APPENDIX 3.3: CLUSTER ANALYSIS

Cluster analysis is an empirical classification technique aimed at subdividing observations into a certain number of groups. Since the number of groups is unknown *a priori*, feasible solutions require that each group is more-or-less homogeneous and distinct from other groups (Davis, 2002). The technique works with a measure of similarity and aims at an optimal subdivision of the sample according to a given criterion.

Our original datasets X consist of n objects and D variables, in which each row vector x is a composition. The objects represent the river samples (n=20) for the C fraction and (n=13) for the S fraction. The variables represent the measured element concentrations for the C and S fractions (D=10). We applied Ward's cluster analysis on the clr-transformed compositional data of the C and S fractions separately. The Aitchison distance δ_a between the observed vector x and its estimate $\hat{\mathbf{x}}$ is the square root of:

$$\delta_a^2(\mathbf{x}, \hat{\mathbf{x}}) = \sum_{i=1}^D \left\{ \log \left(\frac{x_i}{g(\mathbf{x})} \right) - \log \left(\frac{\hat{x}_i}{g(\hat{\mathbf{x}})} \right) \right\}^2$$
(3.2A8)

where $g(\mathbf{x})$ is the geometric mean of the components of \mathbf{x} and $g(\hat{\mathbf{x}})$ the corresponding function of $\hat{\mathbf{x}}$. The use of clr-transformed compositional data implies that the conventional Euclidian distance employed by Ward's method corresponds to the Aitchison distance defined for compositional data (Pawlowsky-Glahn and Olea, 2004).

APPENDIX 3.4: PERMUTATION TEST

A permutation test is a stochastic simulation (randomization) method, which is used to determine whether an observed effect, such as a difference between two means or the correlation between two variables, is significant at a user-specified level α . The null hypothesis in this case is that clustering of the data is attributable to a random effect (sampling error). This hypothesis is tested by means of repeated column-wise randomization of the original data, which does not affect the characteristics of the marginal distributions (means and standard deviations of alr-transformed columns), but destroys the covariance structure of the data set. All randomized data sets thus represent realizations of the measurement process under the null hypothesis.

Repeated randomizations (in our case 1000 times) allow us to construct an empirical distribution of Aitchison distances, which approximates the sampling distribution under the null hypothesis. The full analysis comprises the following steps:

- 1) Transform the original data set to log ratios by means of the alr-transformation (Eqn. 3.2A2);
- 2) Randomize each column of the alr-transformed data matrix separately;
- 3) Carry out the inverse alr-transformation of randomized data (Eqns. 3.2A3, 3.2A4);
- 4) Transform the randomized data by means of the clr-transformation (Eqns. 3.2A5, 3.2A6);
- 5) Apply Ward's cluster analysis to the clr-transformed data;
- 6) Save all Aitchison distances;
- 7) Repeat steps 2 to 6 at least 1000 times;
- 8) Sort the Aitchison distances to obtain a cumulative distribution function (CDF);
- 9) Determine the critical distance corresponding to significance level α;
- 10) Apply Ward's cluster analysis to the clr-transformed original data;
- 11) Partition the original data set into statistically significant clusters (separated by distances which exceed the critical distance).

Chapter 4

Sediment supply to the Northern Adriatic Basin over the past 19.000 years: data-model comparison using a mass-balance approach

4.1 INRODUCTION

The natural unit in the "source-to-sink" view of earth-surface dynamics is the sediment dispersal system, consisting of a drainage basin in which sediments are generated (the source) and a sedimentary basin in which they are deposited (the sink). Source-to-sink analysis of sediment dispersal systems attempts to make optimal use of geo(morpho)logical information through integration of observations and models of earth-surface dynamics and the stratigraphic record. Knowledge of rates of mass transfer from source to basin on geological timescales forms an essential link between stratigraphic and geomorphologic modelling (e.g. Leeder, 1997; Weltje et al., 1998; Paola and Swenson, 1998; Yoo et al., 2007). However, direct comparisons of sediment fluxes in the two domains are almost non-existent, and conservation of mass, a basic principle of physics, plays a subordinate role in quantitative models of earth-surface evolution and analysis of sediment dispersal systems. The difficulty of implementing mass conservation constraints on the stratigraphic record is attributable to its incompleteness and transient nature (Sadler, 1981; Sommerfield, 2006; Jerolmack and Sadler, 2007), which is a manifestation of spatio-temporal variability of erosion and deposition. Of particular importance for understanding the formation of shelf stratigraphy and implementing mass conservation constraints on the stratigraphic record is the time scale at which transience gives way to persistence. On continental shelves and coastal plains this transition usually takes place on a time scale of 103 to 104 years (Jerolmack and Sadler, 2007).

In basins which behave as closed systems on geological time scales, the quantity of sediment supplied by the source equals the quantity of sediment deposited in the sink, because mass is conserved. However, even under these conditions, net basin-wide mass-accumulation rates cannot be directly translated into rates of sediment supply (Brommer et al., 2009). Apart from the practical problems related to the limited precision of stratigraphic data, the main complicating factor is recycling of sediments, which causes sediments deposited in a given time interval to be reworked and incorporated into

younger units (Einsele, 2000). Hence, even in closed basins, direct calculation of long-term sediment supply rates from the stratigraphic record is only valid if the quantity of sediment subjected to intrabasinal erosion and recycling is insignificant relative to the amount of sediment supplied to the basin (Einsele and Hinderer, 1998). As a general rule, only lithosomes in closed basins that are bounded by conformable (non-erosional) surfaces are expected to contain the quantity of sediment supplied during the time interval corresponding to that unit (Brommer et al., 2009).

Brommer et al. (2009) analysed a high-resolution seismic-stratigraphic data set from the Northern Adriatic basin (Italy; Fig. 4.1), which spans the last 19 kyr, to obtain basin-wide mass accumulation rates. Because the Northern Adriatic acted as a closed system, this record should reflect the history of sediment supply over the same interval, modulated by effects of sediment recycling due to spatio-temporal erosion and redistribution of sediments. Quantification of the uncertainties of the estimates obtained by Brommer et al. (2009) allowed a probabilistic comparison of basin-wide mass-accumulation rates across the five time intervals. They were unable to reject the null hypothesis that the millennial-scale averages of net basin-wide mass-accumulation rates are equal (at the 10% significance level). This result seems to indicate that there are limits to the reconstruction of climatically forced changes in sediment supply rates from the stratigraphic record, as postulated by Jerolmack and Sadler (2007).

In this Chapter, we will apply the most recent version of BQART/HydroTrend, a numerical model of water and sediment delivery from fluvial drainage basins to river mouths (Kettner and Syvitski, 2008; Syvitski and Milliman, 2007) to simulate sediment supply to the Northern Adriatic based on palaeo-climate proxies derived from Global Circulation Models and drainage-basin physiography. The HydroTrend model was designed to simulate discharges of present-day fluvial drainage basins. Its predictive capabilities have been demonstrated in a series of tests on modern rivers (Syvitski et al., 2005; Syvitski and Milliman, 2007; Syvitski and Kettner, 2007). Although the model has also been applied in reconstructions of basin-fill histories (Overeem et al., 2005; Kubo et al., 2006), its performance over long time scales has not been formally evaluated. The fact that the Adriatic basin is a closed system allows us to perform a data-model comparison based on the principle of mass balance, which serves as the first quantitative test of the BQART/HydroTrend model on geological timescales.

A quantitative mass balance study of the closed Adriatic basin spanning the time interval from 19 ka BP to the present requires independent estimates of supply and accumulation rates. In addition, a statistically rigorous comparison of these rates should be carried out, which implies that the uncertainties associated with all estimates must be quantified. In the first part of this Chapter, we use the BQART/HydroTrend model (Syvitski and Milliman, 2007; Kettner and Syvitski, 2008) to derive estimates of average basin-wide sediment supply rates, and estimate the associated uncertainties for five time intervals

spanning the last 19.000 years. In the second part, we compare the data on basin-wide mass accumulation presented by Brommer et al. (2009) with the BQART/HydroTrend modelling results, and discuss the implications for stratigraphic modelling.

4.2 SETTING

4.2.1 The Adriatic Basin

The narrow and elongated land-locked Adriatic basin (200x800 km) is bounded by the Dinarides to the East, the Alps to the North and the Apennines to the West (Fig. 4.1). The Northern Adriatic Basin mainly receives sediments from the North and West (Cattaneo et al., 2003). The Northern Adriatic shelf is shallow and has a low gradient (0.05°). The Mid-Adriatic Deep (MAD), a depression in the centre of the Adriatic, acted as a sediment trap during the last glacial maximum (Cattaneo et al., 2003; Ridente and Trincardi, 2005). Deglacial sea level rise, which commenced ≈21 ka BP, caused a dramatic increase in volume and area of the Adriatic basin. Owing to changing oceanographic conditions, a counter-clockwise longshore current established at ≈14 ka BP (Cattaneo and Trincardi, 1999). From that time on, fine-grained sediment dispersed to the Adriatic Sea by Alpine and Apennine Rivers was conveyed to the south to form an elongate shore-parallel prodelta of the Alpine and Apennine Rivers. The prodelta extends to the area south of the Gargano peninsula. Remnant sandy deposits, representing a series of drowned barrier-lagoon complexes formed during relative sea level rise, are present in the axial part of the Northern Adriatic shelf (Storms et al., 2008).

The deposits of the past 19 kyr, which comprise the Transgressive and Highstand Systems Tracts (TST and HST, respectively), have been subdivided into five lithosomes that can be traced throughout the present onshore and offshore of the Northern Adriatic basin. Correggiari et al. (2001) subdivided the Highstand Systems Tract (HST) into an upper or Little Ice Age unit (HST-2; 0.4 - 0 ka BP) and a lower unit (HST-1: 5.5 - 0.4 ka BP). These two units are bounded by conformable surfaces, the lowermost of which represents the maximum flooding surface (MFS). The three lithosomes comprising the Transgressive Systems Tract, which contain the record of abrupt deglacial sea level rise, are the upper unit (TST-3; 11.3 - 5.5 ka BP), the middle unit (TST-2; 14.8 - 11.3 ka BP), and the lower unit (TST-1; 19.0 - 14.8 ka BP) (Cattaneo and Trincardi, 1999). These units are separated by unconformable ravinement surfaces, which the exception of the lower TST unit, which is bounded locally by the maximum regressive surface (MRS; Trincardi et al., 1994). Figure 4.2 illustrates the stratigraphic record of the Adriatic Basin and the five time slices used by Brommer et al. (2009) to derive basin-wide mass accumulation rates.

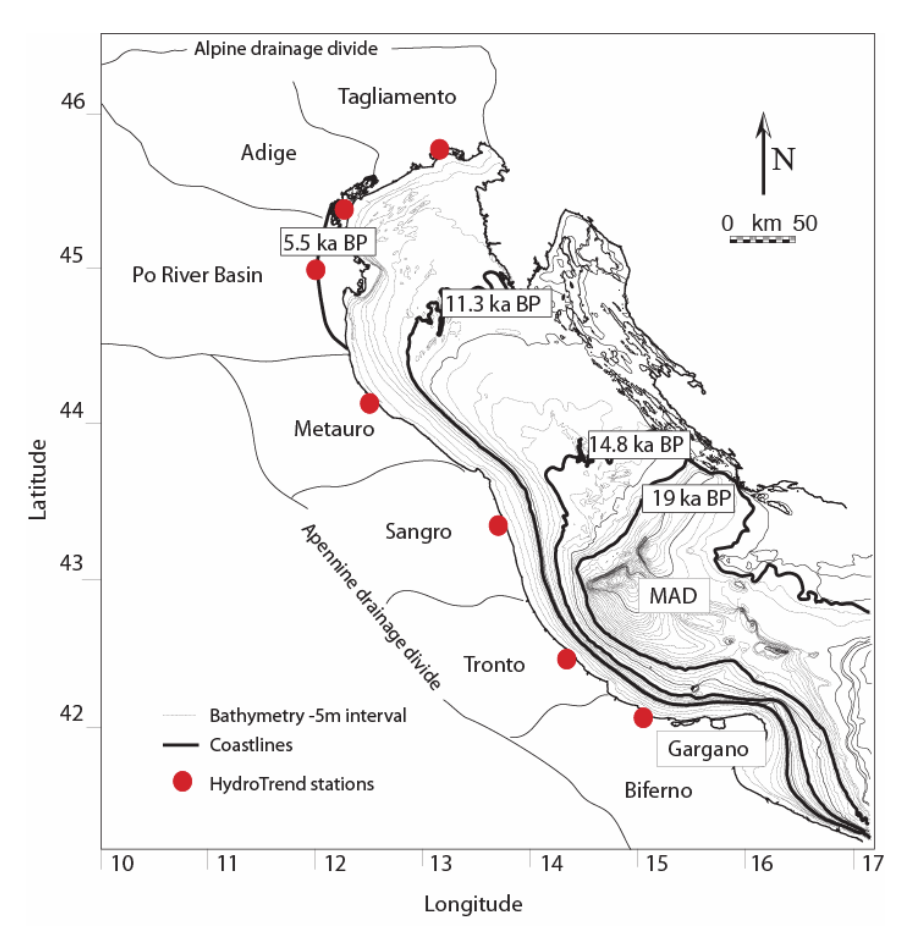


Figure 4.1: Adriatic Basin, Italy. The red dots indicate the HydroTrend stations with corresponding river basins and source areas.

4.2.2 River basins

Broadly speaking, the river basins surrounding the Northern Adriatic Sea fall into three groups: the Eastern Alpine river basins, the Po River basin, and the Apennine river basins. However, given the variability of river-basin characteristics, such as basin area, maximum elevation, and dominant lithology, a further subdivision was required. In total, seven groups of river basins were distinguished to represent the source areas of the Northern Adriatic basin fill (Fig. 4.1).

The Eastern Alpine drainage basins were subdivided into two source areas. Rivers belonging to the Tagliamento source area predominantly drain carbonate lithologies (limestones and dolostones) of the Calcareous Southern

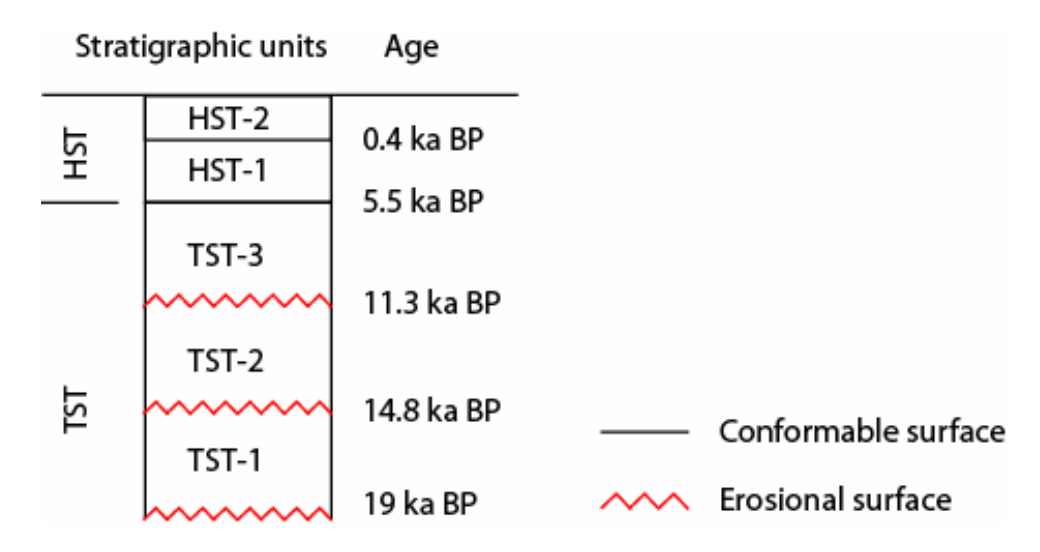


Figure 4.2: Stratigraphic record of the Adriatic Basin spanning the time interval of 19.000 years (after Brommer et al., 2009).

Alps (Castellarin and Vai, 1982). These rivers have drainage basins with similar dimensions. The Adige River was excluded from the Tagliamento group because its drainage basin is much larger. In addition, the Adige cuts into metamorphic rocks of the Austroalpine platform in its upper reaches, and into porphyries of the Atesine platform in its lower reaches (Dinelli and Lucchini, 1999). The maximum elevation in the Eastern Alpine basins is approximately 3500 m.

The Po River Basin, which drains both the Alps and Apennines, is the largest river basin in the study area (≈75.000 km²). The western Alps consist of metamorphic rocks of the crystalline basement (micaschist, gneiss, phyllites and marbles) and various kinds of intrusive rocks (granites, syenites, peridotites). The tributaries from the central Alps mainly drain sedimentary rocks such as limestones and dolostones. The Apennine tributaries of the Po River drain shales, marls and sandstones (Dinelli and Lucchini, 1999). The maximum elevation in the Po Basin is approximately 4200 m.

The Apennine rivers are characterized by their short courses (~150 km) and steep profiles (Cattaneo et al., 2003). We subdivided the Apennine drainage basins into four groups (Fig. 4.1). Rivers corresponding to the northernmost source area (Metauro group) drain the Northern Apennine succession, which is mainly composed of sandstones and (calcareous) mudstones of the Marnoso-Arenacea Formation (Dinelli and Lucchini, 1999). The Central Apennine Rivers of the Tronto group mostly drain turbidites (sandstones and calcareous mudstones) of the Laga Formation, as well as Pliocene (calcareous) mudstones (Dinelli and Lucchini, 1999). The rivers corresponding to the Sangro group

mainly drain limestones and dolostones of the Apennine Mesozoic platform (Dinelli and Lucchini, 1999). In addition, the rivers within the Sangro group are larger and the average elevation in their drainage basins exceeds that of the other Apennine source areas. The last group of rivers correspond to the Southern Apennine Biferno source area. These rivers drain limestones and dolostones of the Apennine Mesozoic platform, Oligo-Miocene turbidite deposits, and Plio-Pleistocene sands and calcareous mudstones (Dinelli and Lucchini, 1999).

4.3 SEDIMENT SUPPLY MODEL

We used the BQART equation (Syvitski and Milliman, 2007) in conjunction with the HydroTrend model (Kettner and Syvitski, 2008) to estimate liquid and solid discharge to the Adriatic basin over a time span of 19.000 years in time steps (epochs) of 200 years. Both models were designed to predict liquid and solid discharges of present-day fluvial drainage basins. The above authors have described and discussed these models in considerable detail. In this Chapter, we apply the BQART/HydroTrend model in a slightly different way: a brief discussion of the components that are relevant to our numerical experiment is provided below.

The long-term average suspended sediment discharge (Qs) of a fluvial drainage basin is based on the BQART Equation for $T \ge 2$ °C (Syvitski and Milliman, 2007):

$$Qs = \omega B \left(\frac{Q}{Q_0}\right)^{0.31} A^{0.5} RT \tag{4.1}$$

where Qs is the long-term average sediment load [Mt yr¹], A is the drainage area [km²], R is the maximum elevation in the drainage basin [km], and T is the basin-averaged temperature [°C]. Q is the long-term average discharge [km³ yr¹]. $Q_0 \equiv 1$ [km³ yr¹] is a reference value introduced to form a non-dimensional ratio of long-term average discharge. The constant $\omega = 0.0006$ Mt yr¹¹ °C¹¹ km²².

B [-] is an aggregated variable, which accounts for geological and human impact factors (Syvitski and Milliman, 2007):

$$B = L(1 - T_e)E_h \tag{4.2}$$

where L [-] represent lithology-specific erodibility (L > 0), T_e [-] is the trapping efficiency of reservoirs and lakes ($0 \le T_e < 1$), and E_h [-] is human impact ($E_h > 0$).

Syvitski and Milliman (2007) proposed discrete values for lithology-specific erodibility (essentially a geometric series ranging from 0.5 to 3.0). The trapping efficiency (T_e) allows suspended sediment discharge to be scaled according to prevailing environmental conditions (e.g. glaciers), which control the retention of sediments in reservoirs. HydroTrend calculates sediment-trapping efficiency of reservoirs based on their location in the river network and their volume (Kettner and Syvitski, 2007). Syvitski and Milliman (2007) discuss estimation of the human impact factor (E_h), based on a combination of population density and per capita Gross National Product.

No attempt was made to simulate the bedload component of the rivers draining the Adriatic Basin. The northern Adriatic shelf is a muddy system, and the quantity of bedload delivered to the river mouth is negligible relative to the uncertainty associated with the total sediment load (see below).

4.4 INPUT DATA

4.4.1 Area (A) and elevation (R)

The physiography of the drainage basins, captured with A and R, remains constant over the duration of the simulation. The locations of the HydroTrend stations were fixed at the present-day coastline (for the high-gradient Alpine and Apennine river basins) or at the position of the coastline at the time of maximum flooding (in case of the low-gradient Po River basin; Fig. 4.1). This approach allows us to compare model predictions of sediment supply passing through these stations to the amount of sediment deposited downstream in the Adriatic Basin. River basin area (A) and maximum elevation (R) of the drainage basins (Table 4.1) were derived from the Shuttle Radar Topography Mission (SRTM) digital elevation models (http://srtm.usgs.gov/).

Table 4.1: BQART/HydroTrend input parameters

	7 110 1711	iyaro i i ci.	ia ilipat j	paramet
River Basin	B	A_{ref}	A_{tot}	R
Tagliamento	0.4	2656	11544	2.60
Adige	0.4	14441	-	3.85
Po	0.4	74259	-	4.75
Metauro	1.5	1381	14850	1.70
Tronto	1.5	1248	2748	2.45
Sangro	1.5	1712	5892	2.80
Biferno	1.5	1285	5436	2.05

4.4.2 Sediment storage and release (B)

The aggregated variable B reflects the long-term balance between rates of sediment generation L and sediment storage $(1-T_e)E_h$ in the fluvial drainage

basin (Eq. 4.2). Instead of estimating L, T_e and E_h separately (cf. Syvitski and Milliman, 2007), we estimated B directly from quantitative analysis of the present-day sediment budget (Chapter 3). The northern Adriatic mud belt is predominantly sourced by two geochemically distinct types of sediment. On average, the Po and Adige rivers combined supply ≈ 17 Mt yr⁻¹, whereas the mean annual supply of the Apennines equals ≈ 25 Mt. An excellent fit between the modern sediment budget and BQART model predictions for present-day climate conditions is obtained by setting B = 0.4 for the Po and Adige rivers, and B = 1.5 for the Apennine rivers. We assume that the values of B for the eastern Alpine rivers are identical to the Adige. We have used these values for the entire time interval covered by the simulation (Table 4.1), and have chosen to neglect possible variations in B attributable to sediment trapping in lakes and to human influence, which seems reasonable given the geological time scale covered by our modelling exercise.

4.4.3 Discharge (Q) and temperature (T)

Present-day temperature and precipitation data were derived from the National Oceanic and Atmospheric Administration (NOAA) database (http://www.noaa.gov/). Estimates of palaeo-temperature (T) and precipitation (P) were derived from output of the Community Climate Model Version 1 (CCM-1) (Kutzbach et al., 1998). The CCM-1 is a physical climate model, similar to other coupled atmosphere and ocean circulation models (Boville and Gent, 1998). The most appropriate boundary conditions for the component models in CCM-1 are the fluxes at the earth's surface. This philosophy is configured as a flux coupler (see Bryan et al., 1996 for further references). Palaeo-boundary conditions for climate simulations with the CCM-1 (Kutzbach et al., 1998) are (1) ice-sheet topography, (2) atmospheric carbon dioxide concentrations (CO₂ level), (3) orbital parameters and (4) length of seasons (days). The grid resolution is 3.5° latitude by 3.5° longitude. Ten simulated years of LGM climate (21 ka BP) in the form of daily temperature and precipitation were available to constrain the paleo-climate record (Kettner and Syvitski, 2007).

The averaged LGM and present-day values of T and P were interpolated over time using the normalized $\delta^{18}{\rm O}$ curve obtained from the GRIP ice core (Dansgaard et al., 1993) as a forcing factor, in order to construct a continuous 19-kyr-long record. These two variables were converted to discharges and basin-averaged temperatures by HydroTrend (Kettner and Syvitski, 2008), based on a water-balance model (Syvitski et al., 1998) and drainage-basin hypsometry, respectively. Because B, A, and R were kept constant during the simulations, all variability of sediment supply is assumed to reflect climate change. The climate-related input variables, discharge (Q) and temperature (T), are depicted in Figure 4.3.

4.5 UNCERTAINTY ANALYSIS

According to standard rules of error propagation, the RSS (root-sum-squares) approximation for relative errors may be used to derive the fractional uncertainty of the BQART/HydroTrend model under the assumption that the uncertainties of input variables are uncorrelated (Taylor, 1982). Hence, the uncertainty of the model output (Eqn. 4.1) can be expressed as:

$$\frac{\delta Qs}{Qs} = \sqrt{\left(\frac{\delta B}{B}\right)^2 + 0.31 \left(\frac{\delta Q}{Q}\right)^2 + 0.5 \left(\frac{\delta A}{A}\right)^2 + \left(\frac{\delta R}{R}\right)^2 + \left(\frac{\delta T}{T}\right)^2} \tag{4.3}$$

The fractional uncertainty for a DEM-derived basin area (A) is based on a geometric argument (Syvitski et al., 2003):

$$\frac{\delta A}{A} \approx 3.5 \sqrt{\frac{\Delta A}{A}} \tag{4.4}$$

where ΔA [km] is the resolution of the DEM. The SRTM dataset has a resolution of 0.09 km. The average source area in our case study is 10.000 km², which implies that the fractional uncertainty in A is:

$$\frac{\delta A}{A} = 0.003\tag{4.5}$$

The fractional uncertainty of maximum elevation R in a DEM-derived basin is (Syvitski et al., 2003):

$$\frac{\delta R}{R} = 0.01\tag{4.6}$$

The fractional uncertainty of Q, based on simulated precipitation data by CCM-0 and CCM-1 during the LGM (Kutzbach et al., 1998; Bartlein et al., 1998) is estimated as:

$$\frac{\delta Q}{O} = 0.30\tag{4.7}$$

LGM surface temperatures simulated with the CCM-1 are accurate to within 2^0 C (Kutzbach et al., 1998). The average basin temperature used for our study is 15^0 C. Hence, the relative error of T is estimated as:

$$\frac{\delta T}{T} = 0.13\tag{4.8}$$

The aggregated variable B of the BQART equation comprises three variables: L, T_e and E_h (Eqn. 4.2). The fractional uncertainty of B is therefore:

$$\frac{\delta B}{B} = \sqrt{\left(\frac{\delta L}{L}\right)^2 + \left(\frac{\delta T_e}{T_e}\right)^2 + \left(\frac{\delta E_h}{E_h}\right)^2} \tag{4.9}$$

Syvitski and Milliman (2007) provided guidelines for estimation of L, T_e and E_h . The difficulty of accurately estimating the three parameters included in B (Eqn. 4.3) is known as the identifiability problem (Merritt et al., 2003). An infinite set of parameter combinations could be invoked to "explain" a given value of B if insufficient information is available to constrain at least two out of three parameters, because the individual parameters cannot be resolved by calibration of model output to data. As shown in Chapter 3, B can be estimated from quantitative analysis of the present-day sediment budget. From this perspective, B represents a long-term average of sediment generation and storage in the fluvial drainage basin. Treating B as a single variable eliminates the need to resolve the values and associated uncertainties of its components, which are poorly known.

Estimation of the uncertainty associated with B may be attempted by means of "inverted chi-squared fitting" (Press et al., 1992). Because the northern Adriatic Sea is a closed basin and the principle of mass balance should apply, the data-model fit should be satisfactory. Hence, a distinct lack of fit may be attributed to the uncertainty associated with B. This approach may be implemented by initially setting $\delta B=0$, and substituting the estimated relative errors of A, R, Q, and T into Equation 4.3 to obtain the minimal fractional uncertainty of BQART/HydroTrend model output:

$$\left[\frac{\delta Qs}{Qs}\right]_{\min} \cong 0.21 \tag{4.10}$$

to give the following expression for the total uncertainty of model output:

$$\frac{\delta Qs}{Qs} = \sqrt{\left(\frac{\delta B}{B}\right)^2 + \left[\frac{\delta Qs}{Qs}\right]_{min}^2} \tag{4.11}$$

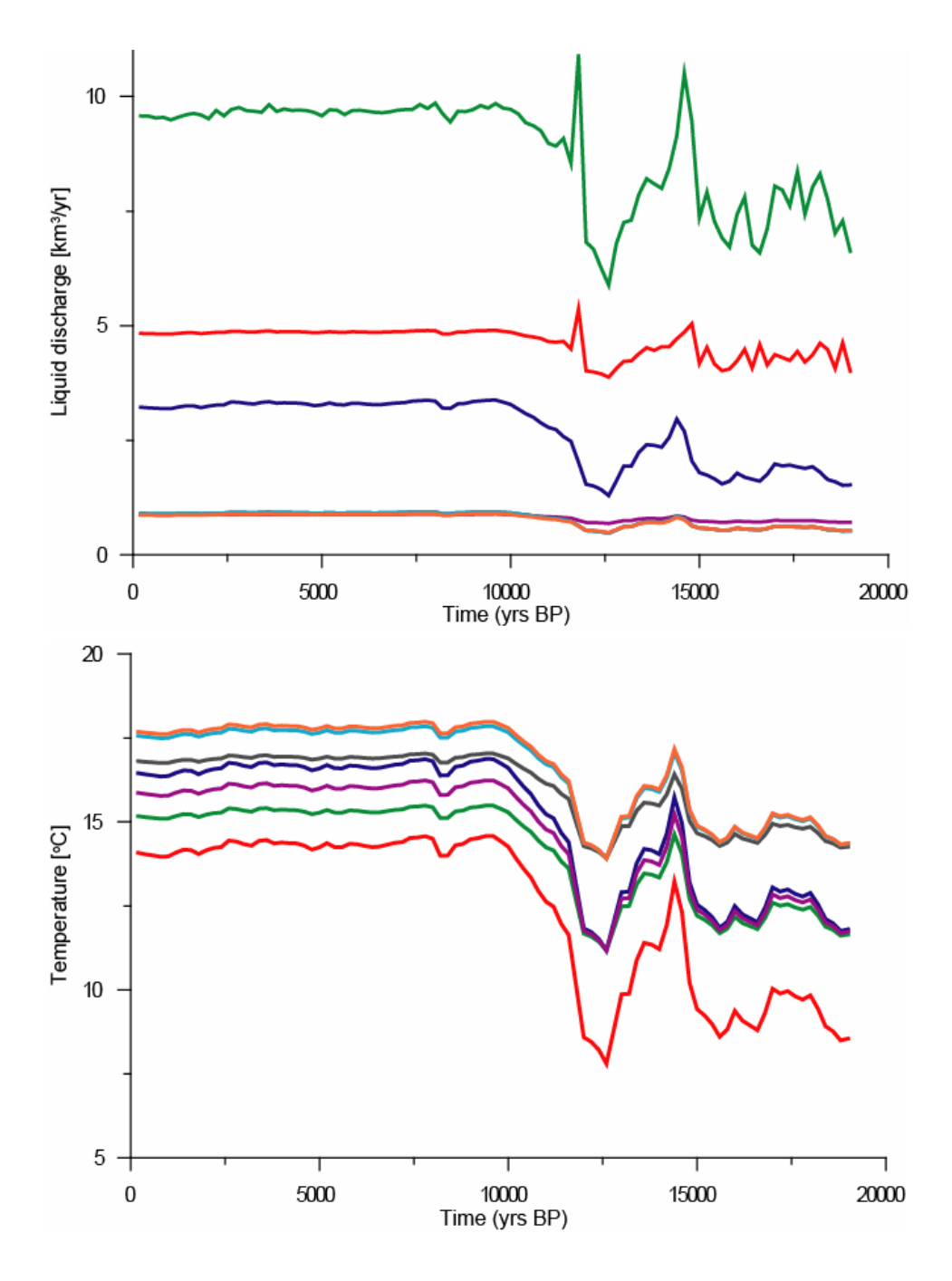


Figure 4.3: Discharge (Q) and temperature (T) of the Tagliamento, Adige, Po, Metauro, Sangro, Tronto, and Biferno Rivers.

4.6 UPSCALING OF MODEL OUTPUT

Apart from the Po and Adige, there are numerous small rivers feeding the Northern Adriatic basin. As explained above, these smaller rivers were subdivided into five contiguous source areas, based on dominant catchment lithology, size of the drainage area, maximum drainage-basin elevation, and river length. The total quantity of sediment supplied by each source area was estimated by modelling of one representative river from each source area (Tagliamento, Metauro, Tronto, Sangro and Biferno; Fig. 4.1), whose output was scaled up to the total drainage area covered by the source using the following procedure.

Let Q = qA, where q is the liquid discharge produced per unit area of the drainage basin [km yr⁻¹]. We assume that the values of q, B, R and T within each source area are constant, and define a constant k:

$$k = \omega BRT \left(\frac{q}{q_0}\right)^{0.31} \tag{4.12}$$

where k [Mt yr⁻¹] is the characteristic parameter of the source area, and $q_0 \equiv 1$ [km yr⁻¹] is the value needed to non-dimensionalize the term within brackets. Equation 4.2 thus simplifies to:

$$Qs_{ref} = k \left(\frac{A_{ref}}{A_0}\right)^{0.81} \tag{4.13}$$

If the source area consists of *n*+1 basins (the reference basin which has been modelled plus *n* other basins), the following holds:

$$A_{tot} = A_{ref} + \sum_{i=1}^{n} A_{i}$$
 (4.14)

Upscaling of Qs using the size of the entire source area can be performed in one step:

$$Qs_{tot} = k \left(\frac{A_{tot}}{A_{ref}}\right) \left(\frac{A_{ref}}{A_0}\right)^{0.81}$$
(4.15)

Substitution of Equation 4.14 into Equation 14.5 demonstrates that this is equivalent to calculation of the sum of *Qs* produced in *n*+1 basins separately:

$$Qs_{tot} = k \left\{ \left(\frac{A_{ref}}{A_0} \right)^{0.81} + \sum_{i=1}^{n} \left(\frac{A_i}{A_{ref}} \right) \left(\frac{A_{ref}}{A_0} \right)^{0.81} \right\}$$
(4.16)

Transformation of simulated rates of sediment delivery (Qs) from the seven source areas to basin-wide estimates of sediment supply was carried out as follows:

- 1) The seven source-area sediment discharges (Qs_{tot}) were summed to obtain basin-wide Qs values for each 200-year epoch.
- 2) The basin-wide Qs values [Mt yr⁻¹] were converted to sediment mass [Gt] delivered in each 200-year epoch.
- 3) The sediment masses delivered in each epoch were summed to obtain total masses supplied to the basin over time intervals corresponding to the lithosomes in the Adriatic basin (M_s). Time intervals corresponding to Northern Adriatic lithosomes are given in Figure 4.2.
- 4) The masses of sediment supplied to the basin over time intervals corresponding to the lithosomes (M_s) were converted into average rates of basin-wide sediment supply (S_s), expressed in units of Gt kyr⁻¹.

4.7 STATISTICAL ANALYSIS OF RESULTS

4.7.1 Model output

The results of our simulations are illustrated in Figure 4.4, in the form of sediment discharge of the Po River Basin and the total sediment discharges of the Eastern Alpine and Apennine river basins. Sediment discharge from the Po River and the Eastern Alpine basins fluctuated strongly between 19 ka BP and 12.5 ka BP, because the Alps were glaciated during this time interval, and a steady rise in temperature caused intense melting of the glaciers. From 12.5 ka BP to the present-day, sediment discharge from the Po River and the Eastern Alpine basins remained more or less constant. Sediment discharge of the non-glaciated Apennine basins remained more or less constant throughout the entire 19-kyr time interval.

Table 4.2 presents the sediment masses [Gt] estimated from the stratigraphic record (M_a) (Brommer et al., 2009) and the simulation results (M_s) . In Table 4.3 we present the rates of sediment accumulation estimated from the stratigraphic record (S_a) , taken from Brommer et al., 2009) and the simulated rates of sediment supply (S_s) .

Table 4.2: Estimated sediment masses [Gt] from stratigraphic record (M_a) and modelling results (M_s) .

Lithosome /	D	ata	Mo	del
time interval	M_a	δM_a	M_s	δM_s
HST-2	18	2	18	4
HST-1	236	28	224	47
TST-3	212	40	262	55
TST-2	116	16	123	26
TST-1	158	22	141	30
HST	254	28	242	51
TST	486	48	526	110
HST+TST	740	56	768	161

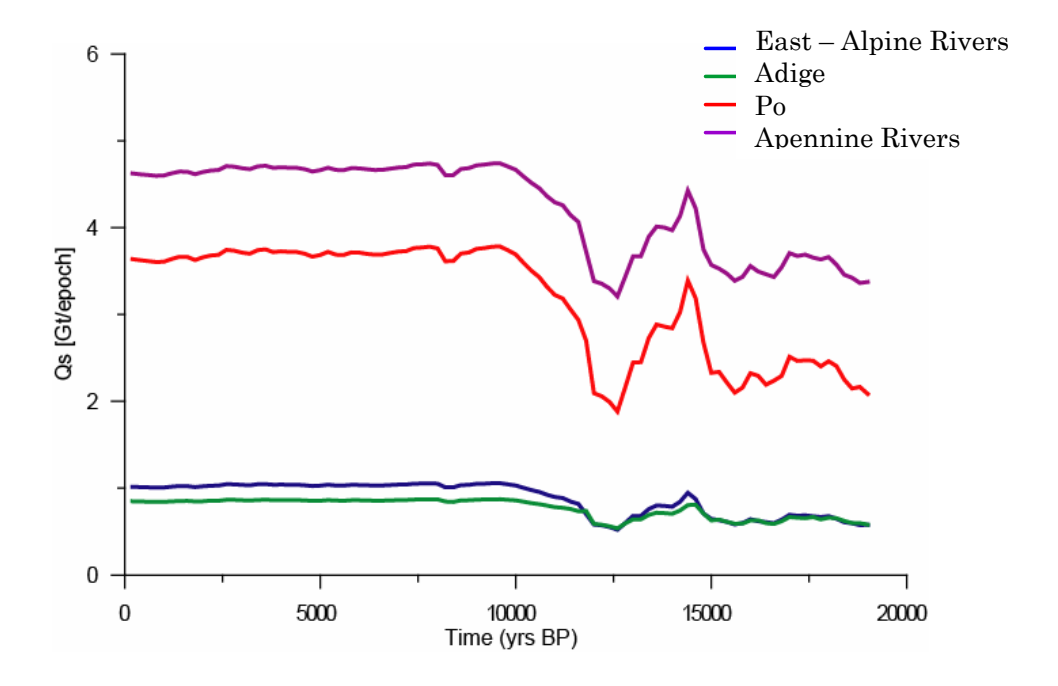


Figure 4.4: Total sediment discharge (Qs) of the East-Alpine, Po, Adige, and Apennine source areas.

Table 4.3: Estimated rates of sediment accumulation and supply [Gt kyr⁻¹] from stratigraphic record (S_a) and modelling results (S_s).

Lithosome /	D	ata	Mo	del
time interval	S_a	δS_a	S_{s}	δS_s
HST-2	45	7	45	9
HST-1	46	6	44	9
TST-3	37	7	45	10
TST-2	33	7	35	7
TST-1	38	8	34	7
HST	46	5	44	9
TST	36	4	39	8
HST+TST	39	3	40	8

4.7.2 Statistical test

Strictly speaking, the five sediment supply rates constitute a time series, which means that they may be serially correlated. However, since we are only assessing the probability that the five estimates are equal, their time order, and consequently, the presence or absence of serial correlation, is irrelevant. This means that statistical analysis of the results may be carried out by means of an appropriate two-sample test. A modified version of the well-known Z-test (e.g. Taylor, 1982; Davis, 2002) was used to carry out pair-wise comparisons of sediment masses and rates of supply in the presence of uncertainties. Brommer et al. (2009) give a derivation of the test statistic.

If $x_1 \pm \delta x_1$ and $x_2 \pm \delta x_2$ are two values (with absolute uncertainties) and we wish to test for equality, we calculate their log-ratio y.

$$y = \ln\left(\frac{x_1}{x_2}\right) \tag{4.17}$$

The absolute uncertainty of y is given by:

$$\delta y = \sqrt{\left(\frac{\delta x_1}{|x_1|}\right)^2 + \left(\frac{\delta x_2}{|x_2|}\right)^2} \tag{4.18}$$

and the test statistic Z is defined as:

$$Z = \frac{-|y|}{\delta y} \tag{4.19}$$

We can test the hypothesis H_0 : $x_1 = x_2$ (which is equivalent to Z = 0) by evaluation of the integral of the standard normal distribution N(0,1):

$$P(H_0) = 2\int_{-\infty}^{Z} \frac{1}{\sqrt{2\pi}} e^{-x^2/2} dx$$
 (4.20)

The value of $P(H_0)$ represents the probability of observing a difference greater than or equal to $|x_1 - x_2|$ if the two are in fact identical. The null hypothesis (equality of two rates) is considered acceptable if $P(H_0)$ exceeds a significance level α , which was set at 0.1 (this represents the risk of erroneously rejecting the null hypothesis).

4.7.3 Test result

The results of applying the modified Z-test to the five supply rates $(H_0: S_s(j) = S_s(j))$, for $i \neq j$ are given in Table 4.4. The minimum fractional uncertainty of S_s does not allow the distinction of significant variations in basin-wide sediment-supply rates among the five time slices. This means that we cannot reject the hypothesis that the mean rates of basin-wide sediment supply have been constant. Tests of equality for corresponding pairs of masses (M_s, M_a) and rates (S_s, S_a) obtained from data and model are summarized in Table 4.5. The results indicate an excellent overall agreement between data and model, implying that there are no reasons to assume a violation of mass-balance constraints. The results of our test thus indicate that the performance of the BQART/HydroTrend model is more than adequate.

Table 4.4: Probability of pair-wise equality of supply rates (S_s)

	HST-2	HST-1	TST-3	TST-2	TST-1
HST-2	-	-	-	-	-
HST-1	0.94	-	-	-	-
TST-3	1.00	0.94	-	-	-
TST-2	0.41	0.45	0.41	-	-
TST-1	0.35	0.39	0.35	0.91	-

Table 4.5: Data-model comparison of masses (Ms, Ma) and accumulation rates (Ss, Sa).

Lithosome / time interval	M	S
HST-2	1.00	1.00
HST-1	0.83	0.84
TST-3	0.45	0.47
TST-2	0.82	0.84
TST-1	0.65	0.74
HST	0.84	0.84
TST	0.73	0.74
HST+TST	0.87	0.91

4.8 DISCUSSION AND CONCLUSIONS

The results of our sediment-supply simulations with the BQART/HydroTrend model are fully consistent with independent estimates of mass accumulation over the past 19 kyr (Brommer et al., 2009) in terms of the overall mass balance. The excellent fit between rates of sediment supply and accumulation implies that the minimum uncertainty of model predictions (Eqn. 4.10), which is dominated by the palaeo-climate variables Q and T, is more than sufficient to account for the observed deviations. This precludes estimation of the uncertainty of B. In fact, we would have obtained a satisfactory data-model fit if the total uncertainty of model output would have been much smaller than the minimum value adopted in our study. An obvious consequence of this conclusion is that the uncertainties associated with palaeo-climate input variables Q and T should be reduced to realize the full potential of BQART/HydroTrend for palaeo-sediment supply modelling. It should be noted that our decision to calibrate model parameter B by analysis of the present-day sediment budget (Chapter 3) instead of using predefined values for B (Syvitski and Milliman, 2007) turned out to be crucial to the success of the data-model comparison presented in this study. Attempts to apply the BQART/HydroTrend model without such calibrations are unlikely to be equally successful, as this requires estimation of three variables (Eqn. 4.2) which are not well constrained (Syvitski and Milliman, 2007).

A remarkable result of our study is the apparent lack of significant changes in the rate of basin-wide sediment supply among the five time slices considered, which confirms the inferences of Brommer et al. (2009) based on basin-wide net mass-accumulation rates. It should be noted that the time intervals over which we have averaged our simulated basin-wide sediment supply are dictated by the sequence-stratigraphic subdivision of the Adriatic basin fill. Our results do therefore not imply that basin-wide sediment supply has not varied at all. Nevertheless, our results appear to contradict the evidence for order-ofmagnitude changes in fluvial sediment fluxes throughout glacio-eustatic cycles. The frequency band in which variations of sediment supply are widely believed to be concentrated ranges from 10³ to 10⁵ years (Hovius and Leeder, 1998). In the Neogene, this frequency band coincides with glacio-eustatic cycles, which profoundly affected drainage-basin evolution and governed basin-fill architecture through high-amplitude sea level changes. It has been reported that fluvial sediment fluxes have varied significantly since the last glacial maximum (Blum and Törnqvist, 2000; Walling, 2006), and that late-Quaternary deglaciation has led to an acceleration of erosion in glaciated catchment areas (Hallet et al., 1996; Molnar and England, 1990). Compilations of accumulation rates obtained from sediment cores in fluvial drainage basins and delta plains illustrate the order-of-magnitude variations in these data, a phenomenon that has been noted in marine environments as well (Sadler, 1981; Sommerfield, 2006; Jerolmack and Sadler, 2007).

It is important to note that our study covers a much larger area ($\approx 10^5 \text{ km}^2$) than the scale typically associated with geological reconstructions based on sediment cores, which ranges from 10⁻² to 10⁻² km², depending on the spatial heterogeneity of sedimentary architecture in various environments. From a statistical point of view, the five orders-of-magnitude upscaling relative to sediment-core data may well be sufficient to reduce the variance of basin-wide average rates relative to the values noted in the above studies. Another difference between our results and those cited above is that we have not explicitly addressed sediment dynamics upstream of the river mouth. The areal extent of our quantitative mass-balance study is restricted to the marine part of the Northern Adriatic basin at the time of maximum flooding (5.5 ka BP). Hence, we do not exclude order-of-magnitude variations in the rate of sediment production in individual drainage basins. Variations in the rate of sediment production will not be observed in the marine realm, nor predicted by BQART/HydroTrend, provided sediments are temporarily stored in the fluvial drainage basin and released over a comparatively long time span.

The apparent contradiction between the above studies and our inferences may be understood by taking into account the mathematical stability analysis performed by Phillips (2003), who showed that large fluvial drainage basins are likely to be dynamically stable with respect to the rate of sediment export, provided that alluvium is available for transport (transport-limited system). The long-term stability of sediment supply from such basins may be attributable to feedbacks between storage and remobilization of alluvium, which buffers the system against environmental change. Moreover, this analysis implies that hill slopes and fluvial systems within the drainage basin must be unstable in order to maintain stability at the larger scale. The apparent contradiction noted above may thus reflect scale-dependent behaviour

of sediment-dispersal systems, which provides a physical justification for our results. Another reason for long-term stability of fluvial drainage basins is strong external forcing, which overwhelms climatically induced effects on sediment supply. This may be the case for the Apennine drainage basins, which are characterized by high rates of tectonic uplift and are underlain by easily erodible sediments.

Another aspect of sedimentary-system dynamics is the inverse correlation between (local) rates of sediment accumulation and the duration of the time interval covered by the measurements, which reflects incompleteness of the stratigraphic record (Sadler, 1981; Sommerfield, 2006; Jerolmack and Sadler, 2007). By contrast, we consider a closed system, in which rates of sediment supply and accumulation are potentially independent of the duration of the measurement interval and do not display this inverse relation. Although the stratigraphic record is unlikely to be complete at any given location, the fact that sediment cannot leave the system ensures that the principle of mass balance applies and the basin-fill record is complete in terms of the total quantity of sediments preserved over the time span considered.

In conclusion, statistical as well as physical reasoning supports the idea that the limited variability of rates of sediment supply and accumulation inferred from our basin-wide study implies that the variance of sediment supply and accumulation rates is inversely proportional to spatio-temporal scale. The apparent contradiction between observations on different scales indicates that inferences from core data cannot be readily upscaled to obtain quantitative reconstructions of the entire basin fill. A more realistic approach is to use long-term basin-wide rates of sediment supply, either obtained from the stratigraphic record (Brommer et al., 2009) or simulated using the approach outlined in this study, as boundary conditions for stochastic simulation of short-term sediment-supply fluctuations from individual river systems (cf. Morehead et al., 2003). Such high-resolution time series could serve as input to large-scale process-based models of basin filling aimed at examining the local variability of sediment-accumulation rates, in an attempt to shed light on the scale-dependency of preservation in the stratigraphic record.

List of Abbreviations and symbols

Abbreviations

Highstand Systems Tract [5.5 – 0.0 ka BP] HST: HST-1: Lower HST unit [5.5 - 0.4 ka BP] HST-2: Upper HST unit [0.4 - 0.0 ka BP] Last Glacial Maximum LGM: LST: **Lowstand Systems Tract** MAD: Mid-Adriatic Deep MAR: Mass Accumulation Rate Maximum Flooding Surface, separating the TST from the HST [5.5 MFS: Maximum Regressive Surface, separating the LST from the TST MRS: [19.0 ka BP] TST: Transgressive Systems Tract [19.0 – 5.5 ka BP] Lower TST unit [19.0 - 14.8 ka BP] TST-1: TST-2: Middle TST unit [14.8 - 11.3 ka BP] TST-3: Upper TST unit [11.3 - 5.5 ka BP] NOAA: National Oceanic and Atmospheric Administration CCM-1: Community Climate Model Version 1

Symbols

г	٦.			٠.,			-
١-	п	=	non	-dı	mei	nsio	าลโ

[] - non unitensional			
Symbol	Definition	Units	
A	Drainage area	$[km^2]$	
A_{tot}	Total area of source	$[km^2]$	
A_{ref}	Area of reference basin	$[km^2]$	
B	Geological and human impact factor	[-]	
δX	absolute uncertainty of variable X		
E_{h}	Human impact	[-]	
k	Source-area parameter	$[\mathrm{Mt}\;\mathrm{yr}^{\text{-}1}]$	
L	Lithology-specific erodibility	[-]	
M_a	Mass of lithosome	[Gt]	
M_s	Simulated mass of lithosome	[Gt]	
ω	Constant	[kg °C ⁻¹ km ⁻²]	
q	Liquid discharge per unit area	[km yr ⁻¹]	
Q	Liquid discharge	$[\mathrm{km^3~yr^{ ext{-}1}}]$	
Q_0	$Q_0 \equiv 1$ (non-dimensionalizing constant)	$[\mathrm{km^3~yr^{\text{-}1}}]$	
Qs	Suspended sediment load	$[\mathrm{Mt\ yr}^{ ext{-}1}]$	
Qs_{tot}	Sediment load of entire source area	$[\mathrm{Mt\ yr}^{ ext{-}1}]$	

Qs_{ref}	Sediment load of representative river	[Mt yr ⁻¹]
R	Maximum elevation	[km]
S_{a}	Net mass accumulation rate	$[\mathrm{Gt}\;\mathrm{kyr}^{\text{-}1}]$
$S_{\!s}$	Simulated rate of sediment supply	[Gt kyr ⁻¹]
T	Basin-averaged temperature	[oC]
T_e	Trapping efficiency	[-]
Z	Test statistic	[-]

Chapter 5

Sediment budget, growth pattern and stratal architecture of the Late-Holocene Adriatic mud belt: an integrated model

5.1 INTRODUCTION

Continental shelves are often regarded as prime locations to investigate source-to-sink processes and dynamics based on terrigenous sediment records (Sommerfield, 2007). About 90% of the sediment generated by erosion on land is deposited on continental shelves, where it is (temporarily) stored in major deltas, as shelf deposits and on the continental slope. Dispersal of fine-grained sediment on continental shelves has been the subject of intensive research (Chen et al., 2000; Diaz et al., 1996; Labaune et al., 2005; Lesueur et al., 2002; Li et al., 1998; Liquete et al., 2007, 2008; Lobo et al., 2004; McCave, 1972; Owen, 2004; Sternberg et al., 1996; Tesson et al., 2005). Numerous studies have shown that dispersal pathways of fine-grained sediments are complex, and the movement of material from river plumes to the nearshore and beyond is accomplished through a variety of transport mechanisms operating on different temporal and spatial scales (Kineke et al., 1996; Mulder and Syvitski, 1995; Goodbred and Kuehl, 1999; Kuehl et al., 2003; Traykovski et al., 2007).

In some areas, detached subaqueous delta deposits or mud belts form far away from parent river mouths (Kuehl et al., 1997; Goodbred and Kuehl, 1999; Cattaneo et al., 2003), which underscores the importance of understanding the fate of fine-grained sediments. Mud belts are typical of low-gradient settings, and are characterized by a substantial component of shore-parallel sediment transport (Cattaneo et al., 2007). They are important building blocks of continental-margin stratigraphic sequences (Vail et al., 1977; Christie-Blick and Driscoll, 1995). Mud belts develop seaward of major deltas, as is the case in the Adriatic and Mediterranean margins, and the continental shelves adjacent to the Amazon and the Yellow River (Nittrouer et al., 1986), the Fly River (Harris et al., 1996), and the Ganges-Brahmaputra (Kuehl et al., 1997). Although increasing attention has been paid to mud belts over the past years (Owen, 2004), very few studies have investigated growth mechanisms and preservation potential of mud belts within the stratigraphic record. The sediment dynamics of these muddy deposits and the physical processes that

govern their formation and preservation have received limited attention (Walsh et al., 2004; Liu et al., 2009).

The late-Holocene mud belt of the Northern Adriatic Sea (Italy) is an exception to the rule, because its evolution and internal geometry are relatively well-known (Trincardi et al., 2004; Cattaneo et al., 2004; Cattaneo et al., 2007; Brommer et al., 2009). Seismic-stratigraphic and core analyses indicate that the present-day circulation pattern, which gives rise to the northern Adriatic mud belt became active at around 14 ka BP (Cattaneo and Trincardi, 1999). From that time on, fine-grained sediment dispersed to the Adriatic Sea by Alpine and Apennine Rivers has been conveyed to the south to form an elongate shore-parallel prodelta of the Alpine and Apennine Rivers. The modern mud belt, which is the subject of this chapter, comprises a series of longshore and cross-shore prograding clinoforms, which have been built after the rate of deglacial sea level rise had decreased sufficiently to halt transgression. In sequence-stratigraphic terms, the Adriatic mud belt belongs to the highstand systems tract (HST), which is bounded below by the maximum flooding surface (MFS) dated at ≈5.5 ka BP.

In this Chapter we aim to analyse the growth mechanism of the northern Adriatic mud belt by presenting a mass-balanced model, which relates temporally and spatially averaged rates of sediment transport to its stratigraphic architecture. Results of a quantitative analysis of mass accumulation patterns across the entire mud belt on a decadal, centennial and millennial time scale (Brommer et al., 2009) will be used to depict the spatial and temporal variability of mass fluxes within the Adriatic Basin. We show that these patterns are closely related to the stratal architecture of the mud belt as inferred from high-resolution seismic cross-sections. We then present a sediment budget model to quantify the long-term average rates of longshore transport, the preservation potential of sediments, and the dispersal of sediments with different provenance (Apennine versus Alpine + Po). The required input data to the sediment budget model have been generated by (1) sediment budget analysis of the Adriatic Basin (Brommer et al., 2009) and (2) quantitative analyses of rates of fluvial sediment supply predicted by the BQART/HydroTrend model (Chapters 3 and 4). The transport rates obtained with the sediment budget model are discussed in the light of their end product, the stratigraphic record. Finally, we discuss how the preserved history of basin filling may shed light on possible future events.

5.2 SYNTHESIS OF PREVIOUS WORK

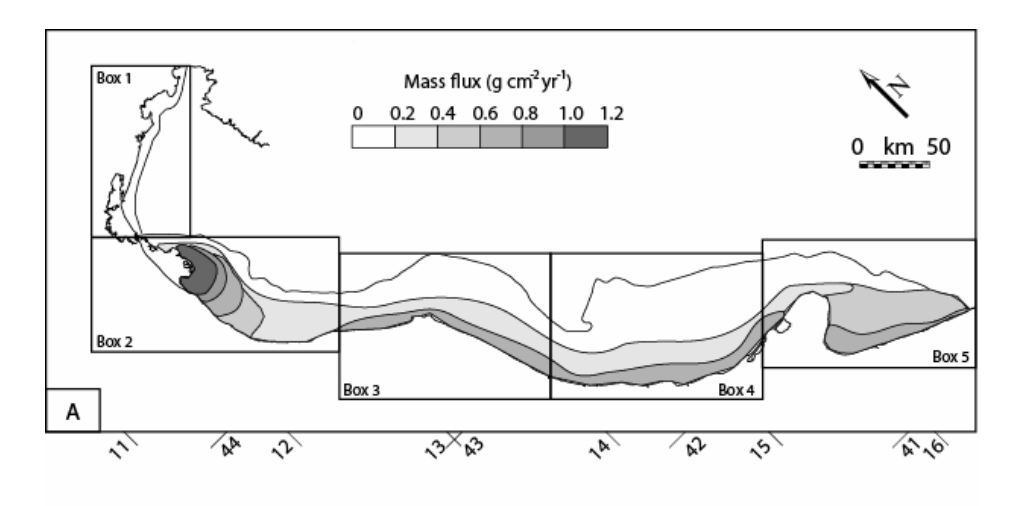
The quantitative sediment budget analysis presented in Brommer et al. (2009) demonstrated that a probabilistic assessment of mass accumulation rates (MAR) in a well-documented "closed" basin allows reconstruction of time-averaged rates of sediment supply, provided the basin fill can be subdivided into conformity-bounded units. The sediment masses of five basin-wide lithosomes and their associated uncertainties were derived by means of stochastic simulation, using high-resolution seismic data, porosity profiles, and

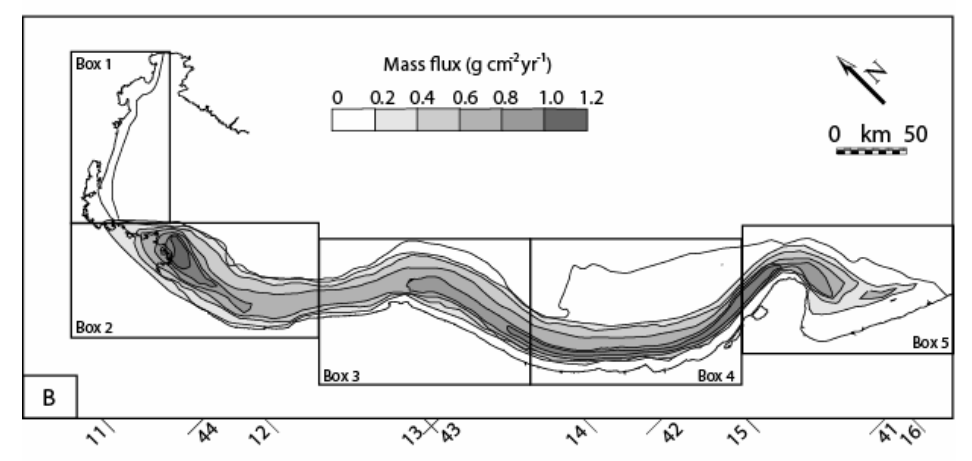
radiocarbon datings. Brommer et al. (2009) compared mass accumulation rates on the three different time scales presented in Figure 5.1. Decadal averaged (modern) mass fluxes [g cm⁻² yr⁻¹] calculated from the data of Frignani et al. (2005) are presented in Fig. 5.1A. Figure 5.1B presents the centennial averaged mass fluxes derived from the thickness distribution of the HST-2 lithosome (0-0.4 ka BP) (Brommer et al., 2009). Figure 5.1C depicts the millennial averaged mass fluxes [g cm⁻² yr⁻¹] derived from the thickness distribution of the HST-1 lithosome (0.4 - 5.5 ka BP) (Brommer et al., 2009).

The spatial variation of mass fluxes brings out systematic differences between decadal, centennial and millennial averages. The decadal average mass flux (Fig. 5.1A) shows that sediments tend to accumulate near the coast and especially off the river mouths of the Po-delta distributaries. On centennial time scales (Fig. 5.1B), sediments are reworked and displaced basinward (cross-shore) along most of the Adriatic coast. In addition, the pattern also shows a net trend of longshore progradation in the most distal part of the lithosome, which reflects the growth of the recent Gargano subaqueous delta (Cattaneo et al., 2003). Other features of interest include the area around the modern Po Delta, showing a rapid progradation, which started around AD1600 (Correggiari, 2001) and the low preservation potential of sediments presently accumulating near the coast. The pattern of millennial average mass fluxes (Fig. 5.1C) is in many ways similar to the centennial average fluxes, albeit without the localized accumulation in front of the modern Po delta. Hence, much of the sediment, which has accumulated over the past decades in the Northern Adriatic is likely to represent a transient stratigraphic record (sensu Jerolmack and Sadler, 2007), and the change from transient to persistent accumulation patterns is estimated to occur at the centennial to millennial time scale, provided that external forcing remains essentially unchanged.

Three seismic cross-sections (KS53, KS11 and AMC 167) illustrate the seismic architecture of the northern Adriatic mud belt (Fig. 5.2). Seismic profiles KS53 and KS11 show an aggrading geometry between the maximum flooding surface (MFS) and the seabed, which suggests that during the formation of the entire HST accommodation space equaled rates of sediment supply in the Central Apennine mud wedge. Seismic cross-section AMC167 shows an aggrading geometry in the lower HST lithosome (HST 1) but a progradational trend in the upper HST lithosome (HST 2). Figure 5.2 captures the information provided by the seismic architectural analysis by plotting the spatial distribution of maximum mass fluxes [g cm-2 yr-1] on three time scales (decadal, centennial, and millennial). Figure 5 clearly illustrates an aggradational architecture of the late-Holocene mud belt along the Apennine coast and a progradational trend in the most distal part, the Gargano subaqueous delta.

In Chapter 3 it was shown that the present-day sediment budget of the Northern Adriatic mud belt can be traced to two geochemically distinct source areas: the Po and Adige rivers (Alpine source) and the Apennine rivers (Apennine source).





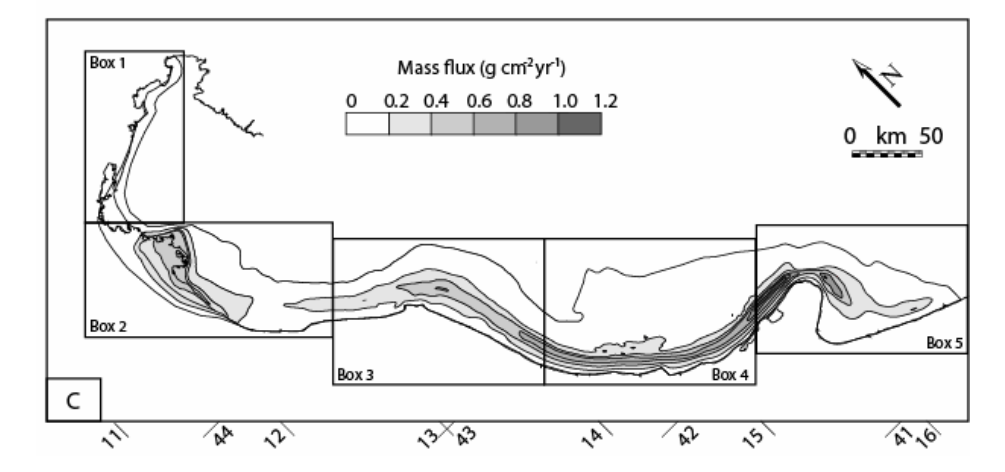
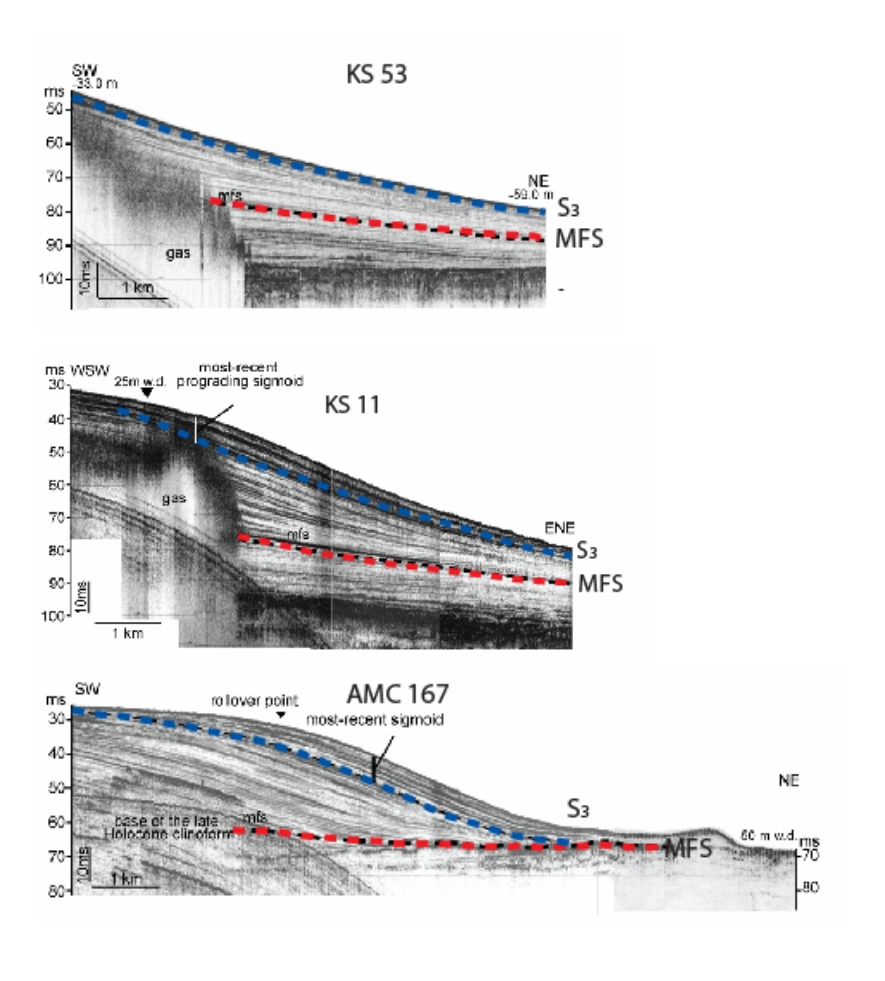


Figure 5.1: Net mass accumulation fluxes of Northern Adriatic mud belt (Italy) over three time intervals. The area has been divided into five contiguous cells for the purpose of sediment budget modelling. A) Decadal scale (present day); B) Centennial scale (HST-2; 1600 AD - present); C) Millenial scale (HST-1; 5.5 - 0.4 ka BP).



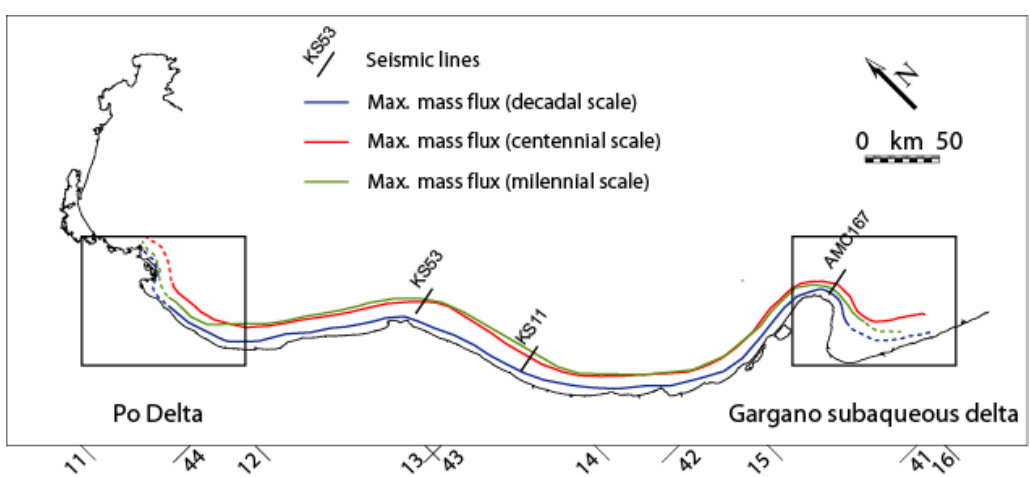


Figure 5.2: Cross-shore maxima of net mass fluxes for the three time intervals considered (coloured lines) and seismic profiles (red dotted line = lower boundary of HST-1 (MFS); blue dotted line = boundary between HST-1 and HST-2).

Integration of the chemical data with bulk accumulation rates (Frignani et al., 2005) allowed mapping of accumulation rates of sediments derived from each of the two major source areas (Po/Adige vs. Apennines) across the mud belt. The results of this analysis were used to calibrate the BQART/HydroTrend model of fluvial sediment supply (Kettner and Syvitski, 2007; Syvitski and Milliman, 2007). In Chapter 4, we used the calibrated BQART/HydroTrend model (Kettner and Syvitski, 2007; Syvitski and Milliman, 2007) to derive estimates of average basin-wide sediment supply rates for five time intervals spanning the last 19 kyr. Data on basin-wide mass accumulation presented by Brommer et al. (2009) were compared with simulations of sediment supply by the BQART/HydroTrend model. The results indicate excellent agreement, as expected under the assumption of closed-basin conditions. The data-model comparison showed that the sediment budget of the northern Adriatic basin over the past 19 kyr can be adequately approximated by calibration of the longterm average sediment generation and storage (B) of river basins with surface sediments.

5.3 SEDIMENT BUDGET MODEL

5.3.1 Introduction

A sediment budget model was developed for the northern Adriatic mud belt to quantify the long-term average rates of longshore transport, the preservation potential of sediments, and the dispersal of sediments with different provenance (Apennine versus Alpine + Po). The area of interest was subdivided into five contiguous cells, covering the entire area of sediment accumulation between Trieste and the Gargano peninsula (Fig. 5.1). The average sediment accumulation rate in each cell was obtained from the sediment masses calculated by Brommer et al. (2009). These data were combined with the rates of fluvial sediment supply predicted by the BQART/HydroTrend model (Chapters 3 and 4) to yield the input data for a sediment-budget model (Table 5.1) from which average rates of longshore transport over three time intervals were estimated.

5.3.2 Mass balance

Because the data-model comparison (Chapter 4) showed an excellent agreement, our first step was to implement a closed sediment budget by calculating the weighted average of accumulation and supply rates across the whole mud belt:

$$F_{tot} = \frac{w_a \sum_{j=1}^{n} S_{aj} + w_s \sum_{j=1}^{n} S_{sj}}{w_a + w_s}$$
(5.1)

where S_a and S_s are the independent estimates of the accumulation and supply rates (Table 5.1, see also Chapter 4), and F_{tot} equals the weighted average of the two totals. The number of cells is equal to n. The weights are defined in terms of the sums of squared absolute errors (variances) of the two estimates (δS_a and δS_s) in order to derive the minimum-chi-squared estimate of the average (mass-balanced) rates:

$$w_a = \frac{1}{\sum_{j=1}^{n} (\delta S_{aj})^2}, \quad w_s = \frac{1}{\sum_{j=1}^{n} (\delta S_{sj})^2}$$
 (5.2a, b)

Table 5.1: Input to sediment budget model

Time slice	Cell	S_a [Mt yr ⁻¹]		S_s [Mt yr-1]		P [-]
		Mean	Stddev	Mean	Stddev	
Present Day	1	2.0	0.3	4.1	0.9	1.0
Present Day	2	12.0	1.4	24.4	5.1	0.8
Present Day	3	6.0	1.0	7.0	1.8	0
Present Day	4	9.0	1.4	6.7	1.4	0
Present Day	5	13.0	2.0	3.7	0.8	0
HST 2	1	3.0	0.5	4.1	0.9	1.0
HST 2	2	7.0	0.8	24.4	5.1	0.8
HST 2	3	2.5	0.4	7.0	1.8	0
HST 2	4	15.0	2.3	6.7	1.4	0
HST 2	5	17.0	2.6	3.7	0.8	0
HST 1	1	2.0	0.3	4.0	0.8	1.0
HST 1	2	3.0	0.5	23.9	5.0	0.8
HST 1	3	9.0	1.4	6.8	1.4	0
HST 1	4	17.0	2.6	6.5	1.4	0
HST 1	5	15.0	2.3	3.6	0.8	0

The weighted mean is used to derive scaling factors for the rates in each cell:

$$F_{D,j} = \frac{F_{tot}}{\sum_{j=1}^{n} S_{aj}}, \quad F_{R,j} = \frac{F_{tot}}{\sum_{j=1}^{n} S_{sj}}$$
 (5.3a, b)

where F_D and F_R are defined as the mass-balanced rates of deposition and fluvial supply, respectively. The mass balance now holds exactly:

$$\sum_{j=1}^{n} F_{D,j} = \sum_{j=1}^{n} F_{R,j} = F_{tot}$$
 (5.4)

Therefore, the sum of fluvial and longshore input equals the sum of deposition and longshore output:

$$\sum_{j=1}^{n} F_{R,j} + \sum_{j=1}^{n} F_{I,j} = \sum_{j=1}^{n} F_{D,j} + \sum_{j=1}^{n} F_{O,j}$$
(5.5)

where F_I and F_O are defined as the mass-balanced rates of longshore input and output, respectively.

5.3.3 Longshore transport

The mass balance (Eqn. 5.5) also applies to each cell:

$$F_{R,j} + F_{I,j} = F_{D,j} + F_{O,j}, \quad j = 1, 2, ..., n$$
 (5.6)

And because the northern Adriatic mud belt is regarded as a closed system, we have the following boundary conditions:

$$F_{I,1} = F_{O,n} = 0$$
 (5.7a, b)

By definition, the rate of sediment removal by longshore transport from the *j*-th cell equals the rate of longshore sediment supply to the next (downstream) cell:

$$F_{O,j} = F_{I,j+1}, \quad j = 1, 2, ..., n-1$$
 (5.8)

If we define the net longshore transport rate as:

$$F_{L,j} = F_{O,j} - F_{I,j}, \quad j = 1, 2, ..., n$$
 (5.9)

and substitute Equation 5.9 into Equation 5.6, we obtain after rearrangement:

$$F_{L,j} = F_{R,j} - F_{D,j}, \quad j = 1, 2, ..., n$$
 (5.10)

Finally, the net longshore transport rate is decomposed into rates of sediment input and output for each cell:

$$F_{O,j} = F_{I,j+1} = \sum_{k=1}^{j} F_{L,k}, \quad j = 1, 2, ..., n-1$$
 (5.11)

5.3.4 Provenance

We keep track of the sediment provenance to predict the composition of the sediment accumulating in each cell. The proportion of eastern Alpine and Po river-derived sediment is defined as p, and its complement, 1-p, equals the proportion of sediment derived from the Apennine rivers. In our long-term and large-scale model, mixing of sediments is assumed to be complete, and the composition of the sediment leaving a cell (p_0) is assumed to be identical to the composition of the sediment, which has been deposited (p_D) :

$$p_{D,j} = p_{O,j}, \quad j = 1, 2, ..., n$$
 (5.12)

The composition of sediment deposited in a cell is determined by the relative contributions of the fluvial and longshore input, and their compositions (p_R and p_I , respectively):

$$p_{R,j}F_{R,j} + p_{I,j}F_{I,j} = p_{D,j}(F_{D,j} + F_{O,j}), \quad j = 1, 2, ..., n$$
 (5.13)

This, when solved for $p_{D,j}$ gives:

$$p_{D,j} = \frac{p_{R,j}F_{R,j} + p_{I,j}F_{I,j}}{F_{D,j} + F_{O,j}}, \quad j = 1, 2, ..., n$$
(5.14)

5.3.5 Preservation Potential

The preservation potential of sediments (R) is an important indicator of stratigraphic completeness. Its long-term average value may be calculated from the rates of sediment influx and deposition:

$$R_{j} = \frac{F_{D,j}}{F_{R,j} + F_{I,j}}, \quad j = 1, 2, ..., n$$
 (5.15)

Equation 5.15 shows that R may be interpreted as the long-term average probability that material entering a cell will be deposited. The assumption of complete mixing (Eqn. 5.12) implies that the preservation potential is independent of sediment provenance. Note that the closed sediment budget (Eqn. 5.4) implies that $R_n \equiv 1$, since it is assumed that no sediment escapes from the most distal part of the mud belt.

Table 5.2: Output of sediment budget model

Time slice	Cell	Vd [Mt yr ⁻¹]	<i>V</i> r [Mt yr ⁻¹]	<i>V</i> i [Mt yr ⁻¹]	<i>V</i> o [Mt yr ⁻¹]	P	R
Present Day	1	2.0	3.8	0.0	1.8	1.0	0.54
Present Day	2	12.2	22.6	1.8	12.1	0.79	0.50
Present Day	3	6.1	6.5	12.1	12.6	0.51	0.33
Present Day	4	9.2	6.3	12.6	9.6	0.34	0.49
Present Day	5	13.3	3.6	9.6	0.0	0.25	1.0
HST 2	1	3.0	4.0	0.0	1.0	1.0	0.76
HST 2	2	7.1	23.7	1.0	17.6	0.78	0.29
HST 2	3	2.5	6.8	17.6	21.9	0.56	0.10
HST 2	4	15.1	6.6	21.9	13.4	0.43	0.53
HST 2	5	17.1	3.8	13.4	0.0	0.34	1.0
HST 1	1	2.0	4.0	0.0	2.1	1.0	0.49
HST 1	2	3.0	24.3	2.1	23.4	0.79	0.11
HST 1	3	8.9	6.9	23.4	21.4	0.61	0.29
HST 1	4	16.8	6.6	21.4	11.2	0.46	0.60
HST 1	5	14.9	3.7	11.2	0	0.35	1.0

5.4 RESULTS

The transport rates obtained from the sediment budget model are summarized in Table 5.2. The modeling results for the three time slices under consideration have been visualized in Figure 5.3. As shown by the raw data of Table 1 and their recomputed estimates of Table 5.2, sediment input (S_s and F_R , respectively) has been essentially constant, both in terms of spatial distribution and composition. Approximately two thirds of the total sediment load has been supplied to the northern part of the Adriatic Basin (cells 1 and 2) over the entire time interval covered by the data. However, rates of long-shore transport and deposition differ among the three time slices.

The present-day situation, which differs considerably from the two older time slices, is characterized by storage of sediment in cell 2 (representing the area of the Po Delta), and an overall similarity of long-shore sediment fluxes between cells 2 to 5. The HST-1 and HST-2 time slices are quite similar to each other, and differ with respect to the present-day situation in terms of the higher long-shore transport rates between cells 2 to 4, which indicates that more sediment was transported southwards to be deposited offshore the Central and Southern Apennines (cells 4 and 5). The main difference between HST-1 and HST-2 reflects an increase of sediment accumulation in the area of the Po Delta (cell 2), which appears to be balanced by a decrease of the accumulation rate in the Northern Apennine offshore (cell 3).

This result is supported by Figure 5.4A, which depicts rates of long-shore transport between the cells (Table 5.2). The average long-shore transport rates during HST-1 and HST-2 times appear to have been similar, except in the area between the Po Delta (cell 2) and the Northern Apennine offshore (cell 3). Figure 5.4A clearly demonstrates that present-day long-shore transport rates are substantially lower than the average rates inferred from the HST-1 and HST-2 units.

The preservation potential of sediments (R) along the Northern Adriatic shelf appears to have varied mainly in the northern part of the mud belt (Fig. 5.4B). In view of the low rates of sediment accumulation in cell 1, the variations of R do not exert a major impact on the stratigraphic record. Significant variations between the time slices are present in cells 2 and 3. Preservation potential has been increasing in the area around the Po delta (cell 2), whereas the area offshore the northern Apennines (cell 3) has experienced a decrease from HST-1 to HST-2, followed by an increase from HST-2 to the present day. The area offshore the central and southern Apennines has been acting as a local depocentres (sink) of mud-belt sediments throughout the time interval under consideration, as illustrated by the large R values of cells 4 and 5 (Note that the preservation potential of the latter equals unity by definition).

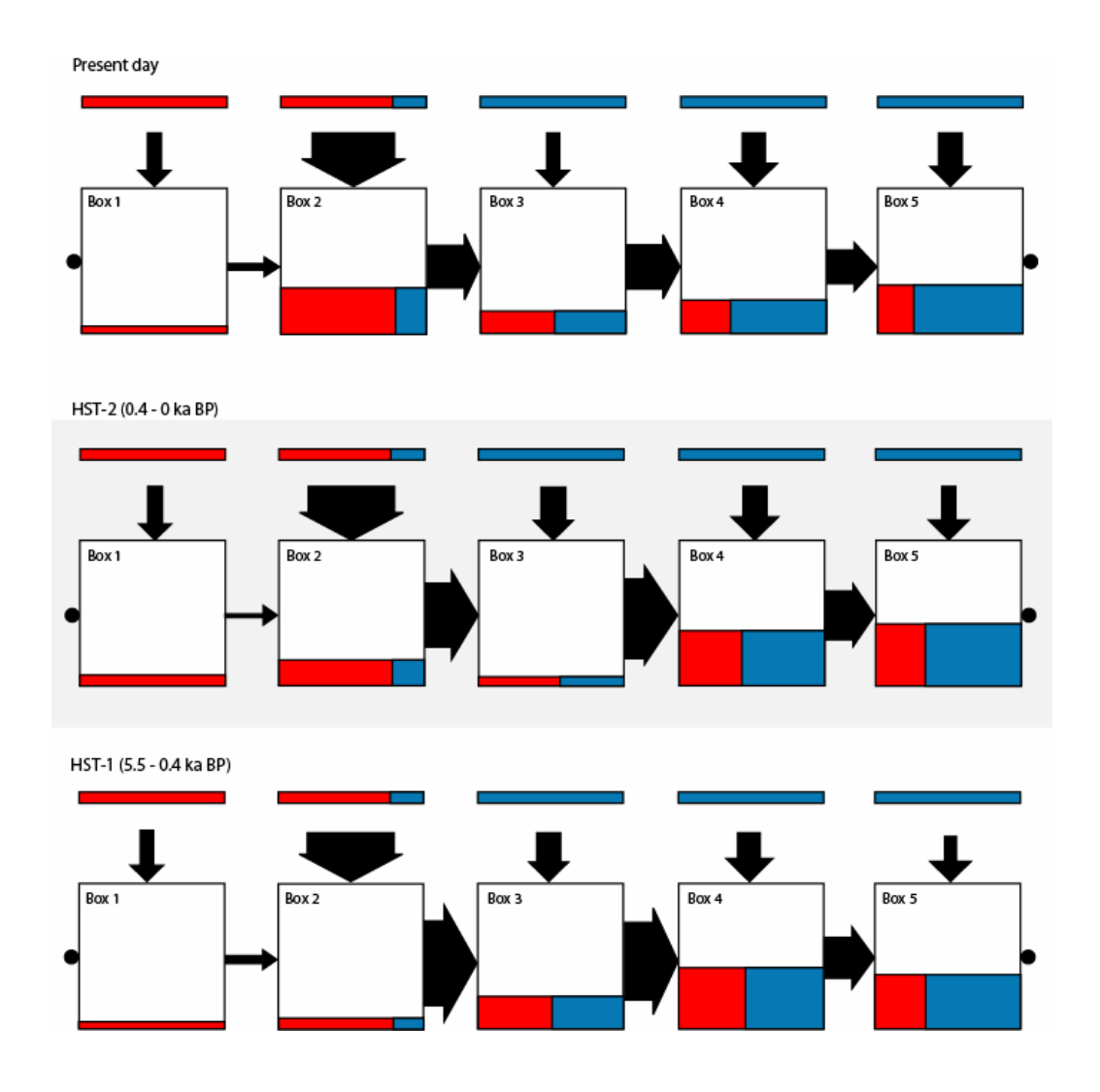


Figure 5.3: Sediment budget models for the three time slices considered (top row: present day; middle row: HST-1; bottom row: HST-1). Locations of the five cells are shown in Figure 5.1. Vertical arrows represent fluvial sediment supply (V_r) [Mt yr⁻¹]; horizontal arrows represent long-shore sediment transport (V_o) [Mt yr⁻¹]; widths of arrows are proportional to magnitudes. Colors represent sediment provenance (red for Alpine and blue for Apennine). Bars above vertical arrows indicate provenance of fluvial sediments; areas within boxes indicate composition of deposits in each cell (mass accumulation rates (V_d) [Mt yr⁻¹] proportional to colored areas). Black dots indicate closed cell boundaries (based on data of Table 5.2).

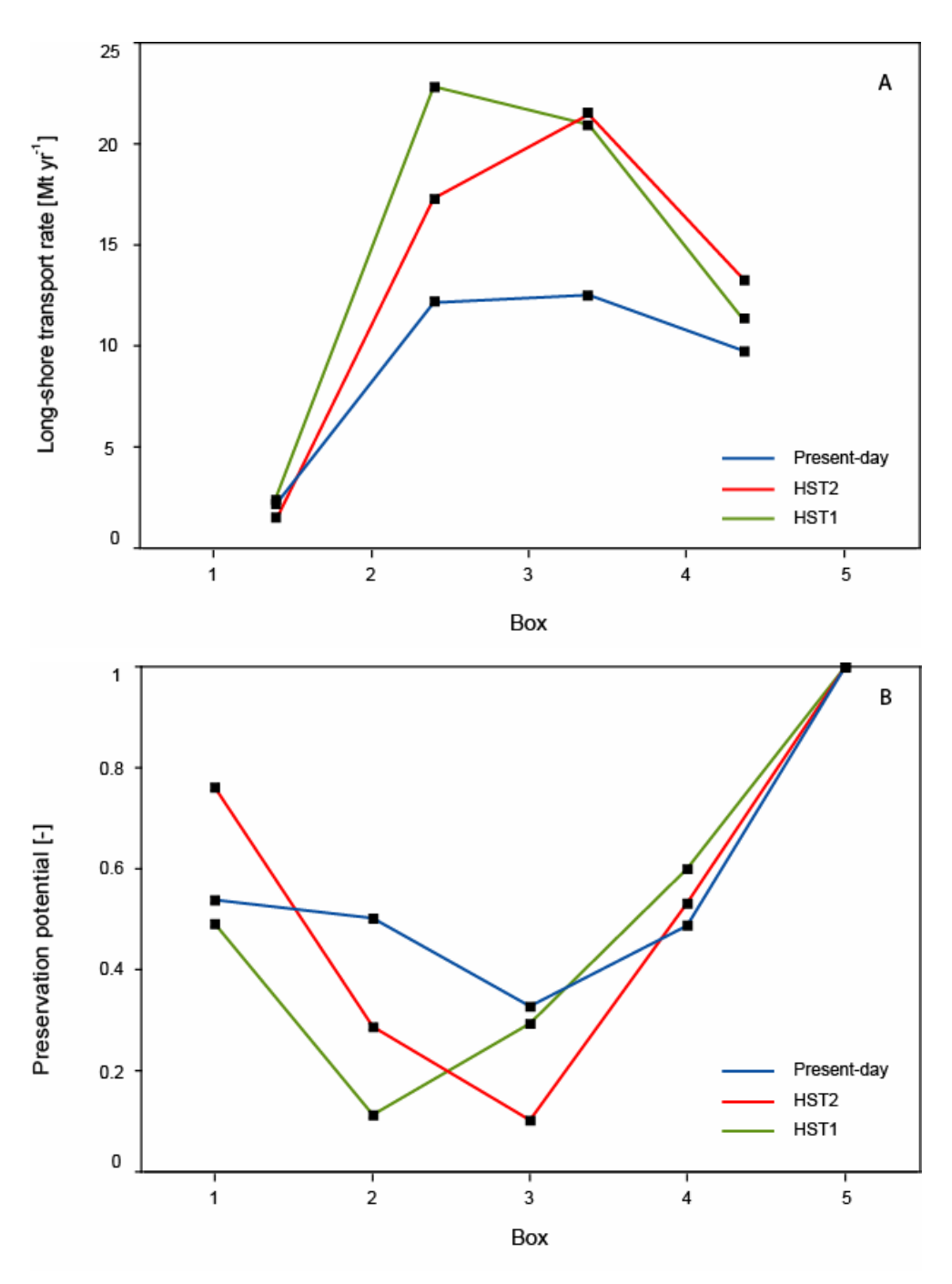


Figure 5.4: A) Longshore sediment transport rates; B) preservation potential (data from Table 5.2).

In order to illustrate the variability of local sediment accumulation rates, we plotted the mass accumulation rate within each cell versus the magnitude of time interval (Fig. 5.5). Although the average basin-wide sediment accumulation rate for the entire mud belt is constant for the three time intervals studied (Brommer et al., 2009) there are substantial differences between time-averaged rates within each cell.

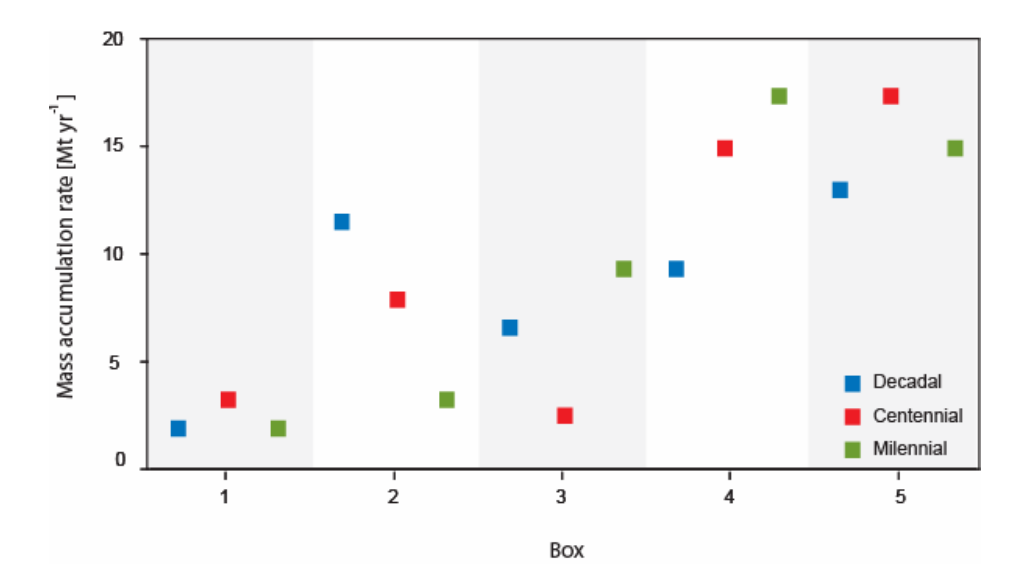


Figure 5.5: Sadler plots of the data. Magnitude of time interval (decadal, centennial, and millennial) versus average accumulation rates within each cell.

5.5 DISCUSSION

5.5.1 Long-term trends

The sediment-budget model illustrates the spatio-temporal patterns of sediment supply, long-shore transport, and deposition, which produced the Northern Adriatic mud belt over the 5.5-kyr time interval corresponding to the highstand systems tract. The palaeoclimate data of the Adriatic region (Chapter 4), which were derived from interpolation of the present-day situation to the Late Glacial Maximum by means of the GRIP ice-core record (Dansgaard et al., 1993), do not suggest major changes in climate forcing of the northern Adriatic basin, which explains the near constant rates of sediment supply to the Adriatic. Similarly, the palaeo-environmental reconstruction of Storms et al. (2008) suggests that changes in oceanographic forcing (waves, tides, thermohaline circulation) are unlikely to have directly affected the formation of the HST. Based on radiocarbon datings of peats in various locations of the

basin, the total sea level rise over the past 5.5 kyr has been estimated to be in the range of 7m (Storms et al., 2008). The latter is likely to have had a significant impact on the coastal stratigraphy, and allowed the mud belt to aggrade by elevating the long-term wave base (depth of closure) for fine-grained sediments. Given the asymptotic decrease in the rate of sea level rise (at least up to the present-day), it is likely that aggradation gradually gave way to cross-shore and long-shore progradation, because the rate of accommodation has been decreasing whereas the rate of supply has been essentially constant.

The temporally and spatially averaged sediment transport patterns of the HST-1 and HST-2 lithosomes are very similar. The majority of Alpine sourced sediment has been transported southward, indicating a low preservation potential of Alpine sourced sediment in the Northern part of the Adriatic Basin. The only substantial difference between the two lithosomes appears to be in the area between the Po Delta and the Northern Apennine offshore (cells 2 and 3), which indicates that Alpine sourced sediment has been retained around the offshore Po Delta during HST-2 times. This pattern is consistent with the derived maximum mass flux patterns from the seismic-stratigraphic analysis presented in Figure 5.2. Centennially-averaged maximum mass fluxes are observed to be the farthest offshore, a likely effect of the outbuilding and growth of the modern lobate Po Delta over the past four hundred years. According to Stefani and Vincenzi (2005) the modern Po Delta came into existence by human intervention in the Po Delta plain at the beginning of the 17th century (1604 AD) to prevent siltation of the Venice lagoon (Bondesan, 1990). This effect clearly shows up in our results.

5.5.2 Transience versus persistence

Differences between the oldest units (HST1 and HST2) on the one hand, and the present-day situation on the other hand are striking. Whereas the preservation potential of the older sediments in the Po Delta and Northern Apennine area (cells 2 and 3) is low, present-day long-shore transport rates indicate that Alpine sourced sediments have a high probability of preservation. Palinkas and Nittrouer (2007) compared decadal-scale sediment accumulation patterns to the instantaneous depocentres of sedimentation around the Po Delta following a major flood in the fall of 2000. The analysis showed that the depocentres of decadal-scale accumulation correspond to the instantaneous depocentres of flood sedimentation. This has led the authors to conclude that high-energetic events such as floods are important in forming and shaping stratigraphy around the Po Delta area. Palinkas and Nittrouer (2007) concluded that 50% of the present-day Alpine derived sediment remains within 50km of the Po Delta on a decadal time scale.

Under the assumption that oceanographic conditions in the Adriatic Basin have not changed substantially over the time interval represented by the HST, and the magnitude-frequency relation of river floods will remain unchanged, differences between the stratigraphic record (units HST-1 and HST-2) and the

present-day (decadal average) sediment dispersal pattern imply that the latter is transient (sensu Jerolmack and Sadler, 2007). In other words, the present-day sediment dispersal pattern is unlikely to be incorporated into the stratigraphic record. It is much more likely that the Adriatic shelf will undergo a series of high-energetic events in the coming decades that will provide the mechanism to remove a large quantity of sediment from its temporary repository around the Po Delta and transport it southward, in order to match the persistent character of the mud belt.

5.5.3 Local versus basin wide measurements

It is widely known that sediment accumulation rates on continental shelves show an inverse relation to the time scale over which they are measured. Sadler (1981) documented this in detail by plotting 25,000 accumulation rates measured in cores against the time span over which they have been calculated. His synthesis showed that there is a huge range in rates (up to eleven orders of magnitude), which reflects the number and length of intervals of non-deposition or erosion factored into the measurements. Because only a small fraction of elapsed time is normally represented by sediment preserved in the geological record, measurements of sediment accumulation rates from modern environments show much larger values than sediment accumulation rates determined from radiocarbon dating or inferred from the (bio) stratigraphic record. This implies that sediment accumulation rates representing a given time interval can only be used to infer sediment dynamics on that specific time scale, and any attempt to up- or down-scale such inferences is fraught with difficulty.

If we examine the variability of sediment-accumulation rates over the three time intervals considered (Fig. 5.5) in the light of the model proposed by Sadler (1981) for 'open' systems, we conclude that only cell 2 follows the classic pattern for an 'open' system, in which the preservation potential is inversely proportional to the length of the time interval. Cell 4 shows exactly the opposite, which is a logical consequence of the fact that the Adriatic mud belt is a 'closed' system. Cells 1, 3 and 5 do not show clear trends. Despite the fact that 'missing time' in a closed system does not automatically imply 'missing sediment', local accumulation rates obtained from analysis of sediment cores are not representative of the entire system and should be interpreted with great caution.

5.6 CONCLUSIONS

The mass-balanced stratigraphic model presented in this study illustrates that the transformation of transience to persistence in the HST of the northern Adriatic mud belt takes place on a centennial time scale under present-day forcing. The interplay of instantaneous deposition of sediments from major river floods and instantaneous removal of sediments from temporary repositories by storm events controls the short-term variability of local net

accumulation rates. The stratigraphic record shows that long-term patterns of supply, transport and deposition appear to be stable. The system is sensitive to large-scale perturbations only, such as the construction of the modern (artificial) Po delta, which upsets this natural balance.

The mud belt shows local variability of mass accumulation and long-shore transport rates, although the basin-wide average mass accumulation rate has been essentially constant. This variability may be understood in terms of the local balance between supply and accommodation, which varied over time. Despite the fact that the Adriatic mud belt is a 'closed' system, our results show that data obtained from a small area such as a sediment core can only be used to infer location-specific processes. Up- and down-scaling in time and space is fraught with difficulty, even in this comparatively straightforward setting. According to Griffiths (1996), the determination of temporal and spatial zones of predictability is one of the most pressing needs in stratigraphy. This poses severe limitations on the use of proxies derived from local stratigraphic records and indicates that the development of methods to bridge temporal and spatial scales in stratigraphy and palaeoceanography is a prerequisite for a more consistent use of proxies in geological reconstructions.

Chapter 6

Sustainable coastal zone management: a concept for forecasting long-term and large-scale coastal evolution

6.1 INTRODUCTION

Coastal areas are amongst the most heavily populated areas around the world and are the place of intensive economic development. At present, approximately 44 percent of the global human population lives within 150 km of the coastal zone (Cohen et al., 1997). Population growth and economic pressure in the coastal zone will continue to increase not only in the near future, but also centuries from now. Especially in the light of projected global climate change (IPCC, 2007) it is of paramount importance to comprehend the long-term (decades to centuries) and large-scale (10-10² km²) evolution of the coastal zone for sustainable coastal management and related coastal impact assessments. For instance, coastal authorities in the United Kingdom are faced with the need to forecast coastal evolution on a time scale of 100 years, and are required to present a sustainable "vision" of the coast (Defra, 2004). Within these sustainable visions, Shoreline Management Plans (SMPs) are developed which are targeted at determining future coastal defense policies and strategic long-term planning of shoreline evolution. Forecasts of coastal changes and quantitative risk assessments spanning this time interval are the key requirements (Burgess et al., 2001). However, present coastal research still mainly focuses on forecasting coastal system evolution in response to changes in hydrodynamic processes and sea level on rather small temporal scales, e.g. the tidal cycle. The overall trend or direction the coastal system evolves to on longer temporal scales can greatly affect and alter the impact of smaller-scale processes, but still little is known on how to account for changes in long-term system evolution. We aim to illustrate how geologic information from the (sub) surface combined with the quantification of sediment budgets helps assessing the long-term trend of the coastal system. The long-term trend provides the boundary conditions for processes and system evolution on smaller temporal and spatial scales.

Furthermore, we will describe how the prediction of coastal changes can be enhanced when a holistic "source to sink" view is adopted. We define the coastal zone as the transitional region between land and sea within a sediment dispersal system (Fig. 6.1). A sediment dispersal system is the natural unit in

This Chapter is based on: Brommer, M.B., and Bochev-van der Burgh, L.M. Towards sustainable coastal management: a conceptual approach to forecasting long-term and large-scale coastal evolution. Journal of Coastal Research, 25, 181-188

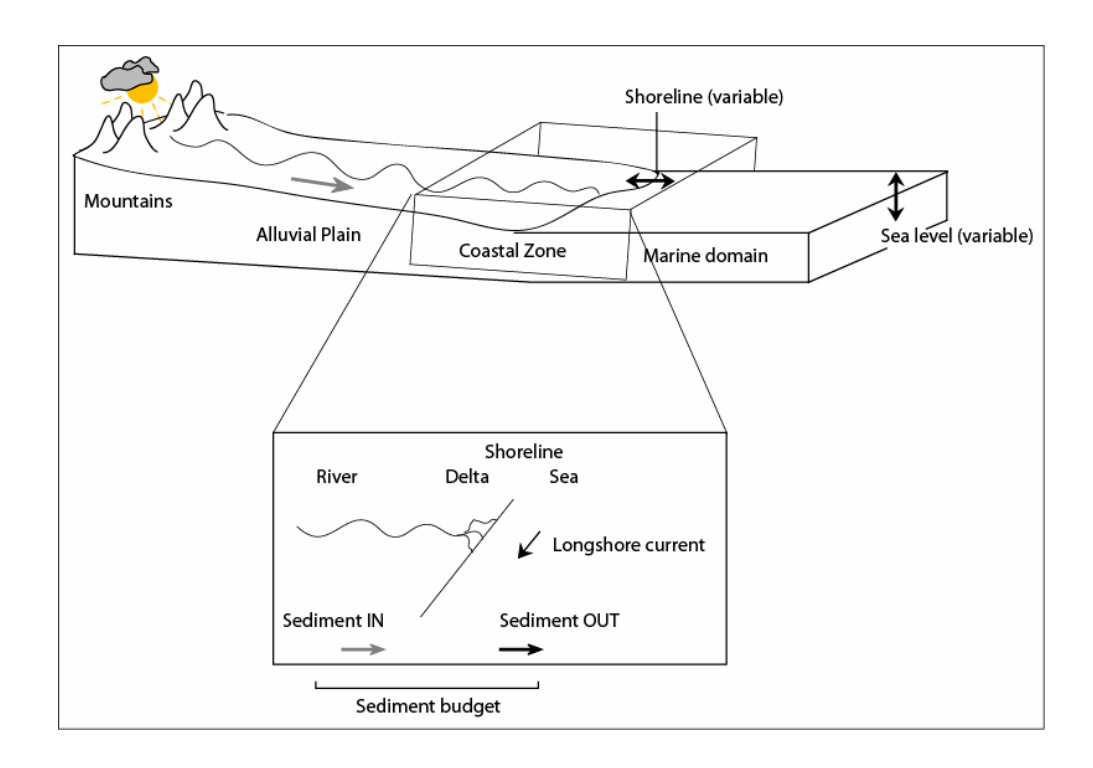


Figure 6.1: Illustration of the coastal zone as a component of a sediment dispersal system.

the source-to-sink view of earth-surface dynamics. It comprises an erosional basin in which sediments are generated (the source) and a sedimentary basin in which they are deposited (the sink). The recent trend in the earth-science community to consider earth-surface processes within a source-to-sink framework has been fuelled by the prospect of providing new insights into the responses of our planet to (anthropogenic) environmental perturbations (Chapter 4). This development is exemplified by the Community Surface Dynamics Modeling System (CSDMS; http://csdms.colorado.edu), which is aimed at developing, supporting and disseminating integrated software modules that predict the erosion, transport, and deposition of sediment and solutes in landscapes and sedimentary basins.

This Chapter is organized as follows. First, we will discuss how different scientific disciplines regard and study the natural system and which temporal and spatial domain forms the focus of their research activities. Most disciplines study system evolution at specific predefined temporal and spatial scales. As a consequence, different research approaches as well as modeling techniques arise, which only can be applied to these often narrow bandwidths of temporal and spatial scales. Secondly, the role of sediment dynamics in understanding

long-term coastal evolution is discussed. Several case studies are mentioned, which illustrate the usefulness of sediment budgets in understanding and forecasting long-term system behaviour. We introduce a conceptual framework in which the research topics of the different scientific disciplines are placed. Within this framework, we discuss the gaps in present coastal zone management activities. We will end with the conclusions and recommendations.

6.2 SCIENTIFIC DISCIPLINES AND THEIR VIEW ON THE COASTAL SYSTEM

6.2.1 Stratigraphic community

Stratigraphers study the result of past sedimentary processes and conditions by analyzing the stratigraphic record. Data usually at hand to the stratigrapher include detailed analysis of the subsurface based on sediment cores and seismic or electromagnetic interpretation (e.g. high-resolution seismics and Ground Penetrating Radar (GPR)), and numerical models to test hypotheses on sedimentary system evolution. Paleoclimate records are used to formulate the boundary conditions and associated uncertainties. The main objectives are to infer sedimentary system evolution from the stratigraphic record and relate the inferences to processes such as changes in climate, sea level and sediment supply. However, several complications arise. First of all, the stratigraphic record is seldom complete (Tipper, 2000). Secondly the inability to scale inferred processes and mechanisms from a specific site up to larger spatial and temporal scales, thirdly sedimentary system evolution involves non-linear and sometimes chaotic behaviour (Lorenz, 1993: Smith, 1998; Werner, 1999; Meijer, 2002), and finally, the problem of nonuniqueness, the notion that more than one model construction can produce the same output (Oreskes et al., 1994), although this problem is well known in other disciplines as well.

A potential step to include is to predict the evolution of sedimentary (coastal) systems for the coming hundreds years based on a combination of knowledge on present-day processes and stratigraphic data with other types of (geological) information. To achieve such a goal, dynamic stratigraphic modelling could play a central role in linking the present processes to the stratigraphic record (Syvitski and Hutton, 2001).

6.2.2 (Geo)morphological community

(Geo)morphologist study land forms, and more specifically, they are interested in how sediment is distributed within a system. From studying landforms, (geo)morphologists deduce process information. Since the 1970s, emphasis in geomorphologic research shifted towards examining the mutual interactions and changes between landforms and the processes acting on these landforms. These processes are hydrodynamic and/or aerodynamic forces involving the

motion of sediment, as they occur at different temporal and spatial scales. These processes are called morphodynamic processes (Wright and Thom, 1977), or morphodynamics Coastal systems are the result of the continuous adaptation between coastal morphology and water motion. This is called the morphodynamic loop (Beven, 1996). It is, however difficult to deduce process knowledge from merely studying forms, although this is often done. Also, geomorphologists reconstruct past environmental conditions by studying land forms. Whereas stratigraphers are primarily concerned with the subsurface, the (geo)morphologists are mainly focused on the earth surface. However, forecasting system evolution by studying land forms is difficult, especially on longer time and spatial scales. Some attempts are made in this regard. Statistical techniques, based on data/measurements are used to forecast system evolution (e.g. bulk statistical methods as the mean and standard deviation and also more advanced techniques as Empirical Orthogonal Function analysis). For a full discussion on statistical techniques and their use in forecasting system evolution, see e.g. Larson et al., 2003 and Southgate et al., 2003.

6.2.3 Coastal engineering community

The coastal engineering community - as opposed to the stratigraphic and morphological community -, focuses on the measurement and simulation of coastal processes on smaller spatial and temporal scales, i.e. seconds to decades. Coastal engineers use the following methods to study the problem of interest: (1) small-scale measurements, usually laboratory experiments (2) process-based numerical models, often calibrated on results of the laboratory measurements and (3) behaviour-oriented models. Given the impossibility to design one model that covers the wide range of processes operating at different spatial and temporal scales in the coastal zone, coastal engineers use different model approaches. Process-based models are useful for simulating the smallerscale hydrodynamic processes, whereas behaviour-oriented models are designed to cope with difficulties regarding the prediction of large-scale phenomena. These latter models do not take into account complete process knowledge, but rather use empirical relationships between system variables and, as a result, assumptions are made with regard to the governing processes. Another disadvantage of behaviour oriented models is the often crude spatial coastal schematization, which makes it difficult to evaluate the effects of e.g. smaller-scale coastal policy measures, such as beach nourishments on a local scale. Process-based models have, in general, a more sound scientific basis. This is mainly because small-scale processes are easier to measure and can often be simulated by means of laboratory experiments. A disadvantage is the restricted range of temporal and spatial scales over which they can be implemented (Bras et al, 2003). Furthermore, since the process of interest is isolated in laboratory experiments, interactions between processes and dynamic feedback mechanisms, which do occur in nature are not accounted for (Haff, 1996). In addition, the geological framework and system boundary conditions are absent in the laboratory. Process-form interactions and transformations, however, all become more pronounced on larger scales (Wright and Thom, 1977). Also, processes that may be ignored at the small scale can have significant effects on the large scale and vice versa (de Vriend et al., 1993).

Present coastal engineering research still mainly focuses on forecasting system evolution in response to changes in hydrodynamic processes and sea level on small spatial and temporal scales. In consideration of long-term coastal morphodynamic predictions, the general objective of the coastal engineering community is to evaluate how coastal systems evolve over time in response to local changes in sediment transport due to human interventions such as the construction of groynes (small-scale) or breakwaters (large-scale) (for further references see Battjes, 2006). However, time in this perspective is limited to months and sometimes years due to the duration of modelling efforts (computer time) but also to the non-linear and chaotic behaviour of natural phenomena.

6.3 SCIENTIFIC DISCIPLINES AND THE PRIMARY SCALE RELATIONSHIP

In natural scientific research it is assumed that temporal and spatial scales are closely linked, so we can describe a process or phenomenon in terms of its characteristic scale (de Vriend, 1991). This direct coupling between the scales of processes and the scales of forms is called the primary scale relationship (de Vriend, 1991). The primary scale relationship assumes that processes operating on a certain scale level are in dynamic interaction with morphological behaviour on a similar scale. This means that morphological behaviour at a certain scale is mainly the result of processes operating at the same scale (de Vriend et al., 1993; de Boer, 1992). The primary scale relationship assumes that processes operating at a smaller scale than the scale of interest can be considered as noise, whereas the larger scale processes impose the boundary conditions to the scale under consideration. Hence, it is assumed that there is no dynamic interaction between processes and behaviour at different scale levels. The primary scale relationship reflects a hierarchy structure in morphological systems: every morphological system consists of and physically contains a hierarchy of ever smaller, higher-level systems (intrinsic conditions). The system, however, is at the same time part of a hierarchy of ever larger, lower-level systems (extrinsic conditions, de Boer, 1992; Malanson, 1999; Cowell et al., 2003). In a hierarchy, a higher and a lower level system are linked by an exchange of matter and/or energy.

Recent developments in the field of coastal research, based on the assumption of a hierarchy structure in coastal morphological systems, were made by Cowell et al. (2003) who introduced the 'Coastal Tract' as a framework for the aggregation of processes in the modeling of low-order, i.e. large-scale, coastal change. This framework is based on Wright and Thom (1977) and altered by Terwindt and Battjes (1990)). The Coastal Tract Cascade (Fig. 6.2) provides a framework for separating lower-order coastal change from morphodynamics on

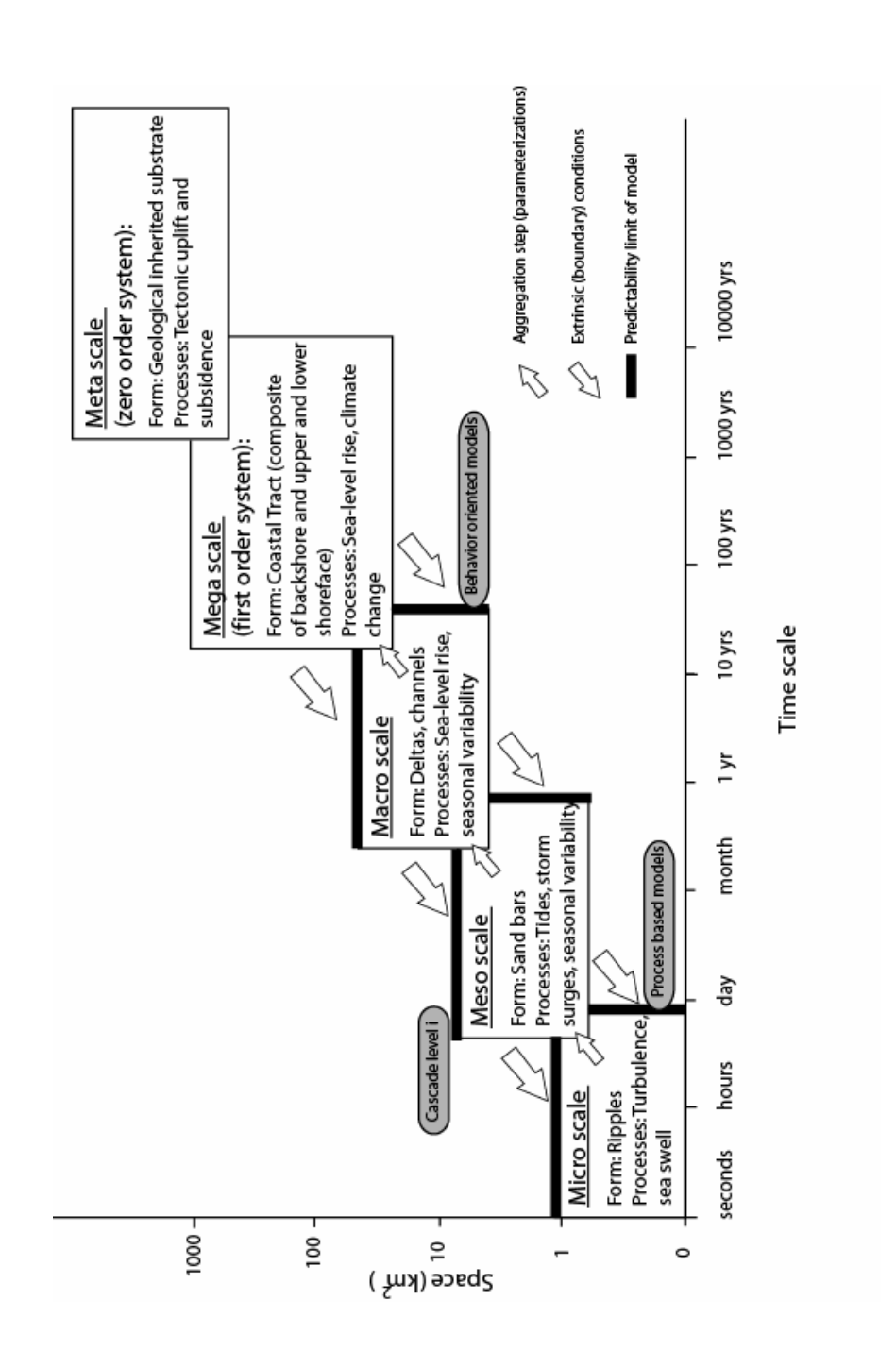


Figure 6.2: Coastal Tract Cascade (after Cowell et al., 2003)

smaller scales. The Coastal Tract, the largest compounded morphological feature, forms the first-order level in this hierarchy structure, which is constrained by the zero-order system, i.e. tectonic movements and the geologically inherited substrate. Each level in the hierarchy sees the lower levels as boundary conditions and the higher levels as intrinsic processes. At successively higher levels in the hierarchy, these intrinsic processes lose their relevance to the level of interest and may be treated as 'unimportant' (noise) or must be generalized (parameterized) for representation at the scale of interest. The coupling between the different scales -and, hence, the coupling of different morphological models- in this approach is still not thoroughly understood.

Authors as Church (1996), Phillips (1992), Werner (1999) and Van Vuren (2005) doubt the tenability of the primary scale relationship, since most natural systems exhibit features of dynamic and stochastic behaviour. Dynamic systems can be extremely sensitive to perturbations (slight changes in initial conditions), which results in a completely unpredictable solution, known as deterministic chaotic behaviour (Phillips, 1992). This implies that the aggregation or upscaling of small scale processes is not suitable for predicting large(r) scale morphologic evolution, which is commonly employed in modeling practices. A promising morphodynamic updating technique to bridge the gap between short-term hydrodynamic changes (daily time scale) and long-term morphodynamic (yearly time scale) behaviour is discussed in Roelvink (2006) who presents a highly dynamic case of the evolution of a tidal inlet to a complex geometry with an intricate pattern of channels and shoals. Further work remains to go from a yearly time scale to a decadal scale.

The discussion on different (coastal) scientific disciplines illustrates that each discipline focuses on certain aspects of system evolution and hence, on a certain temporal and spatial scale domain of coastal evolution. Each discipline is confined by its theoretic consideration, in which a holistic approach is lacking. In the scope of Sustainable Coastal Zone Management, merely upscaling of small-scale process knowledge will yield unrealistic results, as well as omitting the geologic trend, which covers spatio-temporal scales even larger than that required for coastal management planning horizons.

6.4 SEDIMENT DYNAMICS AND LONG-TERM COASTAL EVOLUTION

6.4.1 Sediment fluxes

River sediments are the source of 80 to 90% of beach sand (Summerfield, 1991). Supply-dominated coastal areas are able to prograde during times of rising sea level, provided that the input of sediment in the coastal zone is sufficient to keep pace with sea level rise (McManus, 2002). This is for instance illustrated by the evolution of the Italian shoreline surrounding the Po Delta area in the Adriatic Sea (Nelson, 1970; Stefani and Vincenzi, 2005), and the Kura Delta in the Caspian Sea (Hoogendoorn et al., 2005).

Changes in sediment fluxes and patterns to the coastal zone may alter the stability of the shoreline (Coleman and Wright, 1971). Recent observations reveal that shoreline erosion and reduction in (suspended) fluvial sediment supply are closely related (Frihy, Dewidar and El Banna, 1998; Liquete et al., 2004). Human activities impact sediment production, transport and storage in the river basins and influence thereby the fluvial sediment flux from source to basin (Syvitski et al., 2005), which might not be noticeable on the short-term, but has profound effects on the long-term (Nelson, 1970). Still, little is known to what extent humans interfere with the natural system (Larcombe, 2007). According to Syvitski et al. (2005) the net global reduction in sediment flux to the coastal zone is ≈ 1.4 BT yr⁻¹ over pre-human loads due to sediment retention behind dams. Yang, Zhao and Belkin (2002) demonstrated that decadal river sediment discharge and suspended sediment concentrations (SSC) of the Yellow River (China) had reduced by 34% and 38%, respectively, between the 1960s and 1990s. The decreases of these numbers have been assigned to a combination of dam and reservoir constructions. Giosan et al. (1999) reported a 45% decrease in sediment discharge of the Danube River due to river engineering improvements and dam construction. As a consequence, the shoreline of the Danube Delta in the Black Sea is presently eroding at rates of 20 m yr⁻¹. In the Ebro Delta, Spain, retention of sediment behind dams has led to sediment starvation along the seaward margin (McManus, 2002). In addition, coastal erosion occurs due to the wave-driven longshore current that carries the available sand-sized sediments dispersed by the River Ebro alongshore at a high rate (Sanchez-Arcilla, Jimenez and Valdemoro, 1998). In The Netherlands, it is estimated that the off-shore Dutch coast requires roughly 6 million m³ yr⁻¹ of sand nourishments to maintain the upper shoreface between -6m and +3 m NAP (Dutch Mean Sea Level) with the present rate of relative sea level rise (Mulder, 2000; Elias, 2006). The largest sand losses are observed along the coast adjacent to the Texel Inlet where the effects of the closure of the Zuiderzee are far from damped out (Elias, 2006).

Another example from the Netherlands shows that the current sediment deficit in the diked lowlands of the Netherlands is estimated at 136 ± 67 million m³ yr¹ (Van der Meulen et al., 2007). About 85 % of this volume is the hypothetical amount of sediment required to keep up with sea level rise, and 15% is the effect of land drainage (peat decomposition and compaction). These examples suggest that many coastal areas around the world receive too little sediments in order to keep pace with sea level rise. As a result these coastal areas erode at an alarming pace. In order to prepare a long-term vision that incorporates the natural dynamics of the sediment dispersal system we propose to strive to (1) better understand sources and sinks in the sediment dispersal system on different spatial and temporal scales; (2) quantify within the coastal zone the actual need for sediments in order to determine the sediment budget of the sediment dispersal system; and (3) link the sediment budget to (decadal) shoreline behaviour.

6.4.2 Sediment budgets

The sediment budget concept provides a valuable framework for the quantification of sediment mobilization, delivery, storage and output at the catchment scale (Dietrich and Dunne, 1978), and at a (sedimentary) basin scale (Fig. 6.1). The sedimentation capacity of a site is defined as either the amount of space available for sedimentation or the amount of space from which sediment can be released into transport by erosion. Sediment budgets can be used along with measurements of sediment delivery pathways to determine systematic variations in sediment sources that occur with changes in basin area (Prestegaard, 1988). Establishing a sediment budget provides a means of clarifying the link between upstream erosion and downstream sediment yield and the role of sediment storage effecting non-delivery of sediment at basin outlets (Walling, 1983, 1999).

The quantification of the coastal sediment budget helps determining sediment sources and sinks (or supply and dispersal) to and from the coast, and offers a quantitative understanding on coastal dynamics in response to changes in sea level and sediment supply. The sediment balance, which is the difference between sediment input to and sediment output from a unit area over unit time, must ultimately, be zero. However, in most real world examples the balance is not zero and this introduces a powerful property of the approach (Slaymaker, 2003). A non-zero sediment budget implies that the area defined by the budget must be either eroding or depositing. Consequently, Slaymaker (2003) argues that those time scales at which the sediment budget is either negative or positive can indicate the time scales associated with landform change within that system.

Miselis and McNinch (2006) used this approach and were able to link changes in near shore sediment volume to shoreline change and found that the geologically defined near shore sediment volume is a useful predictor of decadal shoreline behaviour for the Northeastern Outer Banks (USA). Other studies have shown a variety of methods on the quantification of the Holocene coastal sediment budget (Kelley et al., 2005; Locker et al., 2003; Schwab et al., 2000). These studies, however, did not yet link sediment budgets to shoreline changes.

6.4.3 Modelling of sediment supply

Knowledge on rates of mass transfer from source to basin on geological timescales is essential for stratigraphic as well as geomorphologic modelling (Leeder, 1997; Weltje, et al., 1998; Paola and Swenson, 1998). However, long-term records of mass transfer from source to basin are scarce (Kettner and Syvitski, 2007a). Therefore, a lot of effort has been put in developing hydrological transport models, which enable the prediction of sediment flux and discharges of global rivers (Syvitski and Alcott, 1995; Morehead et al., 2003; Syvitski et al., 2005). The climate-driven hydrological model BQART in conjunction with the model HydroTrend provides, for instance, a powerful tool

for generating synthetic water discharges and sediment load records at the river outlet (Syvitski and Milliman, 2007; Kettner and Syvitski, 2007a). The predictive capabilities of the model BQART/HydroTrend have been demonstrated in a series of tests on modern rivers (Syvitski et al., 2005; Kettner and Syvitski., 2007a). In addition, BQART/HydroTrend has been used to simulate the liquid and solid discharge where observational data are limited (Kettner and Syvitski., 2007b), or to evaluate human impacts on suspended sediment loads of rivers (Syvitski et al., 2005). Recently, BQART/HydroTrend has also been used in reconstructions of basin-fill histories (Overeem et al., 2005; Kubo et al., 2006). However, the performance of BQART/HydroTrend over long time scales (20,000 years) has been formally evaluated in Chapter 4 by means of a data-model comparison in the closed Adriatic Basin, Italy, using the principle of mass balance. Chapter 4 demonstrated that simulations of the BQART/HydroTrend model are in agreement with the quantity of sediment derived from the stratigraphic record, for the time interval covering the past 5500 years.

In the scope of an integrated coastal management approach, the use of hydrological models, which generate sediment loads and discharges for past and future time intervals can be important. Simulated sediment loads of the past can be matched to the stratigraphic record of the coastal zone to obtain sediment budgets with an estimate of the bandwidth in which these simulations fall (Chapter 4). Interpretation of the stratigraphic record therefore, provides useful information to past coastal settings, and can also help us to understand present and future changes in the environment. Calculating sediment budgets for a given coastal area and integrating these budgets in forecasting long-term evolution provides a quantitative framework to estimate the future amount of space, and determine future areas of sediment loss (erosion) and sediment storage (deposition) in the coastal zone. Since the stratigraphic record contains the results of sediment transport processes over time periods long enough to distinguish mean depositional trends from fluctuations associated with storms and other unpredictable occurrences, stratigraphic knowledge should be incorporated into (numerical) models to predict future coastal evolution records (Stolper et al., 2005).

Summarized, in Integrated Coastal Zone Management (ICZM), the incorporation of geological knowledge and large spatial and temporal scales in morphodynamic predictions is still underexposed. Yet, geological and morphological knowledge offers great potential to enhance the predictive capability of numerical models, a key tool in river, estuarine and coastal management (de Vriend, 2004). Bringing together information from both domains requires a multi-disciplinary approach, and hence the development of a common language.

6.5 DISCUSSION

6.5.1 Sediment dynamics

The role of the different communities, their research objectives and their temporal and spatial research domain are indicated in Figure 6.3, based on Van der Burgh and Brommer (2006). The "Integrated Coastal Model" (ICM) illustrates the gaps in coastal research activities and planning activities in the framework of sustainable coastal management. Fluvial processes (hinterland characteristics), changes in sediment budget (sediment transport processes) and human activities are at present omitted in forecasting long-term, largescale coastal changes and are therefore indicated with a cross. The mega scale (tectonic movements and the geologically inherited substrate) provides the boundary conditions for the processes, which govern changes in the coastal zone. Process-based and behaviour oriented models in conjunction with global climate change models and sea level rise scenarios are used to simulate future coastal development (present approach in coastal research (Fig. 6.3)). Focus should not only be on sea level rise scenarios but also on changing sediment supply scenarios, hinterland characteristics and socio-economic activities in and around the coastal zone.

6.5.2 Natural versus social systems

Assessing human impacts on the natural system is hindered due to a different notion of scale in the socio-economic sciences. In the natural sciences, choosing a scale level at which phenomena are examined refers to time and space. Scale in socio-economic research however, has a more abstract meaning and can often not be expressed in terms of temporal and spatial units. Therefore, assessing the impacts of socio-economic processes remains a difficult and ambiguous task, since this requires a thorough understanding on human behaviour. In addition, motives of people change rapidly, so forecasting human behaviour and associated socio-economic changes on long timescales are surrounded by great uncertainty. At present, models to simulate the effects of human interferences are poorly developed. Different techniques have been developed to express socio-economic processes in spatial entities. One of such techniques is agent-based modeling (ABM). Another technique to express socioeconomic changes are land-use models, which simulate the effects of people on nature and landscape. For instance, spatially detailed land-use maps of the Netherlands for the year 2030 have been constructed by de Nijs et al., (2004), in which the effects of different national economic and demographic scenarios were taken into account. However, present land use models do not take into account the mutual interactions between the natural and socio-economic system (Fig. 6.4).

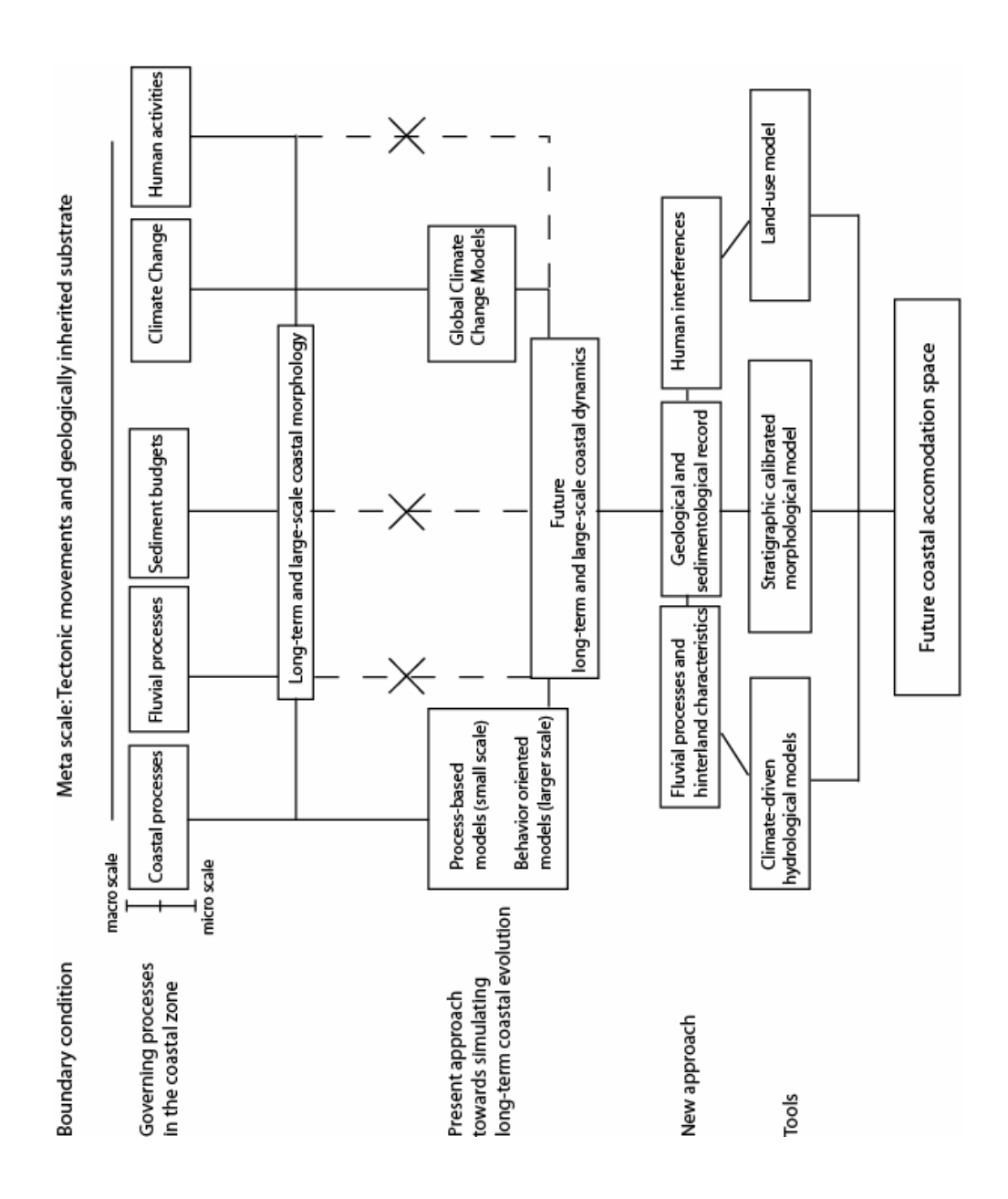


Figure 6.3: The Integrated Coastal Model. A multi-disciplinary integrated approach to enhance future coastal development scenario-building (Modified from: Van der Burgh and Brommer, 2006).

6.5.3 Linking human impact to natural coastal dynamics

Both ABMs and land use models are promising tools for assessing socioeconomic impacts in time and space. They may produce output that can be linked as probabilistic model input to *natural* morphodynamic predictions. How to link the socio-economic/ human system to the natural (long-term) system remains a challenging question. The problem of linking natural and social systems is widely acknowledged (Nicholls and Klein, 2005). So far, most social research in densely populated deltas and coastal zones has focused on socioeconomic changes in isolation from the natural system. Ideally, we should have a means to quantify the human impacts in the coastal zone. The quantification of changes in the coastal sediment budget is a potential approach to enhance forecasting of coastal evolution Elias (2006). The author demonstrated that for the Western Wadden Sea (The Netherlands) the sediment deficit after closure of the Zuiderzee is still at least 5 to 6 millions m³ yr⁻¹ to obtain equilibrium. Sediment budget studies such as these underscore not only the importance of understanding how human impacts alter the natural dynamics of the coastal system, it also quantifies the actual sediment need in the coastal system.

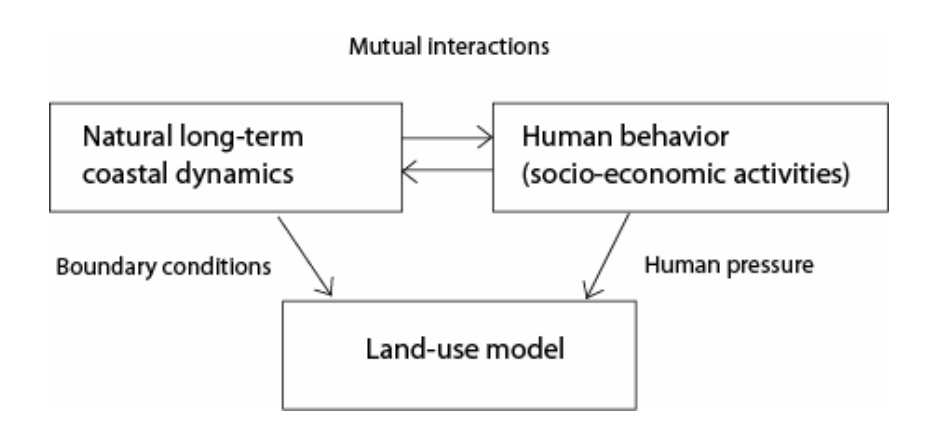


Figure 6.4: Coupling the natural long-term coastal evolution to a land-use model (From: Van der Burgh and Brommer, 2006).

6.5.4 Morphodynamic forecasts

Studying past coastal behaviour provides datasets upon which numerical models can be calibrated. It is often possible to reconstruct coastal development by means of historical maps and documents (McManus, 2002; Nelson, 1970). When compared to present-day digital elevation or terrain models, volumetric changes of the coastal area over a certain time interval can be calculated. This 'historic' result can then be compared to volumetric changes determined by means of numerical modeling. Sha (1989) quantified the evolution of an ebb-delta complex (Texel inlet, The Netherlands), which enabled comparison to

reconstructions from historical maps (Schoorl, 1973). Correggiari et al. (2005) estimated the volume of several off-shore delta lobes of the Po River, and compared their evolution with historical data. These are promising results, and suggest that if both estimates are in reasonable agreement, we may use the outcome to estimate a future budget as a result of changes in hinterland, sea level or human interferences.

6.5.5 Uncertainties

Forecasts of natural and social dynamics (and their mutual influence) are surrounded with great uncertainties. We propose the construction of long-term probabilistic scenarios as one of the means to deal with these uncertainties and variability. Probabilistic scenarios provide a range of morphodynamic states. These scenarios can lead to answers on how future social and natural changes affect the development of the coastal zone that accommodates a variety of activities that are valuable in environmental and economic perspectives. Quantitative modeling of this interaction, at all relevant scales is therefore needed.

6.6 CONCLUSIONS

In this Chapter, we have illustrated the importance of integrating different types of scientific information in forecasting long-term coastal evolution. The combined use of numerical models simulating sediment (BQART/HydroTrend) and stratigraphic information to estimate sediment budgets may provide a useful calibration technique for forecasting system evolution. The impact of human activities on long-term coastal evolution should as well be accounted for. Different disciplines adopt different theories, which are restricted to a certain temporal and spatial domain. We should aim to integrate these different types of information in the scope of sustainable coastal zone management. Rather than striving for a single-valued prediction, we should aim for providing probabilistic scenarios on coastal evolution in which relevant components contributing to uncertainties have been properly analyzed.

References

Agarwal, R.G., Gardner, D.C., Kleinsteiber, S.W. and D.D. Fussell (1999), Analyzing well production data using combined-type-curve and decline-curve analysis concepts. *SPE Reservoir Evaluation and Engineering*, *2*, 478-486.

Aitchison, J. (1986), The statistical analysis of compositional data. Chapman and Hall, London.

Alvisi, F. and M. Frignani (1996), ²¹⁰Pb-derived sediment accumulation rates for the central Adriatic Sea and crater lakes Albano and Nemi (central Italy). *Mem. Ist. Ital. Idrobiol*, *55*, 303-320.

Amorosi, A., Colalongo, M.L.Fusco, F., Pasini, G. and F. Fiorini (1999), Glacio-eustatic control of continental-shallow marine cyclicity from late Quaternary deposits of the Southeastern Po plain, Northern Italy. *Quaternary Research*, 52, 1-13.

Amorosi A. and S. Milli (2001), Late Quaternary depositional architecture of Po and Tevere river deltas (Italy) and worldwide comparison with coeval deltaic successions. *Sedimentary Geology*, 144, 357-375.

Amorosi, A., Centineo, M.C., Colalongo, M.L., Pasini, G., Sarti, G. and S.C. Vaiani (2003), Facies architecture and latest Pleistocene-Holocene Depositional history of the Po Delta (Comacchio Area), Italy. *Journal of Geology*, 111, 39-56.

Amorosi, A., Centineo, M.C., Colalongo, M.L. and F. Fiorini (2005), Milennial-scale depositional cycles from the Holocene of the Po Plain, Italy. *Marine Geology*, 222-223, 7-18.

Asioli, A., Trincardi, F., Lowe, J.J., Ariztegui, D., Langone, L. and F. Oldfield (2001), Sub-millennial scale climate oscillations in the central Adriatic during the Late-glacial: palaeoceanographic implications. *Quaternary Science Reviews*, 20, 1202-1221.

Asioli, A. (1996), High resolution foraminifera biostratigraphy in the central Adriatic basin during the last deglaciation: a contribution to the PALICLAS project. *Mem. Ist. Idrobiol, 55,* 197-217.

Athy, L.F. (1930), Density, porosity, and compaction of sedimentary rocks. *AAPG Bull.*, 14, 1-24.

Bahr, D.B., Hutton, E.W., Syvitski, J.P.M. and L.F. Pratson (2001), Exponential approximations to compacted sediment profiles. *Computers and Geosciences* 27, 691-700.

Bartlein, P.J., Anderson, K.H., Anderson, P.M., Edwards, M.E., Mock, C.J., Thompson, R.S., Webb, R.S. and C. Whitlock (1998), Paleoclimate simulations for North America over the past 21.000 years: features of the simulated climate and comparisons with palaeoenvironmental data. *Quaternary Science Reviews*, 17, 549-585.

Bass, S.J., Aldridge, J.N., McCave, I.N., Vincent, C.E. (2002), Phase relationships between fine sediment suspensions and tidal currents in coastal seas. *Journal of Geophysical Research*, 107 (C10), 3146–3160.

Bass, S.J., McCave, I.N., Rees, J.M., Vincent, C.E. (2003), Estimating fine sediment fluxes in coastal seas: validity of point measurements. Proc. Int. Conf. on Coastal Sediments 2003, World Scientific Publishing Corp. and East Meets West Productions, Corp.

Battjes, J.A. (2006), Developments in coastal engineering results. *Coastal Engineering*, 53, 121-132.

Bayer, U., and Wetzel, A. (1989), Compactional behaviour of fine-grained sediments – examples from Deep Sea Drilling Project Cores. Geologische Rundschau, 78, 807-819.

Bertrand, A. and MacBeth, C. (2003), Seawater velocity variations and real-time reservoir monitoring. *The Leading Edge*, 22, 351-355.

Blum, M. and Törnqvist, T. (2000), Fluvial responses to climate and sea level change: a review and look forward. *Sedimentology*, 47, 2-48.

Bondesan, M., Castiglioni, G.B., Elmi, C., Gabbianelli, G., Marocco, R., Pirazolli, P.A., Tomasin, A. (1995), Coastal areas at risk from storm surges and sea level rise in north-eastern Italy. Journal of Coastal Research, 11, 1354-1379.

Boudreau, B.P., and R.H. Bennett (1999), New rheological and porosity equations for steady-state compaction. *American Journal of Science*, 299, 517-528.

Boville, B.A. and P.R. Gent (1998), The NCAR Climate System Model, Version One. *Journal of Climate*, 11, 1115-1130.

Bras, R.L., Tucker, G.E. and Teles, V. (2003), Six myths about mathematical modeling in geomorphology In: WILCOCK, P and IVERSON, R. (eds), Prediction in Geomorphology. AGU, USA.

Bruckmann, W. (1989), Typische Akkretionsablaufe mariner Sedimente und ihre Modifikation in einem rezenten Akkretionskeil (Barbados Ridge). Tubinger Geow. Arb., Reihe A, 5., 135pp.

Brommer, M.B., Weltje, G.J., Trincardi, F. (2009), Reconstruction of sediment supply from mass accumulation rates in the Northern Adriatic Basin (Italy) over the past 19.000 years. Journal of Geophysical Research – Earth Surface, doi:10.1029/2008JF000987.

Bryan, F.O., B.G. Kauffman, W.G. Large and P.R. Gent (1996), The NCAR CSM Flux Coupler, NCAR/TN-424+STR, 48pp.

Burban, P.Y., Lick, W., Lick, J. (1989), The flocculation of fine-grained sediments in estuarine waters. Journal of Geophysical Research, 94 (C6), 8323-8330.

Burgess, K.A., Jay, H., Hutchison, J., Balson, P. and Ash, J., (2001), Futurecoast: assessing future coastal evolution. Proceedings DEFRA Conference of River and Coastal Engineers. Keele University, England, 9.3.1-9.3.10.

Carminati, E. and G. Martinelli (2002), Subsidence rates in the Po plain, northern Italy: the relative impact of natural and anthropogenic causation. *Eng. Geol.*, *66*, 241-255.

Castellarin, A. and Vai, G.B. (1982), Guida alla geologica del Sudalpino centro-orientale. *Soc. Geol. It.*, *Guide Geologiche Regionali*, 386 pp.

Cattaneo, A., Correggiari, A.M., Langone, L. and F. Trincardi (2003), The late-Holocene Gargano subaqueous delta, Adriatic shelf: Sediment pathways and supply fluctuations. *Marine Geology*, 193, 61-91.

Cattaneo, A., and F. Trincardi (1999), The late Quaternary transgressive record in the Adriatic epicontinental sea: basin widening and facies partitioning, in *Isolated Shallow Marine Sand Bodies: Sequence Stratigraphic Analysis and Sedimentologic Interpretation* edited by K.M. Bergman and J.W. Snedden, Special Publication 64, pp 127-146, SEPM Tulsa, USA.

Catuneanu, O. (2006), *Principles Of Sequence Stratigraphy*. Elsevier, Amsterdam, 375 p.

Chen, Z., Song, B., Wang, Z., Cai, Y. (2000), Late Quaternary evolution of the sub-aqueous Yangtze Delta, China: sedimentation, stratigraphy, palynology, and deformation. Marine Geology, 162, 423–441.

Church, M., (1996), Space, Time and the Mountain - How Do We Order What We See? *In*: Rhoads, B.L. and Thorn, C.E. (eds). *The Scientific Nature of Geomorphology*. Proceedings of the 27th Binghamton Symposium in Geomorphology held 27-29 September 1996.

Cohen, J.E.; Small, C.; Mellinger, A.; Gallup, J.; Sachs, J.; Vitousek, P.M. and Mooney, H. A. (1997), Estimates of coastal populations, *Science*, 278, 1209-1213

Coleman, J.M. and Wright, L.D. (1971), Analysis of major river systems and their deltas, Technical Report No.95, Coastal Studies Institute, Louisiana State University, Baton Rouge.

Correggiari, A.M., Cattaneo, A. and Trincardi, F. (2005), The modern Po Delta system: Lobe switching and asymmetric prodelta growth. *Marine Geology*, 222-223, 49-74.

Correggiari, A.M., Trincardi, F., Langone, L. and M. Roveri (2001), Styles and failures in the late Holocene highstand prodelta wedges on the Adriatic shelf. *Journal of Sedimentary Research, Section B, 71*, 218-236.

Cowell, P.J.; Stive, M.J.F.; Niedoroda, A.W.; de Vriend, H.J.; Swift, D.J.P.; Kaminsky, G.M. and Capobianco, M. (2003), The Coastal-Tract (Part 1): A conceptual approach to aggregated modelling of low-order coastal change. *Journal of Coastal Research*, 19(4), 812-827.

Curran, K.J., Hill, P.S. Schell, T.M., Milligan, T.G., Piper, D.J.W. (2004), Inferring the mass fraction of floc-deposited mud: application to fine-grained turbidites. *Sedimentology*, 51, 927-944.

Dansgaard, W., Johnsen, S., Clausen, H.B., Dahl-Jensen, D., Gundestrup, N.S., Hammer, C.U., Hvidberg, C.S., Steffensen, J.P., Sveinbjornsdottir, A.E., Jouzel, J. and G. Bond (1993), Evidence for general instability of past climate from a 250-ka ice core record. *Nature*, *364*, 218-220.

Davis, J.C. (2002), Statistics and Data Analysis in Geology, Third Edition. Wiley & Sons, New York, 638 p.

Diaz, J.I., Palanques, A., Nelson, C.H., Guillén, J. (1996), Morpho-structure and sedimentology of the Holocene Ebro prodelta mud belt (northwestern Mediterranean Sea). Continental Shelf Research, 16, 435-456.

De Boer, D.H. (1992), Hierarchies and spatial scale in process geomorphology: a review, *Geomorphology*, 4, 303-318

Department for Environment Food and Rural Affairs (2004). Internal Progress Report:

http://www.foresight.gov.uk/previous projects/flood and coastal defence/index.html

De Nijs, T.C.M.; De Niet, R. and Crommentuijn, L. (2004), Constructing landuse maps of the Netherlands in 2030. *Journal of Environmental Management*, 72, 35-42 De Vriend, H.J. (1991), Mathematical modeling and large-scale coastal behaviour (part 1: physical processes). *Journal of Hydraulic Research*, 29, 727-739

De Vriend, H.J.; Capobianco, M.; Chesher, T.; De Swart, H.E.; Latteux, B. and Stive, M.J.F., (1993), Approaches to long-term modelling of coastal morphology: a review. *Coastal Engineering*, 21, 225-269

De Vriend, H.J. (2004), Fluvial and estuarine morphology: recent advances in modelling. Keynote address to Int. conf. on Hydro-Science and -Engineering (ICHE 2004), Brisbane, Australia. In: Altinakar, M.S. (ed.): Advances in Hydros-Science and -Engineering Volume VI (full paper on CD-ROM, ISBN 0-937099-13-9).

Dietrich, W.E. and Dunne, T. (1978), Sediment budget for a small catchment in mountainous terrain. *Zeitschrift fur Geomorphologie*, 29, 191-206. Dinelli, E. and Lucchini, F. (1999). Sediment supply to the Adriatic Sea basin from the Italian Rivers: geochemical features and environmental constrains. *Giornale di Geologia*, 61, 121-132.

Eisma, D., Schuhmacher, T., Boekel, H., Van Heerwaarden, J., Franken, H., Lann, M., Vaars, A., Eijgenraam, F., Kalf, J. (1990), A camera and image analysis system for in situ observation of flocs in natural waters. Netherlands Journal of Sea Research, 27, 43–56.

Eisma, D., Dyer, K.R., van Leussen, W. (1997), The in-situ determination of the settling velocities of suspended fine-grained sediment – a review. In: Burt, N., Parker, R., Watts, J. (Eds.), Cohesive Sediments – Proc. of INTERCOH Conf. (Wallingford, England). John Wiley & Son, Chichester, pp. 17–44.

Einsele, G. and M. Hinderer (1998), Quantifying denudation and sediment-accumulation systems (open and closed lakes): basic concepts and first results. *Palaeogeography, Palaeoclimatology, Palaeoecology, 140,* 7-21.

Einsele, G. (2000), Sedimentary basins: Evolution, Facies, and Sediment Budget. Springer-Verlag, Berlin, 792 p.

Elias, E.P.L. (2006), Morphodynamics of Texel Inlet. Delft, The Netherlands. Delft University of Technology, Ph.D. thesis, 200p.

Fain, A.M.V., Ogston, A.S., Sternberg, R.W. (2007), Sediment transport event analysis on the western Adriatic continental shelf. Continental Shelf Research, 27, 431-451.

Farabegoli, E., Onorevoli, G. and C. Bacchiocchi (2004), Numerical simulation of Holocene depositional wedge in the southern Po Plain-northern Adriatic Sea (Italy). *Quaternary International*, 120, 119-132.

Favalli, M. and M.T. Pareschi (2004), Digital elevation model construction from structured topographic data: the DEST algorithm. Journal of Geophysical Research, 109, F04004, doi: 10.1029/2004JF000150.

Frignani, M., Langone, L., Ravaioli, M., Sorgente, D., Alvisi, F. and S. Albertazzi (2005), Fine-sediment mass balance in the western Adriatic continental shelf over a century time scale. *Marine Geology*, 222-223, 113-133.

Frihy, O.E., Dewidar, K.M. and El Banna, M.M. (1998), Natural and human impact on the northeastern Nile delta coast of Egypt. *Journal of Coastal Research*, 14, 1109-1118.

Galloway, W.E. (1989), Genetic stratigraphic sequences in basin analysis I: Architecture and genesis of flooding-surface bounded depositional units. *American Association of Petroleum Geologists Bulletin*, 73, 125-142.

George, D.A., Hill, P.S., Milligan, T.G. (2007), Flocculation, heavy metals (Cu, Pb, Zn) and the sand-mud transition on the Adriatic continental shelf, Italy. Continental Shelf Research, 27, 475-488.

Gibbs, R.J., Matthews, M.D., Link, D. (1971), The relationship between sphere size and settling velocity. Journal of Sedimentary Petrology, 41, 7-18.

Giles, M.R. (1996), *Diagenesis – A Quantitative Perspective*. Kluwer Academic Publishers, Dordrecht, 435 pp.

Giosan, L.; Bokuniewicz, H.; Panin, N. and Postolache, J. (1999), Longshore sediment transport pattern along the Romanian Danube delta coast. *Journal of Coastal Research*, 15, 859–871.

Goodbred Jr, S.L., Kuehl, S.A. (1999), Holocene and modern sediment budgets for the Ganges-Brahmaputra river system: Evidence for highstand dispersal to flood-plain, shelf, and deep-sea depocenters. Geology, 27, 559-562.

Haff, P.K. (1996), Limitations on Predictive Modeling in Geomorphology. In: Rhoads, B.L. and Thorn, C.E. (eds.), *The Scientific Nature of Geomorphology*. Proceedings of the 27th Binghamton Symposium in Geomorphology, 337-358.

Hallet, B., Hunter, L. and J. Bogen (1996), Rates of erosion and sediment evacuation by glaciers: A review of field data and their implications. *Global and Planetary Change 12*, 213-235.

Harris, C.K., Sherwood, C.R., Signell, R.P. (2004), Sediment dispersal mechanisms within the Adriatic Sea: insights from the EuroStrataform Program. EOS: Transactions of the American Geophysical Union, Ocean Sciences Meeting Supplement, 84(52), Abstract OS52E—07, Portland, OR, January, 2004.

Hill, P.S., Milligan, T.G., Geyer, W.R. (2000), Controls on effective settling velocity of suspended sediment in the Eel River flood plume. Continental Shelf Research, 20, 2095-2111.

Hoogendoorn, R.M.; Boels, J.F.; Kroonenberg, S.B.; Simmons, M.D.; Aliyeva, E.; Babazadeh, A.D. and Huseynov, D. (2005), Development of the Kura Delta, Azerbaijan: a record of the Holocene Caspian sea level changes. Marine Geology, 222-223, 359-380.

Hovius, N. and M. Leeder (1998), Clastic sediment supply to basins. *Basin Research*, 10, 1-5.

Huang, Z., and Gradstein, F.M., 1990. Depth-porosity relationship from deep sea sediments. Scientific Drilling 1, 157-162.

Hunt, J. R. (1986), Particle aggregate breakup by fluid shear. In: Estuarine Cohesive Sediment Dynamics, A. J. Mehta (Ed.), pp. 85–109, Springer, New York.

Intergovernmental Panel on Climate Change, (2007), Fourth Assessment Report. Climate Change 2007: Synthesis Report. http://www.ipcc.ch/ipccreports/ar4-syr.htm

Jerolmack, D.J., and Sadler, P. (2007) Transience and persistence in the depositional record of continental margins. *Journal of Geophysical Research*, 112, F03S13, doi: 10.1029/2006JF000555.

Kelley, J.T.; Barber, D.C.; Belknap, D.F.; Fitzgerald, D.M.; van Heteren, S. and Dickinson, S.M. (2005), Sand budgets at geological, historical and contemporary time scales for a developed beach system, Saco Bay, Maine, USA. *Marine Geology*, 214, 117-142.

Kettner, A.J., and Syvitski, J.P.M. (2007), Predicting Discharge and Sediment Flux of the Po River, Italy since the Last Glacial Maximum, in *Analogue and Numerical Forward Modelling of Sedimentary Systems; from Understanding to Prediction* edited by P.L. de Boer et al., Special Publication 39, IAS.

Kettner, A.J. and J.P.M. Syvitski (2008), HydroTrend v.3.0: a climate-driven hydrological transport model that simulates discharge and sediment load leaving a river system. *Computers and Geosciences*, *34*, 1170-1183

Kirchner, J.W., Finkel, R.C., Riebe, C.S., Granger, D.E., Clayton, J.L., King, G. and W.F. Megahan (2001), Mountain erosion over 10 yr, 10 ky, and 10 my time scales. *Geology*, 29, 591-594.

Kineke, G.C., Sternberg, R.W., Trowbridge, J.H., Geyer, W.R. (1996), Fluid mud processes on the Amazon continental shelf. Continental Shelf Research 16, 667-696.

Konert, M., Vandenberghe, J. (1997), Comparison of laser grain size analysis with pipette and sieve analysis: a solution for the underestimation of the clay fraction. Sedimentology, 44, 523-535.

Kranck, K., Milligan, T.G. (1992), Characteristics of suspended particles at an 11-hour anchor station in San Fransisco Bay, California. Journal of Geophysical Research, 97, 11373-11382.

Kranck, K., Smith, P.C., Milligan, T.G. (1996a), Grain-size characteristics of fine-grained unflocculated sediments I: 'one-round' distributions. Sedimentology, 43, 589-596.

Kranck, K., Smith, P.C., Milligan, T.G. (1996b), Grain-size characteristics of fine-grained unflocculated sediments II: 'multi-round' distributions. Sedimentology, 43, 597-606.

Kubo, Y., Syvitski, J.P.M., Hutton, E.W.H., and Kettner, A.J. (2006), Inverse Modeling of post Last Glacial Maximum transgressive sedimentation using 2d-SedFlux: Application to the northern Adriatic Sea. *Marine Geology, 234*, 233-243

Kuehl, S.A., Levy, B.M., Moore, W.S., Allison, M.A. (1997), Subaqueous delta of the Ganges-Brahmaputra river system. Marine Geology, 144, 81-96.

Kutzbach, J., Gallimore, R., Harrison, S., Behling, P., Selin, R. and F. Laarif (1998), Climate and Biome simulations for the past 21.000 years. *Quaternary Science Reviews*, 17, 473-506.

Kuehl, S.A., Carter, L., Gomez, B., Trustrum, N. (2003), Holistic approach offers potential to quantify mass fluxes across continental margins, Eos, 84, no. 38, 379-388.

Labaune, C., Jouet, G., Berné, S., Gensous, B., Tesson, M., Delpeint, A. (2005), Seismic stratigraphy of the deglacial deposits of the Rhône prodelta and of the adjacent shelf. Marine Geology 222–223, 299–311

Langone, L., Asioli, A., Correggiari, A.M. and F. Trincardi (1996), Age-depth modelling through the late Quaternary deposits of the central Adriatic basin. *Mem. Ist. Ital. Idrobiol, 55,* 177-196.

Larcombe, P. (2007), Continental shelf environments. In: Perry, C. and Taylor, K. (eds.), *Environmental Sedimentology*. Blackwell Publishing, Oxford, pp 441.

- Larson, M.; Capobianco, M.; Jansen, H.; Rozynski, G.; Southgate, H.N.; Stive, M.; Wijnberg, K.M. and Hulscher, S.J.M.H. (2003), Analysis and Modeling of Field Data on Coastal Morphological Evolution over Yearly and Decadal Time Scales. Part 1: Background and Linear Techniques, *Journal of Coastal Research*, 19(4), 760-775
- Leeder, M. (1997), Sedimentary basins: Tectonic recorders of sediment discharge from drainage catchments. *Earth Surface Processes and Landforms*, 22, 229-237.
- Le Roux, J.P. (2002), Application of the Hofmann shape entropy to determine the settling velocity of irregular, semi-ellipsoidal grains. Sedimentary Geology, 149, 237-243.
- Lesueur, P., Tastet, J.P., Weber, O. (2002), Origin and morphosedimentary evolution of fine-grained modern continental shelf deposits: the Gironde mud fields (Bay of Biscay, France), Sedimentology, 49, 1299–1320.
- Li, G., Wei, H., Yue, S., Cheng, Y., Han, Y. (1998), Sedimentation in the Yellow River delta, part II: suspended sediment dispersal and deposition on the subaqueous delta. Marine Geology, 149, 113–131.
- Liquete, C.; Canals, M.; Arnau, P.; Urgeles, R. and Durrieu de Madron, X., (2004), The Impact of Humans on Strata Formation along Mediterranean Margins. *Oceanography*, 17, 70-79.
- Liquete, C., Canals, M., Lastras, G., Amblas, D., Urgeles, R., De Mol, B., De Batist, M., Hughes-Clarke, J.E. (2007), Long-term development and current status of the Barcelona continental shelf: A source-to-sink approach. Continental Shelf Research, 27, 1779–1800.
- Liquete, C., Canals, M., De Mol, B., De Batist, M., Trincardi, F. (2008), Quaternary stratal architecture of the Barcelona prodeltaic continental shelf (NW Mediterranean). Marine Geology, 250, 234–250
- Liu, H., He, Q., Wang, Z.B., Weltje, G.J. & Zhang, J. (2009) Dynamics and spatial variability of near-bottom sediment exchange in the Yangtze Estuary, China. Estuarine, Coastal and Shelf Science, doi:10.1016/j.ecss.2009.04.020
- Lobo, F.J., Sánchez, R., González, R., Dias, J.M.A., Hernández-Molina, F.J., Fernández-Salas, L.M., Díaz del Río, V., Mendes, I. (2004), Contrasting styles of the Holocene highstand sedimentation and sediment dispersal systems in the northern shelf of the Gulf of Cadiz. Continental Shelf Research, 24, 461–482.

Locker, S.D.; Hine, A.C. and Brooks, G.R. (2003), Regional stratigraphic framework linking continental shelf and coastal sedimentary deposits of west-central Florida. *Marine Geology*, 200, 351-378.

Lorenz, E.N. (1993), The essence of chaos. UCL Press, London, 227 pp. Lowe, J. J., Blockley, S. P. E., Trincardi, F., Asioli, A., Cattaneo, A., Matthews, I. P., Pollard, M., and Wulf, S. (2007), Age modelling of late Quaternary marine sequences in the Adriatic: towards improved precision and accuracy using volcanic event stratigraphy. *Continental Shelf Research*, 27, 560-582.

Malanotte-Rizzoli, P., Bergamasco, A. (1983), The dynamics of the coastal region of the Northern Adriatic Sea. Journal of Physical Oceanography, 13, 1105-1130.

Malanson, G.P. (1999), Considering Complexity, Department of Geography, University of Iowa, 746-752

Manning, A.J., Bass, S.J., Dyer, K.R. (2006), Floc properties in the turbidity maximum of a mesotidal estuary during neap and spring tidal conditions. Marine Geology, 253, 193-211.

McCave, I.N. (1984), Erosion, transport and deposition of fine-grained marine sediments. In: Fine-Grained Sediments: Deep Water Processes and Facies, Stow, D.A.V., Piper, D.J.W. (Eds.), pp. 35–69.

McCave, I.N., Hall, R. (2006), Size sorting in marine muds: Processes, pitfalls, and prospects for paleoflow-speed proxies. Geochemistry, Geophysics, Geosystems, 7, 1-37.

McManus, J. (2002), Deltaic responses to changes in river regimes. *Marine Chemistry*, 79, 155-170.

Merritt, W.S., Letcher, R.A., and A.J. Jakeman (2003), A review of erosion and sediment transport models. *Environmental Modelling & Software, 18*, 761-799.

Meybeck, M., and C.J. Vörösmarty, (2005), Fluvial filtering of land-to-ocean fluxes: from natural Holocene variations to Anthropocene. *Comptes Rendus Geoscience*, 337, 107-123.

Meijer, X.D. (2002). Quantitative three-dimensional modelling of Quaternary continental passive margins. Utrecht, The Netherlands. Utrecht University, Ph.D. thesis, no. 221, 87p.

Mikkelsen, O., Milligan, T.G., Hill, P.S., Moffatt, P. (2004), INSSECT—an instrumented platform for investigating floc properties close to the bottom boundary layer. Limnology and Oceanography, Methods 2, 226–236.

Mikkelsen, O.A., Hill, P.S., Milligan, T.G. (2007), Seasonal and spatial variation of floc size, settling velocity and density on the inner Adriatic shelf (Italy). Continental Shelf Research, 27, 417-430.

Milligan, T.G., Cattaneo, A. (2007), Sediment dynamics in the western Adriatic Sea: From transport to stratigraphy. Continental Shelf Research, 27, 287-295.

Milligan, T.G., Hill, P.S., Law, B.A. (2007), Flocculation and the loss of sediment from the Po River plume. Continental Shelf Research, 27, 309-321.

Molnar, P. and England, P. (1990), Late Cenozoic uplift of mountain ranges and global climate change: chicken or egg? *Nature*, 346, 29-34.

Mulder, T., Syvitski, J.P.M. (1995), Turbidity currents generated at river mouths during exceptional discharge to the world oceans. Journal of Geology, 103, 285-298.

Morehead, M.D., Syvitski, J.P.M., Hutton, E.W.H., Peckham, S.D. (2003), Modeling the temporal variability in the flux of sediment from ungauged river basins. *Global and Planetary Change 39*, 95-110.

Nelson, B.W. (1970), Hydrography, sediment dispersal, and recent historical development of the Po river delta, Italy, in *Deltaic Sedimentation, Modern and Ancient* edited by J.P. Morgan, Special Publication 15, pp 152-184, SEPM, Tulsa, USA.

Nicholls, R. J. and Klein, R.J.T. (2005), Climate change and coastal management on Europe's coast. In (Eds R Allan, U. Förstner, W. Salomons, J. Vermaat, W. Salomons, L.Bouwer and K. Turner) Managing European Coasts: Past, Present and Future. Springer Berlin Heidelberg, pp 540.

Nittrouer, C. A. and Kravitz, J.H. (1996), STRATAFORM: A program to study the creation and interpretation of sedimentary strata on continental margins. Oceanography, 9, 146-152.

Oreskes, N.; Shrader-Frechette, K. and Belitz, K. (1994), Verification, validation, and confirmation of numerical models in the Earth Sciences. *Science*, 263, 641-646.

Overeem, I., Syvitski, J., Hutton, E. and Kettner, A.J. (2005), Stratigraphic variability due to uncertainty in model boundary conditions: A case-study of the New Jersey Shelf over the last 40,000 years. *Marine Geology*, 224, 23-41.

Owen, R.B. (2004), Modern fine-grained sedimentation – spatial variability and environmental controls on an inner pericontinental shelf, Hong Kong. Marine Geology, 214, 1-16.

Palinkas, C.M., and C.A. Nittrouer (2007), Modern sediment accumulation on the Po shelf, Adriatic Sea. *Continental Shelf Research*, 27, 489-505.

Paola, C., and J. Swenson (1998), Geometric constraints on composition of sediment derived from erosional landscapes. *Basin Research*, 10, 37-47.

Park, S.C., Lee, H.H., Han, H.S., Lee, G.H., Kim, D.C. and D.G. Yoo (2000), Evolution of late Quaternary mud deposits and recent sediment budget in the southeastern Yellow Sea. *Marine Geology*, 170, 271-278.

Pawlowsky-Glahn, V., Olea, R.A. (2004), Geostatistical analysis of compositional data. Studies in Mathematical Geology 7, International Association for Mathematical Geology, Oxford University Press, New York, pp. 181.

Phillips, J.D. (1992). Qualitative Chaos in Geomorphic Systems, With an Example from Wetland Response to Sea Level Rise. *Journal of Geology*, 100, 365-374.

Phillips, J.D. (2003). Alluvial storage and the long-term stability of sediment yields. Basin Research, 15, 153-163.

Poulain, P. (2001), Adriatic Sea surface circulation as derived from drifter data between 1990 and 1999. Journal of Marine Systems, 29, 3-32.

Prestegaard, K.L. (1988). Morphological controls on sediment delivery pathways. In: Bordas, M.P. and Walling. D.E. (eds). Sediment budgets. IAHS publication 174 Proceedings of the Porto Alegre Symposium, December 1988, 533-540.

Preti, M. (1999), The Holocene transgression and the land-sea interaction south of the Po Delta. Giornale di Geologia, 61, 143-159.

Puls, W, Kuehl, H, Heymann, K. (1988), Settling velocity of mud flocs: results of field measurements in the Elbe and the Weser estuary. In: Dronkers, J., van Leusen, W. (Eds), Physical processes in estuaries. Springer-Verlag, Berlin, pp 404-424.

Ridente, D. and F. Trincardi (2005), Pleistocene "muddy" forced-regression deposits on the Adriatic shelf: A comparison with prodelta deposits of the late Holocene highstand mud wedge. *Marine Geology*, 222-223, 213-233.

Roelvink, J.A. (2006), Coastal morphodynamics evolution techniques. Coastal Engineering, 53, 277-287.

Sadler, P.M. (1981), Sediment accumulation rates and the completeness of stratigraphic sections. *Journal of Geology, 89*, 569-584.

Sanchez-Arcilla, A., Jimenez, J.A. and Valdemoro, H.T. (1998), The Ebro delta: morphodynamics and vulnerability. *Journal of Coastal Research*, 14, 754–772.

Schaller, M. and T.A. Ehlers (2006), Limits to quantifying climate driven changes in denudation rates with cosmogenic radionuclides. *Earth and Planetary Science Letters*, 248, 153-167.

Schoorl, H. (1973), Zeshonderd jaren water en land. Wolters-Noordhoff, Groningen, 534 pp.

Schwab, W.C.; Thieler, E.R.; Allen, J.R.; Foster, D.S.; Swift, B.A. and Denny J.F. (2000), Influence of inner-continental shelf geologic framework on the evolution and behaviour of the barrier-island system between Fire Island Inlet and Shinnecock inlet, Long Island, New York. Journal of Coastal Research, 16, 408-422.

Sha, L.P., 1989 Holocene-Pleistocene interface and three-dimensional geometry of the ebb-delta complex, Texel inlet, the Netherlands. Marine Geology, 89, 207-228.

Syvitski, J.P.M. and Alcott, H.M. (1995), RIVER3: Simulation of water and sediment river discharge from climate and drainage basin variables. Computers and Geosciences, 21, 89-101.

Slaymaker, O., 2003. The sediment budget as conceptual framework and management tool. Hydrobiologia, 494, 71-82.

Smith, P., 1998. Explaining chaos. Cambridge University Press, Cambridge, 193 pp.

Sommerfield, C.K. (2006), On sediment accumulation rates and stratigraphic completeness: Lessons from Holocene ocean margins. *Continental Shelf Research*, 26, 2225-2240.

Southgate, E.H.N.; Wijnberg, K.M.; Larson, M.; Capobianco, M. and Jansen, H. (2003), Analysis of Field Data of Coastal Morphological Evolution over Yearly and Decadal Time Scales. Part 2: Non-Linear Techniques, *Journal of Coastal Research*, 19(4), 776-789

Stefani, M. and S. Vincenzi (2005), The interplay of eustasy, climate and human activity in the late Quaternary depositional evolution and sedimentary architecture of the Po Delta system. *Marine Geology*, 222-223, 19-48.

Stolper, D.; List, J.H. and Thieler, E.R. (2005), Simulating the evolution of coastal morphology and stratigraphy with a new morphological-behaviour model (GEOMBEST), *Marine Geology*, 218, 17-36.

Storms, J.E.A., Weltje, G.J., Terra, G., Cattaneo, A. & Trincardi, F. (2008) Coastal dynamics under conditions of rapid sea level rise: Late Pleistocene to Early Holocene evolution of barrier-lagoon systems on the northern Adriatic shelf (Italy). Quaternary Science Reviews, 27, 1107-1123.

Summerfield, M. A. (1991), Global Geomorphology: An introduction to the study of landforms, Longman Singapore Publishers (Pte) Ltd., pp. 537.

Syvitski, J.P.M., Morehead, M.D. and M. Nicholson (1998), HydroTrend: A climate-driven hydrologic-transport model for predicting discharge and sediment load to lakes or oceans. *Computers and Geosciences*, 24, 51-68.

Syvitski, J.P.M. and Hutton, E.W.H. (2001), 2D SEDFLUX 1.0C: An advanced process-response numerical model for the fill of marine sedimentary basins. Computers and Geosciences, 27, 731–754.

Syvitski, J.P.M., Peckham, S.D., Hilberman, R. and T. Mulder (2003), Predicting the terrestrial flux of sediment to the global ocean: a planetary perspective. *Sedimentary Geology*, 162, 5-24.

Syvitski, J.P.M., Vörösmarty, C.J., Kettner, A.J. and P.A. Green (2005), Impact of Humans on the Flux of Terrestrial Sediment to the Global Coastal Ocean. *Science 308*, 376-380.

Syvitski, J.P.M., and A.J. Kettner (2007), On the flux of water and sediment into the Northern Adriatic Sea. *Continental Shelf Research*, 27, 296-308.

Syvitski, J.P.M. and A.J. Kettner (2007), On the flux of water and sediment into the Northern Adriatic Sea. *Continental Shelf Research*, 27, 296-308.

Syvitski, J.P.M. and J.D. Milliman (2007), Geology, geography, and humans battle for dominance over the delivery of fluvial sediment to the coastal ocean. *Journal of Geology*, 115, 1-19.

Taylor, J.R. (1982), An Introduction to Error Analysis: The Study of Uncertainties in Physical Measurements. University Science Books, Mill Valley, USA, pp 270.

Terwindt, J.H.J. and Battjes, J.A., 1990. Research on large-scale coastal behaviour. Proceedings 22nd Coastal Engineering Conference, A.S.C.E., New York.

Tesson, M. Labaune, C., Gensous, B. (2005), Small rivers contribution to the Quaternary evolution of a Mediterranean littoral system: The western gulf of Lion, France. Marine Geology, 222–223, 313–334.

Tipper, J.C. (2000). Patterns of stratigraphic cyclicity. *Journal of Sedimentary Research*, 70, 1262-1279.

Tomadin, L., 2000. Sedimentary fluxes and different dispersion mechanisms of the clay sediments in the Adriatic Basin. *Rend. Fis. Acc. Lincei*, 11, 161-174.

Traykovski, P., Wiberg, P.L., Geyer, W.R. (2007), Observations and modeling of wave-supported sediment gravity flows on the Po prodelta and comparison to prior observations from the Eel shelf. Continental Shelf Research, 27, 375–399.

Trincardi, F., Corregiari, A.M. and M. Roveri (1994), Late quaternary transgressive erosion and deposition in a modern epicontinental shelf: the Adriatic semi-enclosed basin. *Geo-Marine Letters*, 14, 41-51.

Sternberg, R.W., Cacchione, D.A., Paulson, B., Kineke, G.C., Drake, D.E. (1996), Observations of sediment transport on the Amazon subaqueous delta. Continental Shelf Research, 16, 697-715.

Trincardi, F., Cattaneo, A., Asioli, A., Correggiari, A.M, and L. Langone (1996), Stratigraphy of the Late Quaternary deposits in the central Adriatic basin and the record of short-term climatic events. *Mem. Ist. Ital. Idrobiol*, *55*, 39-70.

Trincardi, F., Cattaneo, A., Correggiari, A.M. (2004), Mediterranean Prodelta Systems: Natural evolution and human impact investigated by EURODELTA. Oceanography, 17, 34-45.

Vail, P. R, Mitchum, R.M., Todd, R.G., Widmier, J.M., Thompsom, S., Sangree, J.B., Bubb, J.N., Hailejid, W.G. (1977), Seismic stratigraphy and global changes in sea level. In: Payton, C.E. (eds) Seismic stratigraphy – applications to Hydrocarbon Exploration. AAPG Memoir 26, 49-212.

Van der Burgh, L.M. and Brommer, M.B. (2006), All you need is space: long-term and large-scale sustainable development in deltaic areas. *In*: ROYAL HASKONING (ed.), *Innovative solutions for the delta*, special publication, 114p.

Van der Meulen, M.J.; Spek, van der, A.; Lange, de, G.; Gruijters, S.H.L.L.; Gessel, van, S.; Nguyen, B.L.; Maljers, D.; Schokker, J.; Mulder, J.P.M. and Krogt, van der, R.A.A. (2007), Regional sediment deficits in the Dutch Lowlands: Implications for Long-term land-use options. *Journal of Soils and Sediments*, 7, 9-16.

Van Vuren, B.G. (2005), Stochastic modelling of river morphodynamics. Delft, The Netherlands. Delft University of Technology, Ph.D. thesis, 295p.

Walling, D.E., 1983. The sediment delivery problem. *Journal of Hydrology*, 65, 209-237.

Walling, D.E. (1999), Linking land use, erosion and sediment yields in river basins. *Hydrobiologia*, 410, 223-240.

Walling, D.E. (2006), Human impact on land-ocean sediment transfer by the world's rivers. *Geomorphology*, 79, 192-216.

Weltje, G.J. (1997), End-member modeling of compositional data: numerical-statistical algorithms for solving the explicit mixing problem. Mathematical Geology, 29, 503-549.

Weltje, G.J., Meijer, X.D. and P.L. de Boer (1998), Stratigraphic inversion of siliciclastic basin fills: a note on the distinction between supply signals resulting from tectonic and climatic forcing. *Basin Research*, 10, 129-153.

Weltje, G.J., and M.A. Prins (2003), Muddled or mixed? Inferring palaeoclimate from size distributions of deep-sea clastics. *Sedimentary Geology*, *162*, 39-62.

Weltje, G.J., von Eynatten, H. (2004), Quantitative provenance analysis of sediments: review and outlook. Sedimentary Geology, 171, 1-11.

Weltje, G.J. (2004), A quantitative approach to capturing the compositional variability of modern sands. Sedimentary Geology, 171, 59-77.

Werner, B.T. (1999), Complexity in Natural Landform Patterns, *Science*, 284, 102-104

Wright, L.D. and Thom, B.G., 1977, Coastal depositional landforms: a morphodynamic approach, *Progress in Physical Geography*, 1(3), 412-459

Wheatcroft, R.A., Stevens, A.W., Hunt, L.M., and T.M. Milligan (2006), The large-scale distribution and internal geometry of the Fall 2000 Po River flood deposit: evidence from digital X-radiography. *Continental Shelf Research*, 26, 499-516.

White, D.A. and Gehman H.M. (1979), Methods of estimating oil and gas resources. *AAPG bulletin, 63*, 2183-2192.

Yang, S., Zhao, Q. and Belkin, I.M. (2002), Temporal variation in the sediment load of the Yangtze rive and the influences of human activities. *Journal of Hydrology*, 263, 56-71.

Yoo, K., Amundson, R., Heimsath, A.M., Dietrich, W.E., and G.H. Brimhall (2007) Integration of geochemical mass balance with sediment transport to calculate rates of soil chemical weathering and transport on hillslopes. *Journal of Geophysical Research*, 112, F02013, doi: 10.1029/2005JF000402.

Samenvatting

Massagebalanceerde stratigrafie: data-model vergelijking in een gesloten sedimentair systeem (Adriatische Zee, Italië)

Hoe reageert een sedimentair systeem op snelle zeespiegelstijging?

Dit is een fundamentele vraag die niet alleen wetenschappelijk gezien interessant is voor sedimentaire geologen maar ook buitengewoon belangrijk is voor het voorspellen van de effecten van klimaatverandering op laaggelegen kustgebieden.

Vanuit een holistisch perspectief bestaat het sedimentaire systeem uit twee delen: een erosie bekken waar het sediment wordt gegeneerd (de source) en een sedimentair bekken waar sediment wordt afgezet (de sink). Op geologische tijdschalen blijft gemiddeld slechts 10% van het sediment dat in het erosie bekken wordt gegenereerd achter, de resterende 90% wordt afgevoerd naar het sedimentaire bekken waar het sediment afgezet wordt. Het sedimentaire bekken als geheel vormt hierdoor een potentieel rijk archief waaruit informatie geëxtraheerd kan worden voor de reconstructie van processen die verantwoordelijk zijn voor de vorming en totstandkoming van het sedimentaire archief. Echter, het 'lezen' van het stratigrafische archief dient te gebeuren met grote voorzichtigheid: het archief wordt niet instantaan gevormd en wordt gekenmerkt door een grote variabiliteit zowel in ruimte als in tijd. Bovendien is het archief ook niet altijd geheel compleet (Sadler, 1981; Sommerfield, 2006; Jerolmack and Sadler, 2007).

Om beter vat te krijgen op het reconstrueren van processen die bijdragen tot de vorming en totstandkoming van het stratigrafische archief is het essentieel om een verband te leggen tussen het brongebied en het sedimentaire bekken. De link tussen de twee delen in het sedimentaire systeem kan het beste gelegd worden door het kwantificeren van snelheden waarmee sediment getransporteerd vanuit het brongebied naar het sedimentaire bekken op diverse geologisch interessante tijdschalen. Een source-to-sink analyse van het sedimentaire systeem probeert optimaal gebruik te maken van geo(morfo)logische en stratigrafische informatie door observaties van veld data, zoals boorkernen en seismische profielen, en modellen te integreren. Een goed

voorbeeld is het *Community Surface Dynamics Modeling System* (*CSDMS*; http://csdms.colorado.edu), dat zich toelegt op het ontwikkelen, ondersteunen, en verspreiden van geïntegreerde software modulen met betrekking tot het voorspellen van erosie, transport en depositie van sediment in zowel het achterland als het sedimentaire bekken. Het doel om op systematische wijze sediment dynamiek aan de aardoppervlakte te onderzoeken brengt echter wel pertinente vragen naar boven of geologische data sets op dit moment wel de juiste kwantitatieve *benchmarks* kunnen bieden waarmee dergelijke geïntegreerde modellen vergeleken kunnen worden.

Directe vergelijkingen tussen sediment toevoer uit het brongebied en depositie in het sedimentaire bekken zijn er bijna niet. Ook wordt de wet van behoud van massa, een basaal begrip in de fysica, nauwelijks gebruikt in stratigrafische analyses en geologische reconstructies. Omdat het archief zelden compleet is en zeer variabel in ruimte- en tijd, is het ook bijzonder moeilijk om een stratigrafische analyse te maken die voldoet aan het massabalans principe. Men loopt aan tegen een fundamenteel probleem in de aardwetenschappen: geologische data kunnen in ruimte- en tijd niet goed opgeschaald worden. Met betrekking tot het interpreteren van het stratigrafische archief van een sedimentair bekken houdt dit in dat sedimentologische en stratigrafische informatie verkregen uit lokale velddata zoals boorkernen altijd plaatsspecifiek zal zijn en niet representatief zal zijn voor het gehele bekken. Een stratigrafische analyse die zowel voldoet aan het massabalans principe als in staat is geologische data met model data te vergelijken is de eerste stap voorwaarts om geïntegreerde software modulen met betrekking tot het voorspellen van erosie, transport en depositie van sediment te kunnen testen.

Bovengenoemde problemen zijn de bouwstenen van dit proefschrift dat zich als hoofdtaak heeft gesteld om een op het massabalans principe gebaseerde stratigrafische analyse van een gesloten sedimentair systeem te presenteren. Het hart van het proefschrift is het ontwikkelen van een generieke methodologie en deze toe te passen op een zorgvuldig gekozen gesloten sedimentair systeem: de Adriatische Zee, Italië. De hoofdtaak is onderverdeeld in verschillende deeltaken die per hoofdstuk nauwkeurig wordt uitgelegd, beschreven en getoetst.

In hoofdstuk twee wordt ingegaan op het reconstrueren van sediment toevoer van de laatste 19.000 jaar uit het stratigrafische archief van het sedimentaire bekken. Met behulp van een stochastische simulatie, gebaseerd op hoge resolutie seismische profielen, porositeit data. radiocarbon ouderdomsbepalingen, zijn gemiddelde massa accumulatie snelheden en bijbehorende onzekerheden gekwantificeerd voor het gehele bekken voor vijf tijdsintervallen. Het kwantificeren van de onzekerheden is essentieel vanwege de statistische toets die gebruikt wordt om te bepalen of de gemiddelden significant van elkaar afwijken. Het is echter onmogelijk de hypothese te verwerpen dat de gemiddelden van elkaar afwijken (α = 10%) waardoor aangenomen dient te worden dat massa accumulatie snelheden constant zijn

voor elk tijdsinterval. Het onderzoek vergelijkt vervolgens de ruimtelijke verdeling van sediment massa accumulatie op drie tijdschalen: 10-jaar, 100-jaar en 1000-jaar. Hierdoor blijkt dat het sediment op de korte termijn (10-jaar) kust nabij wordt afgezet, maar dat op lange termijn (>100-jaar) het sediment afgevoerd wordt naar het zuidelijke gedeelte van de Adriatische Zee. Het stratigrafische archief is pas blijvend van aard als het tussen de 100- en 1000 jaar oud is. De jongste (bovenste) laag is vluchtig van aard, en wordt gekenmerkt door een lage preservatie potentieel (sensu Jerolmack and Sadler, 2007).

In hoofdstuk drie wordt dieper ingegaan op het sediment budget in het sedimentaire bekken. Het hoofdstuk presenteert een simpele doch effectieve methode waarmee de verspreiding en depositie van fijnkorrelig sediment afkomstig uit meerdere bronnen in het bekken aangetoond wordt. De methode is gebaseerd op het integreren van korrelgrootte data, geochemische analyse van specifieke korrelgrootte klassen, bulk accumulatie snelheden, een numeriek model voor het simuleren van sediment toevoer, en statistische algoritmen speciaal ontworpen voor het rekenen met compositionele data. De geïntegreerde resultaten laten voor twee brongebieden sediment accumulatie kaarten zien voor sediment met een korrelgrootte kleiner dan 63 µm. De twee brongebieden zijn de Apennijnen en de Po en Adige Rivier. Vervolgens zijn de bron specifieke sediment accumulatie data gebruikt om voor de moderne tijd het numerieke sediment toevoer model BQART/HydroTrend te calibreren. Hoewel het moderne sediment transport systeem goed gekwantificeerd kan worden in termen van herkomst, verspreiding en budget, blijkt toch dat bij het vergelijken van het moderne verspreidingspatroon met patronen verkregen uit het stratigrafische archief de huidige patronen niet blijvend van aard zijn en dus ook niet representatief zijn voor het reconstrueren van het gehele bekken.

Hoofdstuk vier slaat de brug naar het verleden. In dit hoofdstuk wordt sediment toevoer data met bijbehorende onzekerheid gesimuleerd met het numerieke model BQART/HydroTrend gedurende een tijdspanne van 19.000 jaar. De gesimuleerde data worden vervolgens op basis van het massabalans principe vergeleken met velddata uit de stratigrafie voor vijf tijdsintervallen (zoals beschreven in hoofdstuk twee). Niet alleen is dit een eerste kwantitatieve test voor het BQART/HydroTrend model op geologische tijdschaal, ook is het een primeur op het gebied van data-model vergelijking van een geheel sedimentair systeem. De resultaten wijzen uit dat beide schattingen met elkaar in overeenstemming zijn waarmee aangetoond wordt dat het numerieke sediment toevoer model ook voor langere tijdschalen ingezet kan worden. De resultaten laten echter ook zien dat het onmogelijk is de hypothese te verwerpen dat de gemiddelde sediment toevoer per tijdsinterval van elkaar afwijkt ($\alpha = 10\%$) waardoor aangenomen dient te worden dat sediment toevoer constant is voor elk tijdsinterval.

Het vijfde hoofdstuk brengt de inzichten verkregen in de voorgaande drie hoofdstukken samen in een massabalans model dat de link legt tussen groei

patronen, stratigrafische architectuur, en variabiliteit van sediment accumulatie in ruimte en tijd. Het massabalans model laat duidelijk zien hoe een sedimentair systeem in tijd en ruimte opbouwt en hoe het uiteindelijk bewaard blijft. Hiermee wordt meer inzicht gegeven aan de beantwoording van de centrale vraag hoe sedimentaire systemen reageren op snelle zeespiegelstijging. Het massabalans model laat tevens duidelijk zien dat stratigrafisch onderzoek slechts zin heeft als het gehele bekken bekeken wordt aangezien uit lokale data slechts lokale fenomenen geïnterpreteerd kunnen worden.

In het laatste hoofdstuk wordt met het hierboven verkregen inzicht een conceptueel model besproken waarin het managen van sedimentaire kustsystemen op verschillende tijd- en ruimte schalen centraal staat.

Acknowledgements

Een bijzondere periode is afgesloten.

Salle, ik wil je hartelijk danken voor het zijn van een enthousiaste promotor, die op de juiste momenten met kritische vragen komt. Dank je wel.

Gert Jan, zonder jou was dit onderzoek nooit op dit niveau gekomen. Ik kijk terug op een heel leerzame wetenschappelijke tijd en ik ben trots op het resultaat: mijn proefschrift Daarbuiten heb ik ook ontzettend met je kunnen lachen, voor mij erg belangrijk, vooral op de congressen die we in het kader van de Europese Samenwerking in vele steden hebben bezocht. Dank je wel voor al je support, inspiratie, en je tomeloze energie om de geologie te kwantificeren.

Whilst in Bologna I stayed at the Institute of Marine Geology. Fabio, you have been a great host and your invitation to participate in one of the Adriatic cruises was very kind. I would also like to thank Anna Correggiari and Antonio Cattaneo for making my stay in Bologna worthwhile. A special thanks goes to Domenico Ridente for help and support throughout my stay. Grazie mille!

Remco, Koen, Wiebke, Jan Cees, Maaike, Rick, Jose, Christiaan, Albert, Irina, Bob, Joep, Rory: ik kijk terug op een heel fijne tijd aan de TUD die ik met jullie allemaal heb gehad. Dank jullie wel.

Wouter, Adriaan en Stefan: dank jullie wel voor prima afstudeerwerk en jullie bijdrage aan het onderzoek.

De aardwetenschap is een boeiend vakgebied. De eerste persoon die me dat duidelijk maakte is helaas niet meer. Orson, dank je wel voor je inspiratie. Ik had je graag mijn proefschrift willen overhandigen.

Aan de VU heb ik fijn samengewerkt in het lab met Martin en Maurice, en uiteraard was Maarten Prins daar om het een en ander te coördineren. Ik kijk terug op een gezellige tijd. Dank jullie wel dat ik altijd welkom was.

Gerald, ik wil jou ook hartelijk danken voor je wetenschappelijke inzichten, je creativiteit, en je support. Voor mij heb je een belangrijke bijdrage geleverd. Dank je wel.

Mijn lieve vriendinnen Annemieke, Lisette, en Femke. Dank jullie wel voor alles waar vriendschap voor staat en wat we samen hebben gemaakt. Ik ben nog steeds verbaasd dat jullie nooit moe zijn geworden van mijn geneuzel over modder. Lieve zus, wat fijn dat je mijn paranimf bent.

Lieve Marjolijn en Pierre, Jonatan en Bregje. Het is altijd goed om elkaar te zien en samen te zijn. Dank jullie wel voor de continue interesse en het luisterende oor. Heel fijn om in de familie te zijn.

Lieve Jon en Marianne, ook al zien we elkaar niet veel ik ben altijd heel blij geweest met jullie aandacht voor de promotie en jullie onuitputtelijke support. Lieve Bol, wat fijn dat ook jij mijn paranimf bent.

Lieve paps en mams, het is zover. Ieder op jullie eigen manier hebben jullie ervoor gezorgd dat ik sta waar ik nu sta. Dank jullie wel voor alle liefde, warmte, en de vrijheid die jullie me altijd hebben gegund.

Lieve Tobias, wat zul je blij zijn dat het nu zover is. Zonder jouw liefde en onvoorwaardelijke steun zou het allemaal een stuk zwaarder zijn geweest. Dank je wel voor alles wat je me geeft en dat je bij me wil zijn wat er ook gebeurd. Je bent lief.

Curriculum Vitae

Marit Bente Brommer attended secondary school at the 'Vossius Gymnasium' in Amsterdam from 1989 to 1995. After two years of extensive travel she returned to Amsterdam and started her university studies in Earth Sciences at the *Vrije* Universiteit. Amsterdam. She graduated in 2002 and after a year with PanTerra Geoconsultants in Warmond she joined the International Water Center in Delft and worked on several geohydrological projects worldwide.

In 2004 Marit started at Delft University of Technology with her PhD research "Mass-balanced stratigraphy: data-model comparison within a closed sedimentary system (Adriatic Sea, Italy)" under the supervision of prof dr Salle Kroonenberg and dr Gert Jan Weltje. Two EU funded programmes (EuroDelta and EuroStrataform) enabled several visits to the Institute of Marine Geology of the National Research Center in Bologna (Italy) and allowed an additional three-months stay in 2004.

Marit has presented her work at numerous conferences and has published several papers in peer-reviewed journals. In 2006 Marit was awarded with the 3^d Prize in the Delta Competition, an initiative of Royal Haskoning. In 2009 she received the TU Delft 'Best paper award 2009' for her paper "Reconstruction of sediment supply from mass accumulation rates in the Northern Adriatic Basin (Italy) over the past 19.000 years", which has been published in the Journal of Geophysical Research.

After her PhD research Marit has joined Royal Haskoning as senior consultant in the Division Coastal and Rivers, and is currently based in Peterborough, United Kingdom. Besides managing coastal protection and flood risk projects both in the UK and overseas, she is responsible for a team consisting of coastal scientists, engineers and modellers.

List of proceedings and publications

2009

Brommer, M.B., Weltje, G.J., and Trincardi, F. Reconstruction of sediment supply from mass accumulation rates in the Northern Adriatic Basin (Italy) over the past 19.000 years. Journal of Geophysical Research, 114, F02008, doi:10.1029/2008JF000987.

Brommer, M.B., and Bochev-van der Burgh, L.M. Towards sustainable coastal management: a conceptual approach to forecasting long-term and large-scale coastal evolution. Journal of Coastal Research, 25, 181-188.

Weltje G.J. and Brommer, M.B. Quantitative analysis of sediment provenance and dispersal: application to recent deposits of the Northern Adriatic mud belt (Italy). Basin Research (submitted).

Brommer, M.B., Weltje, G.J., and Kettner, A.J. Sediment supply to the Northern Adriatic Basin over the past 19.000 years: data-model comparison using a mass-balance approach. Journal of Geophysical Research (submitted).

2008

Facies analysis from high-resolution seismic profiles in the Adriatic Basin, Italy. Invited lecture for the Chinese-Dutch workshop on Geophysical methods and techniques for marine and coastal zone management. Qingdao (PR China), 24-29 march 2008.

Critchley, W.R.S., Brommer, M.B., Negi, G. Local innovation in 'Green Water' management. In: Food and Agricultural Organization (Eds.), Bright spots: reversing the trends in land and water degradation, Special Publication, 150 p.

Sediment dispersal system evolution: inferences from the Northern Adriatic Shelf (Italy). Invited lecture for the Chinese-Dutch workshop on coastal management and geohazards. Yantai (PR China), 21-25 november 2008.

Brommer, M.B. and Laban, C.L. Coastal erosion, monitoring and management. Examples of the British and Dutch Coasts. EU coastal management conference, Sofia, 6-10 October 2008.

2007

Methods and techniques in sedimentary geology. MSc lectures in sedimentary geology for the petroleum industry. Delft (Netherlands), November 2007.

Brommer, M.B., Weltje, G.J., Kettner, A.J., Trincardi, F. A mass-balanced reconstruction of sediment supply to the Adriatic Basin from the Last Glacial

Maximum to the present. In: EGU General Assembly 2007, Vienna, Austria, 15-20 April 2007, Geophysical Research Abstracts.

2006

Brommer, M.B., Weltje, G.J. Prodelta sediment budget analysis. In: EGU General Assembly 2006, Vienna, Austria, 2-7 April 2006, Geophysical Research Abstracts.

Van der Burgh, L.M., Brommer, M.B. All you need is space: long-term and large-scale sustainable development in deltaic areas. In: Royal Haskoning (Eds.), Innovative Solutions for the Delta, pp. 114 (3d prize winning paper Delta Competition)

Brommer, M.B., Weltje, G.J. Sediment budget analysis of a late Holocene prodelta. In: Nederlands Aardwetenschappelijk Congres (NAC) 8, 24-25 April 2006.

The integrated Delta Model. Invited lecture for the ENCORA network. Valencia (Spain), 1-5 December 2006.

Brommer, M.B., Weltje, G.J. Quantitative provenance and sediment budget analysis of the late-Holocene Prodelta in the Adriatic Basin. In: Sediment 2006, 4th Meeting of SEPM Central European Section, Göttingen, 6-11 June, 2006, p.55.

Brommer, M.B., Weltje, G.J., Correggiari, A.M. Prodelta sediment budget analysis: a case study from the Holocene of the western Adriatic Sea. In: EGU General Assembly 2005, Vienna, Austria, 23-29 April 2006, Geophysical Research Abstracts

2005

Rabineau, M., Weltje, G.J., Brommer, M.B., and Dalman, R.A.F. Modelling of continental margin growth in contrasting settings and complementary intervals. EUROSTRATAFORM Workpackage 5, D29, pp 83.

Brommer, M.B., Dalman, R.A.F., Weltje, G.J. Fluvio-deltaic system dynamics: A case study of the Northern Adriatic shelf. 8th International Conference on Fluvial Sedimentology, Delft, the Netherlands, 7-12 August 2005.

2004

Brommer, M.B. Sedimentary Challenge. Natural Resource 6, no.3, p.4-5

Weltje, G.J., Storms, J.E.A., Brommer, M.B. Coastal evolution in the Northern Adriatic Sea: inferences from stratigraphic modelling and analysis of sediment

properties.In: EUROSTRATAFORM Second Annual meeting, Venice, October 20-23, 2004.

Critchley, W.R.S., Brommer, M.B., and Negi, G M.P.S. Rautela, Water Volunteer. LEISA, 19 (3), pp. 25.

2003

Critchley, W.C., Brommer, M.B., Tuyp, W.A.M. World Water Wisdom: Annotated Bibliography of Indigenous Knowledge and Water. Amsterdam, Vrije Universiteit, Centre for International Cooperation. http://www.cis.vu.nl/images_upload/62DA86FB-8C2A-44C4-B086E88C320F0926.pdf

Critchley, W.R.S., Brommer, M.B. Understanding traditional terracing. LEISA, 19 (4), 32-33.

Brommer, M.B., and Critchley, W.R.S. Innovative wastewater recycling in an Indian village: linking the rural with the urban. Urban Agriculture (www.ruaf.org).

Critchley, W.R.S., and Brommer, M.B. Innovation and Infiltration: Human ingenuity in the face of water shortage in Kenia and India. International Symposium on Water, Poverty and Productive Uses of Water at the Household Level, Johannesburg, 21-23 January 2003, pp 74-82.